A lab-on-a-chip device for optical mapping of single DNA molecules

A dissertation

Submitted to the University of Hamburg – Department of Chemistry

In partial fulfillment of the requirements for the degree of

Doctor of Natural Sciences (*Dr. rer. nat.*)

Parisa Bayat

Hamburg 2019

1 Reviewer: Prof. Dr. Robert H. Blick

2 Reviewer: Prof. Dr. Wolfgang Parak

Date of the thesis defense: 22.02.2019

Date of the print approval: 30.03.2019

Dedicated to my family and in the memory of my life hero, my dad.

The work described in this thesis was carried out between August 2015 and December 2018 at the Institutes for Nanostructure and Solid State Physics, and Center for Hybrid Nanostructures, University of Hamburg (DESY campus) in the group of Prof. Dr. Robert H. Blick. During this period, I worked on three manuscripts. One is published as conference proceeding; the second is under the revision process of scientific peer-reviewed journal, and the third is under review for publishing on the webpage of ZEISS Company.

In addition, the project is presented in several international and national conferences / workshops. The publications are mentioned subsequently.

Main Publications:

- **Parisa Bayat**, Franziska Esmek, Fabian Perez-Willard, Tobias Volkenandt, Robert H. Blick, Irene Fernandez-Cuesta, *Sculpturing wafer-scale nanofluidic devices for single molecule analysis*, Submitted to Nanoscale journal (2018).

- **Parisa Bayat**, Fabian Perez-Willard, Tobias Volkenandt, Irene Fernandez-Cuesta, Robert H. Blick, *DNA analysis in nanofluidic devices fabricated by focused ion beam milling and nanoimprint lithography*, ZEISS Application note (2018).

- Irene Fernandez-Cuesta, **Parisa Bayat**, Thomas Klings, Melanie West, Stefano Cabrini, Robert H. Blick, *Plasmonics and nanofluidics for single molecule detection*, MicroTAS proceeding (2016).

Other Publications:

- Jann Harberts, Aune Koitmäe, Robert Zierold, Cornelius Fendler, **Parisa Bayat**, Irene Fernandez-Cuesta, Gabriele Loers, Björn-Philipp Diercks, Ralf Fliegert, Andreas Guse, Carsten Ronning, Magnus Borgström, Gaute Otnes, Robert H. Blick, *Culturing and patch clamping of Jurkat T cells and neurons on Al_2O_3 coated nanowire arrays of altered morphology*, Under revision RSC Advances journal (2018).

- Cornelius Fendler, Christian Denker, Jann Harberts, **Parisa Bayat**, Robert Zierold, Gabriele Loers, Markus Münzenberg, Robert H. Blick, *3D micro scaffolds by direct laser writing for neurite guidance leading to tailor-made neuronal networks*, Advanced Biosystems, p1800329 (2019).

- **Parisa Bayat**, Dietmar Vogel, Raul D. Rodriguez, Sven Rzepka, Bernd Michel, *Thermo-mechanical characterization of copper through-silicon vias (Cu-TSVs) using micro-Raman*

spectroscopy and atomic force microscopy, Microelectronic Engineering, 137, 4 p101 – 104 (2015).

- Dietmar Vogel, Ellen Auerswald, **Parisa Bayat**, Jürgen Auersperg, Sven Rzepka, Bernd Michel, *Stress analyses of high spatial resolution on TSV and BEoL structures*, Microelectronics Reliability, 54, 9–10 p1963 – 1968 (2014).

- Raul D. Rodriguez, Thomas Blaudeck, Jana Kalbacova, Evgeniya Sheremet, Steffen Schulze, David Adner, Sascha Hermann, Michael Hietschold, Heinrich Lang, Stefan Schulz, Dietrich, *Metal nanoparticles reveal the organization of single-walled carbon nanotubes in bundles*, RSC Advances, 6, p15753 – 15758 (2016) in the Acknowledgment.

Conference Contributions and Talks

- **Parisa Bayat**, Irene Fernandez-Cuesta, Franziska Esmek, Thomas Günther, Adam Grundhoff, Stefano Cabrini, Robert H. Blick, *Nanofluidics and plasmonics for in-line optical DNA mapping*, EMN Optoelectronics, Victoria, Canada, Invited Talk (2017).

- **Parisa Bayat**, Franziska Esmek, Thomas Kling, Robert H. Blick, Irene Fernandez-Cuesta, *In-line DNA optical mapping in nanochannels,* COST Action Optical Nanospectroscopy, Lisbon, Portugal, Best Poster Award (2017).

- **Parisa Bayat**, Irene Fernandez-Cuesta, Franziska Esmek, and Robert H. Blick, *Optical mapping of single-DNA molecules at high resolution,* PIER graduate week workshop, Hamburg, Germany, Best Poster Award (2017).

- **Parisa Bayat**, Franziska Esmek, Thomas Kling, Robert H. Blick, and Irene Fernandez-Cuesta, *Plasmonics and nanofluidics for DNA-single molecule studies,* PIER graduate week workshop, Hamburg, Germany, Best Poster Award (2016).

- Irene Fernandez-Cuesta, **Parisa Bayat**, Franziska Esmek, Robert H. Blick, *Nanofluidics and nano-optics for in-line DNA optical mapping*, MNE (Micro and Nano Engineering), Copenhagen, Denmark, Invited Talk (2018).

- Cornelius Fendler, Christian Denker, Gabriele Loers, Jann Harberts, **Parisa Bayat**, Robert Zierold, Markus Münzenberg, and Robert H. Blick, *Three-dimensional micro scaffolds for tailor-made 3D neural network studies,* BPS 18 (Biophysical Society), San Francisco, CA, USA, Poster (2018).

- Jann I. Harberts, Aune Koitmäe, Robert Zierold, Cornelius Fendler, Irene Fernandez-Cuesta, **Parisa Bayat**, Gabriele Loers, M. T- Perez, Gaute Otnes, Magnus Borgström, Heiner Linke, Robert H. Blick, *Solar cell nanowires as approach for single cell direct activation,* BPS 18 (Biophysical Society), San Francisco, CA, USA, Poster (2018).

- **Parisa Bayat**, Irene Fernandez-Cuesta, Tobias Volkenandt, Fabian Perez-Willard, Robert H. Blick, *Fabrication and characterization of nanofluidic devices for DNA analysis using a FIB-SEM instrument*, Microscopy Conference, Lausanne, Switzerland Poster (2017).

- **Parisa Bayat**, Irene Fernandez-Cuesta, Robert Blick, Tobias Volkenandt, Fabian Perez-Willard, Michael Rauscher, *Fabrication and characterization of nanofluidic devices for optical DNA mapping using a FIB-SEM instrument*, MRS 2017 (Materials Research Society), Phoenix, AZ, USA, Poster (2017).

- **Parisa Bayat**, Irene Fernandez-Cuesta, Franziska Esmek, Thomas Kling, Robert H. Blick, *Plasmonics and nanofluidics for DNA-Single molecule detection,* DPG Frühjahrstagung, Dresden, Germany, Poster (2017).

- Irene Fernandez-Cuesta, **Parisa Bayat**, Franziska Esmek, Robert H. Blick, *Optical DNA mapping: labeling and reading single molecules*, New Directions In Biocomputation Workshop, Dresden, Germany, Talk (2017).

- Fabian Pérez-Willard, Tobias Volkenandt, **Parisa Bayat**, Irene Fernández-Cuesta, Robert H. Blick, *FIB fabrication of nanofluidic devices for optical DNA mapping*, EUFN 2017 (European FIB Network), Graz, Austria, Talk (2017).

- Irene Fernandez-Cuesta, **Parisa Bayat**, Franziska Esmek, Robert H. Blick, *Plasmonics and nanofluidics for DNA-single molecule detection*, NIL Industrial day, Berlin, Germany, Talk (2017).

- Irene Fernandez-Cuesta, **Parisa Bayat**, Thomas Klings, Melanie West, Stefano Cabrini, Robert H. Blick, *Plasmonics and nanofluidics for single molecule detection*, MicroTAS 2016 (Miniaturized Systems for Chemistry and Life Sciences), Dublin, Ireland, Talk (2016).

- Irene Fernandez-Cuesta, **Parisa Bayat**, Thomas Klings, Melanie West, Paul J. Schuck, Robert H. Blick, Stefano Cabrini, *Individual nanoparticle detection with a plasmonic*

nanoantenna integrated with a 30 nm x 30 nm nanochannel, Nanolight 2016, Benasque, Spain, Talk (2016).

- **Parisa Bayat**, Franziska Esmek, Irene Fernandez-Cuesta, Robert H. Blick, *Nanofluidics and plasmonics for biosensing*, ESCH 2016 (Emerging Science Convention), Hamburg, Germany, Talk (2016).

- **Parisa Bayat**, Irene Fernandez-Cuesta, Thomas kling, Robert H. Blick, *Plasmonic antenna integrated with nanochannels for DNA single molecule*, Nanolight 2016, Benasque, Spain, Poster (2016).

- **Parisa Bayat**, Irene Fernandez-Cuesta, Melanie West, Stefano Cabrini, Robert H. Blick, *Plasmonics and nanofluidics for DNA-single molecule studies*, Scharbeutz retreat workshop, Germany, Talk (2016).

- **Parisa Bayat**, Dietmar Vogel, Raul D. Rodriguez, Evgeniya Sheremet, Sven Rzepka, Dietrich R. T. Zahn, Bernd Michel, *Stress analysis on copper through-silicon vias (Cu-TSVs) using micro-Raman spectroscopy*, MAM 2014 (Materials for Advanced Metallization), Chemnitz, Germany, Poster (2014).

- **Parisa Bayat**, Dietmar Vogel, Raul D. Rodriguez, Evgeniya Sheremet, Sven Rzepka, Bernd Michel, Dietrich R. T. Zahn, *Stress measurement of copper through-silicon vias with micro-Raman spectroscopy*, DPG Frühjahrstagung, Dresden, Germany, Poster (2014).

- Thomas Blaudeck, Laura Kasper, David Adner, **Parisa Bayat**, Stefan Schulz, *Nanometallization of arrays of carbon nanotube field-effect transistors using a wafer-level stop-and-go microfluidic approach*, MRS 2014 (Materials Research Society), Boston, MA, USA, Poster (2014).

- Dietmar Vogel, Ellen Auerswald, Jürgen Auersperg, **Parisa Bayat**, Raul D. Rodriguez, Dietrich R. T. Zahn, Sven Rzepka, Bernd Michel, *Stress analyses of high spatial resolution on TSV and BEoL structures*, ESREF 2014 (European Symposium on Reliability of Electron Devices, Failure Physics and Analysis), Berlin, Germany, Talk (2014).

- Jana Kalbacova, Raul D. Rodriguez, Thomas Blaudeck, **Parisa Bayat**, Sascha Hermann, Stefan E. Schulz, Dietrich R. T. Zahn, *Integration of gold nanoparticles with wafer-level integrated carbon nanotubes probed by Raman spectroscopy*, DPG Frühjahrstagung, Dresden, Germany, Poster (2014).

- **Parisa Bayat**, Raul D. Rodriguez, Alexander Villabona, Michael Hietschold, Sascha Hermann, Stefan E. Schulz, Dietrich R. T. Zahn, *Characterization of horizontally-aligned carbon nanotubes: impact of tip-induced strain and bias voltage*, DPG Frühjahrstagung, Regensburg, Germany, Poster (2013).

- Jana Kalbacova, Raul D. Rodriguez, Thomas Blaudeck, **Parisa Bayat**, Sascha Hermann, David Adner, Heinrich Lang, Stefan E. Schulz, Dietrich R. T. Zahn, *Integration of gold nanoparticles with wafer-level integrated carbon nanotubes probed by Raman spectroscopy*, ICSFS 17 (International Conference on Solid Films and Surfaces), Rio, Brazil, Poster (2014).

- Susanne Müller, Raul D. Rodriguez, **Parisa Bayat**, Dietrich R. T. Zahn, *Horizontally aligned carbon nanotubes: new insights from tip-enhanced Raman spectroscopy*, 538. Wilhelm and Else Heraeus-Seminar Light at the Nanotip, Physics Center Bad Honnef, Germany, Poster (2013).

- Raul D. Rodriguez, Evgeniya Sheremet, Marius Toader, **Parisa Bayat**, Pramodh Srinivasa, Susanne Müller, Sascha Hermann, Holger Fiedler, Ovidiou D. Gordan, D. J. Thurmer, Daniel Lehmann, S. Knohl, Oliver Schmidt, Michael Hietschold, Stefan Schulz, Dietrich R.T. Zahn, Dietrich R. T. Zahn, *Carbon-based nanomaterials, nanodevices and their nanoscale characterization*, Nanoschool VI, Vilnius, Lithuania, Talk (2012).

- Raul D. Rodriguez, Evgeniya Sheremet, Alexander Villabona, Marius Toader, Pramodh Srinivasa, **Parisa Bayat**, Susanne Müller, Sascha Hermann, Holger Fiedler, Ovidiou D. Gordan, D. J. Thurmer, Daniel Lehmann, S. Knohl, Oliver Schmidt, Michael Hietschold, Stefan Schulz, Dietrich R.T. Zahn, *Investigation of micro- and nano-tubes: towards functional devices*, SMINT Workshop, Chemnitz, Germany, Talk (2012).

Argon ion	Ar^+
Atomic force microscope	AFM
Avalanche photodiode	APD
Base pair	bp
Chemical vapor evaporation	CVD
Chromium	Cr
Computer aided design	CAD
Debye length	λ_D
Deoxyribonucleic acid	DNA
Electric double layer	EDL
Electron-beam	e-beam
Electron beam lithography	EBL
Electron multiplying charge-coupled device	EMCCD
Focused ion beam	FIB
Full width at half maximum	FWHM
Gallium ion	Ga^+
Gold	Au
Gold palladium	AuPd
Helium: neon laser	He:Ne laser
Inductively coupled plasma reactive-ion etching	ICP-RIE
Kaposi's sarcoma-associated herpesvirus	KSHV
Lab-on-a-chip	LOC
Micro-electro-mechanical systems	MEMS
Nano-electro-mechanical systems	NEMS
Nanoimprint lithography	NIL

Next generation sequencing	NGS
Numerical aperture	NA
Persistence length	P
Photoluminescence	PL
Physical vapor deposition	PVD
Point-of-care	POC
Poly(methyl methacrylate)	PMMA
Quantum dot	QD
Quantum yield	QY
Radius of gyration	R_G
Reactive ion etching	RIE
Ribonucleic acid	RNA
Scanning electron microscope	SEM
Silicon	Si
Silicon dioxide	SiO_2
Standard cube centimeter per minute	sccm
Three dimensional	3D
Tris-borate EDTA	TBE
Ultraviolet	UV
Ultraviolet nanoimprint lithography	UV- NIL
Zinc-copper-indium-sulfide core/ Zinc sulfide shell	Zn-Cu-In-S/ZnS

Diseases such as cancer, HIV/AIDS, and malaria are life-threatening, which make an early, reliable diagnosis and treatment a priority. Novel and quick personalized diagnostics methods, which are based on the patients' genetics, can help medical examiners to optimize their prescriptions. Miniaturized lab-on-a-chip approaches are ideal candidates for such medical diagnostic tests and preventive healthcare.

In contrast to commercialized industrialized sequencing tools, this technique deals with a reduced amount of data, which is only correlated to the specific regions of the DNA molecules, instead of sequencing the whole genome. The analysis process is significantly accelerated, but can be complemented by standard sequencing of the whole genome.

On-chip optical mapping using sequence-specific barcoding of DNA molecules, and fabrication of ultra-sensitive integrated micro- and nanofluidic devices for a rapid and efficient mutation sequence validation are developed in this thesis. They only require a small reagent sampling volume, are cost-efficient and accessible outside the research labs.

A robust and reliable fabrication technique for nanofluidic devices is developed, which simplifies available sophisticated but slow methods. The nanofluidic devices are fabricated either by electron beam lithography or focused ion beam milling as an imprint mold. This mold replicates all multi-dimensional patterns at once in only two minutes using nanoimprint lithography technique. The imprint process is the only fabrication step, which is repeated every time, prior to the DNA preparation and analysis.

A method for barcoding kaposi's sarcoma-associated herpesvirus molecules at specific sequences, and characterizing their optical maps in real time is developed. A competitive binding between netropsin and intercalating dyes on λ-DNA is also presented. The characterization technique is based on direct visualization of real time translocation events of individual barcoded-DNA molecules. The DNA molecules are physically confined in the nanochannels of integrated micro- and nanofluidic devices, and the linearized molecules are imaged by a point laser in an epifluorescence microscopy workstation. The emission signal is collected in a high-efficiency single photon avalanche detector and analyzed by custom-made software to create optical maps of single DNA molecules. The proposed method might pave the way to the future lab-on-a-chip detection of cancer cells with minimum concentration at early stages of the disease.

Krankheiten wie Krebs, HIV/AIDS und Malaria sind lebensbedrohlich und erfordern eine frühzeitige, zuverlässige Diagnose und Behandlung. Neuartige, schnelle Diagnosemethoden können Mediziner bei der Therapie unterstützen, die auf das Genom des Patienten zugeschnitten sein sollte. Miniaturisierte Lab-on-a-Chip Methoden sind ideale Kandidaten für verschiedene medizinische Diagnosetests und Gesundheitsvorsorge.

Im Gegensatz zu kommerziellen, industriellen Sequenzierungswerkzeugen ist bei dieser Technologie der Datenumfang begrenzt, da statt des gesamten Genoms nur die signifikanten Teile des DNA-Moleküls berücksichtigt werden. Es ist daher möglich eine schnelle Teilanalyse zu erhalten, die im Anschluss durch die Sequenzierung des gesamten Genoms ergänzt werden kann.

In dieser Arbeit wird eine Herstellungsmethode für ultraempfindliche integrierte Mikro- und Nanofluidik-Chips zur schnellen und effizienten Validierung von Mutationssequenzen sowie ein optisches Mapping auf dem Chip unter Verwendung von sequenzspezifischer Barcodierung von DNA-Molekülen entwickelt. Diese Geräte benötigen nur ein winziges Testvolumen, und sind kostengünstig herzustellen.

Die hier entwickelte Präparationsmethode für nanofluidische Bauelemente ist robust und zuverlässig und vereinfacht bereits existierende, langsame Methoden. Die nanofluidischen Bauelemente werden entweder durch Elektronenstrahllithographie oder fokussiertes Ionenstrahlätzen in einer Prägeform hergestellt. Diese Form reproduziert alle mehrdimensionalen Muster innerhalb von zwei Minuten mittels der Nanoimprint-Lithographietechnik in diesem Schritt. Für die eigentliche DNA-Analyse können daher leicht weitere Geräte geschaffen werden.

Es wird eine Methode entwickelt, mit der Kaposi-Sarkom-assoziierte Herpesvirus-Moleküle an bestimmten Sequenzen barcodiert und deren optische Abbildungen in Echtzeit charakterisiert werden können. Eine kompetitive Bindung zwischen Netropsin und interkalierenden Farbstoffen an λ-DNA wird ebenfalls vorgestellt. Die DNA-Moleküle sind physikalisch in den Nanokanälen integrierter Mikro- und Nanofluidikvorrichtungen eingeschlossen. Die vorgestellte Charakterisierungstechnik basiert auf der Echtzeit-Visualisierung von Translokationsereignissen einzelner barcodierter DNA-Moleküle. Die linearisierten Moleküle werden mit einem Punktlichtlaser in einer Epifluoreszenz-Mikroskopiearbeitsstation abgebildet. Das Emissionssignal wird durch einen hocheffizienten Einzelphotonen-Avalanche-Detektor erfasst und mit einer maßgeschneiderten Software analysiert, um optische Karten einzelner DNA-Moleküle zu erstellen.

Die vorgeschlagene Methode könnte den Weg für die zukünftige Erkennung von Krebszellen mit minimaler Konzentration im Frühstadium der Erkrankung durch Lab-on-a-Chip Analyse ebnen.

Chapter 1:

Introduction

1 Introduction

There is an urgent need for rapid and reliable point-of-care (POC) diagnostics and on-time therapeutics in order to replace the inherently slow and expensive methods in clinics. Adequate treatments and more efficient drugs can be prescribed based on a faster analysis using robust diagnostics tools. To provide a personalized affordable and accessible healthcare, fast personal genetic screening is crucial.[1]

Early deoxyribonucleic acid (DNA) sequencing methods started in 1970s, but the first human genome was only sequenced in 2001 after 13 years of extensive collaborative work, and cost $3 billion.[2] Currently, commercialized sequencing products are available from several companies, such as Pacific Biosciences, Thermo Fisher, Illumina, Genia, Oxford Nanopore Technologies, and Agilent Technologies Inc.. Although the costs of DNA sequencing are reduced drastically, and the tools with parallelized analysis are widely accessible, there still remains room for reduction of costs and the processing time.[3] Commercially available sequencing platforms typically provide a short reading range of (35 – 30,000 bases in length), and give detailed information of all base pairs of DNA fragments. Handling of incredible amounts of data, provide by DNA sequencing is a great barrier in the further development of this technique. Since mutations alter mainly only some sequences of DNA molecules, techniques which can rapidly identify and visualize only the specific mutated parts of single DNA molecules are more efficient in cost and processing time. A rapid identification of mutation leads in early disease diagnosis.

On-chip optical mapping is a method which can visualize the “barcode” of long single DNA molecules. Long DNA molecules are observed directly, as it is not necessary to break the molecules, amplify and reassemble them like in standard “short read” sequencing techniques.[4] This allows minimizing the errors as a result of reassembling of repetitive parts, and preserving the long-range information.[3, 4] Optical mapping does not offer the resolution of sequencing, rather the genomic context; however, it is an attractive candidate in combination with sequencing. Optical mapping can aid the sequence assembly of individual long chromosomal molecules in order to complement the information derived from DNA sequencing. This provides a faster analysis result by reusing the information of sequencing that has been already available in the databases, instead of sequencing the whole genomes of the patients each time. Optical mapping can be significantly more affordable, faster, simpler and more accessible to screen the genetic information, and also tailor a specific application.

Laboratory-on-a-chip (LOC) devices for DNA analysis aim at detecting a known sequence, reading the optical signals, and extracting the genetic code of DNA biomarkers (optical DNA mapping). A LOC is a compact miniaturized integrated device, which scales single or multiple laboratory functions down to a chip-format[5, 6] to easily perform multiple ultra-sensitive single-molecule studies. Recent nanotechnology instrumentations allow fabricating ultra-sensitive lab-on-a-chip devices, which are capable of delivering inexpensive and high throughput

personalized gene expression platforms, based on an individual's knowledge of particular gene sequences or mutations. Using LOC single-molecule technologies such as micro- and nanofluidic chips are active research topics for POC diagnostics and home-based healthcare solutions, such as monitoring lithium in the blood of maniac patients.

1.1 Optical mapping of single DNA molecules

For optical mapping of individual DNA molecules, first a barcode (unique "finger print") is created. Then, the DNA molecules are linearized, and mapped (visualized). There are different techniques to create barcodes, such as cleaving the DNA molecules at specific site sequences using restriction enzymes,[7, 8] fluorescently labeling DNA molecules at specific locations,[9-11] or denaturing the fluorescently labeled molecules.[12] The molecules are then elongated using chemical anchors, molecular combing, optical tweezers, electrostatic / optical trapping, or by translocating through a nanofluidic device. The extended DNA molecules are read out using gel electrophoresis, or with a fluorescence microscope.

To analyze the maps of DNA molecules, individual molecules are isolated. Miniaturized lab-on-a-chip formats like micro- and nanofluidic chips are used to isolate a single molecule from the bulk by reducing the volume around the molecule, and slowing the molecular Brownian motion by limiting the degree of freedom. The isolated single-molecules are elongated in the nanochannels by physical confinements, where they are analyzed. The elongation of molecules in a nanochannel provides a consistent and reproducible degree of extension in contrast to other techniques.

1.2 Lab-on-a-chip devices for optical mapping

Conventional genetic screening laboratories require modern sophisticated equipment, as well as lengthy and elaborate processing by trained personnel. Furthermore, a sample analysis in such laboratory processes requires a large reagent volume, and so, a small sample volume should be very diluted. However, if the system is scaled down, the highly concentrated sample (less dilution) is spatially and temporally isolated in a confined environment (Figure 1.1. (b)). Therefore, the background of the bulk volume is hindered, which results in a good signal-to-noise ratio.

The main driving force behind the development of integrated LOC devices is to push the sensitivity by isolating single molecules from the bulk.[13] A LOC device has typically small dimensions (millimeters to few square centimeters), allowing for small diffusion distances within the device, giving faster reaction times. The diagnostic speed is critical for time-dependent medical treatments, such as diagnosing a viral infection. LOCs are capable of high-throughput screening via large-scale parallelization, and meant to handle ultra-low quantities of biomolecules (pico liters, 10^{-12} l). This leads to cost efficiency of the experiment by using only small amounts of expensive reagents, and also a fast diagnostic speed of minutes instead

of days. In addition, LOC devices are capable of minimizing the amount of human interaction with the analysis, providing safe experimental conditions, reducing in the need for highly trained technicians, and ultimately resulting in a smaller degree of human error.

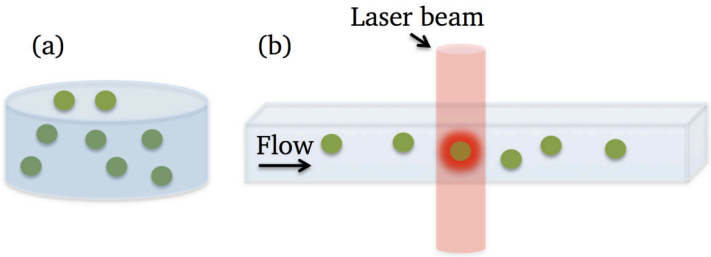

Figure 1.1. Schematic of particles in (a) bulk solution, and (b) confined in a fluid nanochannel with optical excitation. Particles are physically confined and sorted out in a nanochannel, which allows the detection of individual particles, and hinder the background signal.

A nanochannel of a nanofluidic device contains two nanoscale dimensions (width and depth) and possibly one microscale dimension (length), restricting DNA movement along a line. This allows for extracting information which is not accessible in a coiled-up conformation of DNA molecules in a bulk solution. This is a promising technique for visualizing and detecting single DNA molecules to obtain genome mapping.

1.3 Fabrication of lab-on-a-chip devices

With advances in fabrication and detection instrumentation, we are able to detect individual molecules in real-time. These chip-like tools are tailored for precise manipulation of objects, and the fast detection and analysis of analytes with high sensitivity and high throughput. The physical confinement in nanofluidic devices that unfolds the DNA strands is achieved by lithographic methods and nanofabrication. With the advancement of micro- and nanofabrication technology, such as micro-electro-mechanical systems (MEMS) and nano-electro-mechanical systems (NEMS) in recent years, the research fields on single-molecule analysis using nanobio-devices have been expanding. This allows the integration of a large number of interdisciplinary modules on a single chip. However, moving toward commercializable devices, especially biodevices, requires sufficiently reliable and robust systems, which can operate for long terms, even under complex environment.

Nanoimprint lithography (NIL) technique allows for a high-throughput mass-production of LOC devices by using a silicon mold of a nanofluidic pattern that was fabricated by photolithography, electron-beam lithography (EBL), or focused ion beam (FIB) milling. We study a simple structure of an integrated micro- and nanofluidic device, which can easily be complemented by additional functionality (such as valves/pumps). The production of the final LOC device by NIL is easy to fabricate, simple to use for non-experts, cost-efficient and also

biocompatible. In overall, NIL is a robust and accessible technique.

1.4 Analysis of elongated DNA molecules in nanofluidics

Individual molecules are elongated while passing through the nanochannels, and their genetic barcodes are monitored and identified with the aid of fluorescent dyes in an epifluorescence microscope. However, such an analysis with optical microscopes is slow, and detection of emitted signals by a camera includes a large unfocused background signal. In this case, the best achievable resolution is limited by light diffraction ($\lambda/2$ ≈250 nm,[14] which is ≈740 base pairs). To improve the detection resolution and extract more information from the weak emission signals of DNA single-molecules, we monitor the emitted fluorescence of single molecules using an avalanche photodiode in real time (Figure 1.2). In this method, instead of imaging the molecules using a microscope, we record a real time fluorescence intensity profile of DNA biomarkers, which are irradiated by a point illumination laser beam as depicted in Figure 1.2 (b – d). The emitted signal is guided into a 100 μm-diameter pinhole; the out-of-focus signal is eliminated, and the confined signal is recorded by an ultra-sensitive photodiode. This allows improving the resolution of emitted signal and increasing the contrast (signal-to-noise-ratio). In addition, an individual molecule does not repeatedly undergo an absorption-emission fluorescence cycle, as reported in other works, but only pass through the nanochannel once, and its fluorescence will not quench or photo-bleach due to the constant irradiation needed for common still imaging.

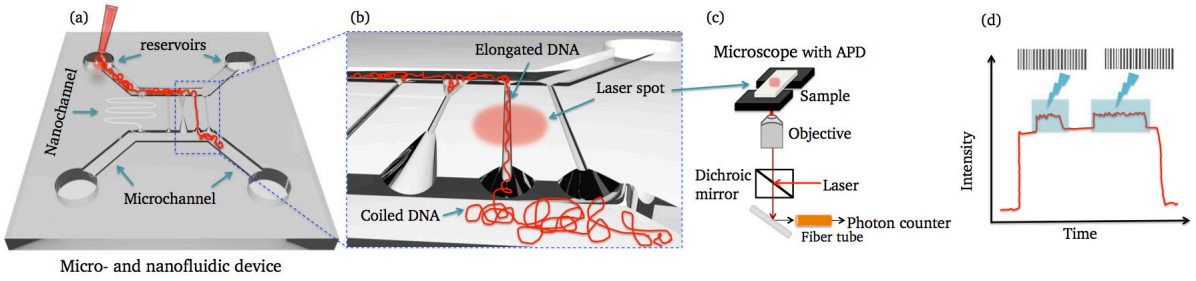

Figure 1.2. Schematic of optical mapping of elongated DNA single-molecules in a micro- and nanofluidic device. (a) the device comprises of two microchannels, which connect the reservoirs to the nanochannels. (b) single DNA molecules are stretched by physical confinements in a nanochannel. A laser spot is focused on the nanochannel where the DNA molecule is elongated. (c) simplified of our optical set up, coupling an inverted epifluorescence microscope with a high efficiency photon counting system to record the emitted signals from the DNA molecules under the laser spot. (d) the genetic barcodes of understudied molecule is visualized by recording the intensity profiles in real time.

In this thesis, fabrication and development of a disposable and inexpensive integrated laboratory-on-a-chip micro- and nanofluidic device for the optical mapping of individual large strand DNA molecules in real-time is presented.

Chapter 2 gives an overview of theoretical background of micro- and nanofabrication techniques, micro- and nanofluidics, DNA molecules and their elongation in the nanochannels, the optical setup of fluorescence microscopy, as well as fluorescent and non-fluorescent optical DNA mapping. The representative fabrication approaches include conventional photolithography, electron-beam lithography, focused ion beam microcopy and nanoimprint lithography.

Chapter 3 includes the nanofabrication methods to form nanoscale channel structures for integrated micro- and nanofluidic devices with the aim of DNA detection and analysis. The complex, multi-scale fluidic circuits are fabricated in a simple, two-minute long imprinting step. The nanofluidic part of the silicon stamp is either sculptured with electron beam lithography or directly milled by focused ion beam. Fabrication of nanochannels with EBL produces well-defined rectangular channels, which guarantee a smooth flow. Direct milling of nanochannels with FIB, however, allows patterning with different cross sections and depths channels, together with 3D funnel-like transient inlets in the same step. Producing such complicated structures with EBL is very time-consuming and difficult. Therefore, stamp fabrication using FIB is a suitable technique for rapid prototyping of different structures. Having a variety of structures (nanochannels with different depths and 3D inlets) integrated in the same device allows studying, optimizing and directly comparing their effects. The silicon stamp is then duplicated into a transparent negative stamp, which is used to replicate tens to hundreds of samples for flow measurements. The last step (sample fabrication) is performed by nanoimprint lithography, which takes only two minutes. We fabricated different silicon stamps including short and long linear/meander nanochannels with different depth and widths. Various 3D funnel-like transient inlets are designed at the entrance of the nanochannels to compare the effect of inlet structures on pre-stretching of DNA molecules, and also decreasing or increasing the speed of DNA molecules. Such inlets optimize the flow and overcome the entropy barrier, which is the result of the size mismatch from microchannels to nanochannels. The robustness and versatility of this technology and DNA testing results evidence the potential applications of imprinted devices in biomedical diagnosis as low cost, disposable lab-on-a-chip devices. The devices are made disposable to solve the issues of contamination and degradation of the sample. The main application fields of such biochips are in clinical diagnostics, for point-of-care testing, and also environmental monitoring.

Flow measurement of DNA molecules in LOC devices is presented in chapter 4. The fabricated devices in chapter 3 are utilized for linearization of DNA molecules to visualize their barcodes in an optical map. Two different techniques of producing optical maps are discussed, (1) using organic fluorescent dyes as color barcodes, as well as (2) using netropsin to create a discrete location mapping along the DNA molecules. Creation of barcodes, the linearization technique, and the detection of in-line fluorescence signals of long molecules in real time within described micro- and nanofluidic devices are discussed.

In the first method, we develop a complementary organic fluorescent dyes labeling scheme that tags specific sequences of kaposi's sarcoma-associated herpesvirus DNA (KSHV) molecules to create a barcode, without cleaving the molecules with restriction enzymes.

Optical mapping of λ-DNA with competitive barcoding using netropsin (a non-fluorescent molecule that has affinity of AT-rich of the DNA molecules) is the second method.

All experiments were conducted at room temperature and the results indicate that these observations correspond to single DNA molecules.

Chapter 2:
Theoretical Background

The first single-molecule detection was measured in the 1960s, a single enzyme activity by the generation of fluorescence.[15] Later, single-molecule detection at low temperature,[16] and room temperature[17] was measured, followed by in the fluid systems.[18]

There are different approaches for studying mechanical properties of DNA molecules, to linearize them, and to optically map the individual DNA molecules. For that, the molecule is either immobilized or flows in a liquid. Either of these two methods, techniques such as magnetic or optical tweezers, molecular combing, hydrodynamic flow, and most recently, nanoconfinement of the molecules in nanofluidics channels[19] can be used. While molecular combing offers a fast overview of the molecules, a uniform readily accessible stretching is not guaranteed. Nanoconfinement is a process that constricts DNA molecules within a narrow structure, lowering the entropy of the molecules and forcing the DNA molecule into a stretched configuration. Elongation of DNA molecules by confinement in nanofluidic channels, allows a uniform stretching for extraction of fluorescent labels attached to specific DNA sequences along long DNA molecules at high precision.

In this chapter, background information is provided on key topics, relevant for the work presented in this thesis. First, fabrication techniques by means of photolithography (fabrication of microfluidics), EBL or FIB milling (fabrication of nanofluidics), and NIL (replication of the whole device in polymer) are described. Then, the DNA and its labeling methods are explained in detail, followed by the fluorescence microscope and avalanche photodiode basic working theory. The two latter tools visualize the molecules to obtain optical DNA mapping.

2.1 Micro- and nanofabrication

The present versatile micro- and nanofabrication techniques have showed a powerful capability of handling a variety of functional materials, which leads the rapid development of micro- and nanofluidics studies and diverse applications.

Lithography techniques are divided into two types: masked lithography and mask-less lithography. In masked lithography, masks or molds (templates) transfer patterns over a large area simultaneously. This type includes photolithography and nanoimprint lithography. On the other hand, mask-less lithography, such as electron beam lithography and focused ion beam lithography fabricates designed patterns by a serial writing. These techniques create ultrahigh-resolution patterns with a minimum feature size of a few nanometers. Despite its precision in nanometer scale fabrication, the throughput of this type is limited by its slow production series, which makes it inappropriate for mass-production.

Fabrication of cost-effective integrated lab-on-a-chip micro- and nanofluidic device, presented in this research is based on double replication of a silicon master stamp. First a silicon master stamp is fabricated. Different silicon master stamps are fabricated in this work. The microchannels are fabricated using photolithography. The nanochannels are sculptured using EBL or FIB milling. Fabrication of a silicon master stamp is a one-time fabrication technique. Then the negative stamp, which is produced from the silicon master stamp, is replicated several times into the final all-transparent and all-polymer device for single molecular analysis. Replication of stamps and also the final device is performed by means of NIL. In this method, a fully functional micro- and nanofluidic sample is fabricated in a two-minutes replication step (only the second replication step), instead of repeating the entire process and starting all over again. All the multi-scale structures on the silicon stamp are duplicated into the final device. The NIL process is simple, quick and cost-efficient, which is a suitable technique for mass-production.

2.1.1 Photolithography

Conventional photolithography or optical lithography is a technique that uses a mask and a light source to transfer the pattern onto a photo-sensitive organic layer. First, a light-sensitive polymer (photoresist) is a spun over a wafer. The mask is placed on the wafer, and the ultraviolet (UV) light with wavelengths in the range of 193-436 nm is illuminated through the opaque features of a photomask and expose a coated photoresist on a substrate. UV-light exposure changes the solubility of the photoresist (polymer chains) in a chemical solvent called developer, leaving the desired pattern on the photoresist. Depending the type of the photoresist, positive or negative tone, the exposed or unexposed area is removed using the developer, respectively. Figure 2.1. depicts the schematic illustration of the main steps in photolithography. This patterned photoresist can be used as a protective layer in subsequent

etching or deposition processes to build topography on the substrate.

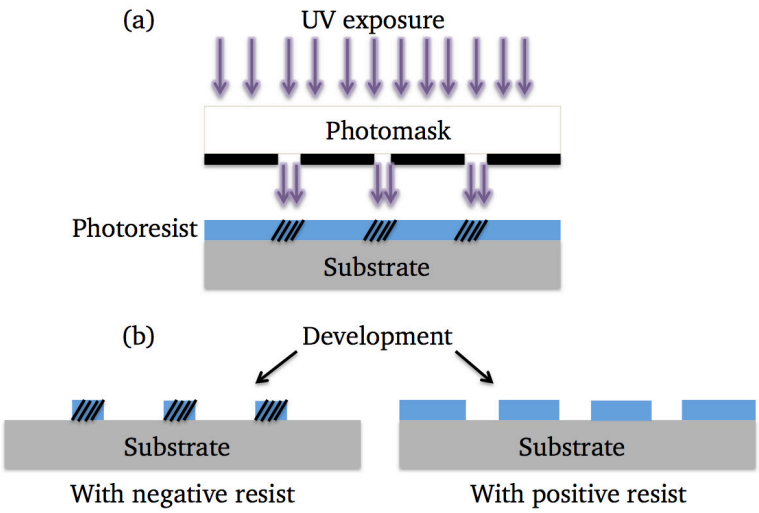

Figure 2.1. Schematic illustration of the main steps of photolithography with negative or positive photoresists. (a) exposure step: photoresist coated on the substrate is exposed to UV light, (b) development step: the exposed/unexposed photoresist is removed by immersion in a developer. The exposed area of the photoresist is removed by developer in the positive tone resist. The unexposed area of the resist is removed by developer using a negative tone resist.

The minimum feature size of conventional photolithography is limited by the diffraction of light. This means the resolution of the resulting pattern is limited by the wavelength of incident light, the ability of the lens to capture the light at wider angles (related to numerical aperture), and other equipment-related parameters.[14] Therefore, photolithography provides patterns with characteristic size around 1 μm practically, which is not suitable for nanofluidic studies. To beat the diffraction limit of light and produce nanometer resolutions, techniques such as EBL, FIB, and/or nanoimprint lithography have been developed.

2.1.2 Electron beam lithography (EBL)

Electron beam lithography creates nanoscale patterns by directly writing a pre-defined path with a focused beam of electrons on a surface covered with a thin film of electron-sensitive resist. The electron beam (e-beam) alters the resist solubility according to the energy of the emitted e-beam, and therefore, either the exposed or unexposed resist area are selectively removed by developing.[20] The purpose is to create small structures in the resist, which can be further transferred to the substrate by reactive ion etching (RIE) or other etching / deposition processes.

The development of EBL tools started in the late 1960s by modifying the design of scanning electron microscope (SEM). Therefore, a typical EBL system closely resembles a SEM. The main difference between a SEM and an EBL is that in an EBL, the beam is scanned

onto the sample according to the instructions coming from the pattern generator, while in a SEM, the beam is raster scanned over the sample in order to collect secondary electrons to form an image. As shown in Figure 2.2., an EBL schematically consists of a chamber, an electron gun, and a column. The column and the chamber are maintained in high vacuum by a set of pumps. The beam of electrons is focused and accelerated to the requested voltage, and deflected onto the substrate. The substrate is typically placed on a laser interferometric stage for accurate positioning. The maximum acceleration voltage or the energy of electrons is typically between 20 and 100 keV. This e-beam spot with a diameter as small as a couple of nanometers is scanned on the surface of the resist in a dot-by-dot fashion to generate patterns in sequence. The feature resolution is limited to critical dimensions of approximately 10 nm due to scattering in the resist. Gaussian beam tools can provide a better spatial resolution of below 5 nm.[21]

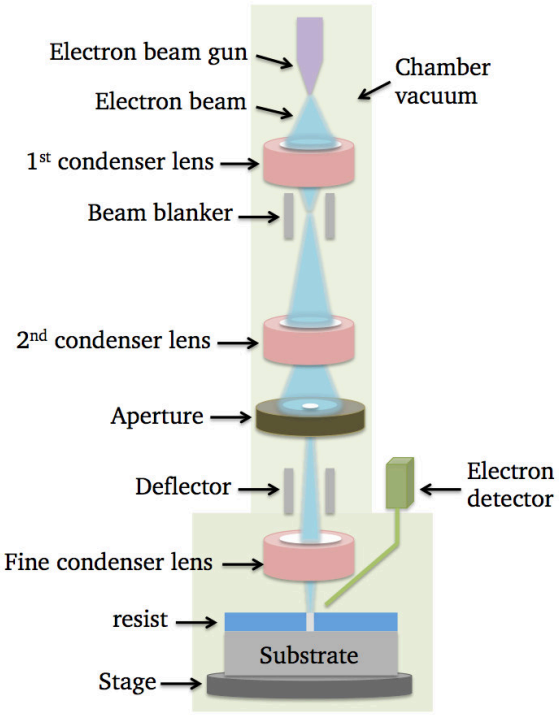

Figure 2.2. Schematic illustration of electron beam lithography, consisting of a vacuum chamber, an electron gun, a column with all the electron optics for focus, scan, and blanking / scanning modes of the electron beam. The e-beam is focused on a resist film to create a pattern by exposing in a dot-by-dot fashion.

EBL is often used for the fabrication of nanochannels. However, as mentioned before, this expensive and slow technique is not well-suited for serial exposure due to its intrinsically low speed.

2.1.3 Focused ion beam (FIB)

Unlike EBL, nanofabrication with FIB is capable of generating specific nanoscale patterns

directly on hard substrates without requiring any resists. FIB uses liquid metal ion source that has a high brightness and a very small emitting area. In the instrumentation of the FIB, a focused beam of ions (typically gallium ions, but can be gold, silicon or germanium) is used to micromachine and etch the structures[22, 23] on the samples, rather than a focused beam of electrons in EBL. The gallium source is heated up and the liquid gallium flows down and wets a sharp tungsten needle. When an extraction voltage is applied, the liquid gallium is pulled into an extremely sharp "Taylor-Gilbert" cone. The gallium (Ga^+) ions are extracted from the top of this cone by field emission. The balancing electrostatic potential produced by the extraction voltage and the liquid surface tension forces causes Ga^+ ions to accelerate through the column to reach ground potential.[24] The higher the acceleration voltage, the faster the ions are travelling as they exit the column. An acceleration voltage of 30 kV is usually used to obtain highest possible lateral resolution and sputtering yield. When the Ga^+ ion energy (acceleration voltage) is bigger than the surface binding energy, the surface atoms will be sputtered.[25-29] This means that the ions lose their energy to the electrons and atoms of the solid,[23, 30] and the elastic and inelastic scattering processes take place on the surface.[31] The inelastic processes generate photons and secondary electrons. The elastic scattering transfers kinetic energy from ions to the sample atoms.[32] When the incident ion reaches the surface, the sample atoms at the surface have enough energy to leave the surface and enter the surrounding vacuum. The atoms are either removed from the vacuum chamber by the pumping system (volatile decomposition product) or they are re-deposited on the surface (solid product).[31] The material removal process is so-called milling. Ion-beam milling selectively carves materials on surfaces at nanoscale precision. Milling of substrate surface is possible due to the heavy mass of ions as compared to that of the electrons. The sputtered material is either removed from the chamber or re-deposited on the surface.

Most FIB instruments are equipped with a combination of SEM and FIB columns, known as dual beam or cross beam, in which the electron beam is used for imaging and the ion beam is used for milling (Figure 2.3.). This allows precise monitoring of FIB operation through the SEM by using the slice-and-view technique. This strategy permits non-destructive imaging at higher magnification and with better resolution as well as more accurate control over the milling process.

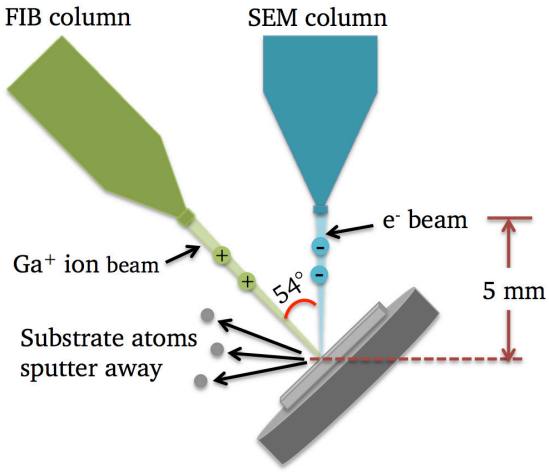

Figure 2.3. Schematic side view of a dual FIB/SEM columns system. The two beams are co-focused at the coincidence point, typically with a 5 mm working distance to the electron beam, which is the optimized position for the majority of operations taking place within the machine. The ion beam is tilted at an angle of 54° with respect to the electron beam. This allows SEM imaging and FIB sample modification without moving the sample.

Gallium is the most popular liquid metal ion source in FIB systems as it has a high surface tension, which is able to maintain stability of the liquid surface against the electric field. It also has a low vapor pressure, where only a few gallium atoms are thermally evaporated into the vacuum as neutrals. Its melting point is slightly above the room temperature, which simplifies the operations[33], makes it compatible with high vacuum and has a long lifetime (up to 1500 hours).

Besides the milling (etching) function of the FIB system, which is the main focus of this thesis for fabrication of nanochannels and 3D structures, deposition of films with precursor gases (similarly to chemical vapor deposition) is also possible. A thin layer of materials such as tungsten, platinum, carbon or insulators can be deposited on the substrates via ion beam.[28]

2.1.4 Nanoimprint lithography (NIL)

Although the traditional EBL and more recently developed FIB milling techniques have high resolution in generating nanoscale structures, both technologies have the disadvantages of low throughput and being expensive. In contrast, nanoimprint lithography is a parallel high throughput technique, which is capable of creating nanometer scale features in wafer scale at low cost.

NIL is based on direct mechanical deformation of the resist material, as a substitute to the use of photons or electrons to modify the chemical and physical properties of the resist like other lithographic approaches. Therefore, nanopatterning by NIL achieves resolutions beyond the limitations set by light diffraction or beam scattering.

NIL is a simple and quick technique to transfer the pattern of a stamp (mold) onto a moldable film on a substrate through mechanical contact.[34] Therefore, the imprint mold is typically fabricated with another nanolithography process (e.g., EBL, FIB, etc.) as a high resolution template, and then the replication of all patterns is conducted by NIL. The imprint molds are generally made by silicon or quartz because of their stiffness and process compatibility, and also to avoid a thermal expansion mismatch.[35]

Nanoimprint lithography can be a thermal imprinting[32] or curing a liquid resist by UV light at ambient. The latter is the replication technique in this work, and so, this technique is discussed in detail.

Ultraviolet nanoimprint lithography (UV-NIL)

A thin layer of imprint resist is first casted or spun onto the substrate. A hard UV-transparent mold with predefined micro- and nanoscale patterns is then brought into contact with the substrate and they are pressed together under a certain load (step 1). This photopolymerizable low-viscous liquid film is squeezed between the stamp and the sample substrate. Subsequently, the resist layer is cross-linked and solidified by the UV light (step 2). After the curing process, the hard mold is removed, leaving the reverse nanostructures on the resist layer (step 3) as shown in Figure 2.4. This process is performed at room temperature at a moderate pressure.[34] The molds or stamps are normally made in silicon, dielectric materials (e.g, silicon dioxide or silicon nitride), metals (e.g., nickel), or polymeric materials that have a sufficient Young modulus. The molds are hard and have a high mechanical strength.

In order to cure/solidify the liquid polymer with UV light, at least one side (stamp or substrate) should be transparent. No residual resist remaining in the contact area when the mold (stamp) is coated with a monolayer of an anti-sticking material.

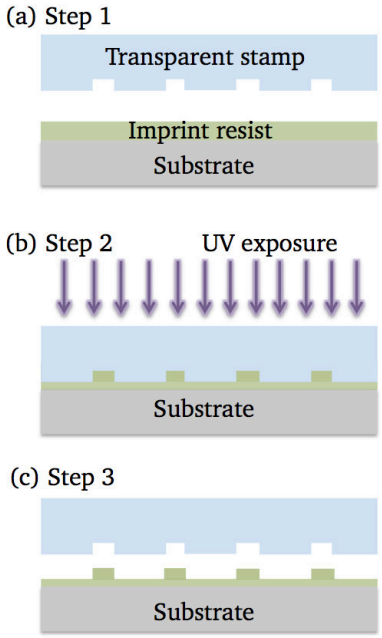

Figure 2.4. Schematic representation of ultraviolet nanoimprint lithography (UV-NIL) process. (a) step 1: coating; low-viscosity UV-curable monomer as a compliant polymer layer is casted onto substrate. The transparent stamp (mold) is brought into contact with the polymer film on the substrate. (b) step 2: imprinting and UV curing; the squeezed polymer is cured by crosslinking under UV light radiation which directly passes through the backside of the transparent mold. (c) Step 3: demolding; The transplant mold is released from the substrate. The rigid polymer on the substrate contains all the micro- and nanoscale structures of the mold.

2.2 Micro- and nanofluidics

A fluid is a substance (gas/liquid) which deforms continuously under an applied shear stress. Fluidics refers to handling of the liquids and/or gases. Fluid phenomena in micro- and nanofluidic systems can be driven by a variety of methods, such as applied pressure, electric or magnetic field.

2.2.1 Flow in the channels

A good example of LOC devices is the micro- and nanofluidics. Microfluidics are systems for manipulating fluids in channels with a cross section dimension of less than 100 micrometers. Nanofluids are suspensions of nanoparticles in a base fluid, which is typically water. Nanofluidics is the study of the behavior, manipulation, and motions of fluid flow that is confined to nanochannel structure of below 100 nm, at least in one of the dimensions (depth / width).[35, 36] Some researchers also use the term nanochannels to describe channels in the range of 100 nm to 1 μm.[36] Low reagent consumption (in the range of zeptoliter) is a big advantage in medical applications, chemical and materials synthesis, diagnostics for low-resource or remote settings, rapid processing and drug discovery. Confinement of the volume

in such small size for studying single-molecules results in low energy consumption, and alters the Brownian motions.[37] Brownian motion is the random movement of single molecules caused by the bombardment from other small molecules in the solution.

Our focus in this thesis is the utilization of nanofluidics for characterization of single-molecules and specifically stretching single molecules with potential applications for single-molecule sequencing and optical mapping of genomic length DNA molecules at high resolution in a quick manner.

2.2.2 Unique features of transport in the nanofluidics

The large surface-to-volume ratio in the nanofluidics results in capillarity-induced negative pressure in water and diffusion-limited reaction.[35] Capillary force originates from the adhesion between the liquid and the solid surface molecules, and the cohesion between the liquid molecules. In nanofluidic experiments, channels are usually filled by capillary action. Diffusion is the transport of particles from a higher concentration region to lower concentration by random motion. The diffusion is unwanted in the fluidic experiments.

There are generally three forces that have an influence on the transport of solvents through the nanochannels: the external driving forces (e.g., an electrical potential gradient or a pressure gradient), the colloidal forces (e.g., electrostatic, van der Waals and hydrophobic interactions), and the friction forces between the wall and the solvent molecules.[36] Several intermolecular forces are absent or negligible in microchannels, such as van der Waals forces (0.1–50 nm), and electrostatic forces (1–100 nm from the nanochannel wall).[35]

Van der Waals forces predominantly act at distances smaller than 2 nm and are always attractive. Electrostatic forces exist where an electrical double layer is created. This force can be repulsive or attractive and depends on the electrolyte concentration, and the nanochannel wall surface charges. This feature is discussed in detail in the following section.

Stronger intermolecular forces occur in smaller nanochannels.[35] However, the channel feature dimension should be in the range of biomolecules size, in order to selectively control the transport or elongate the DNA molecules[35] in a linearized state without folding back. As the feature size decreases, the process complexity increases and the choice of the fabrication approach as well as the production yield decrease. Nevertheless, with developed techniques such as EBL and FIB milling, confinement of individual molecules in nanochannels is possible.

Electric double layer (EDL)

We consider a nanochannel with ideally flat walls and without surface adsorption. When such a channel connects two reservoirs and an aqueous solution flows in the channel, a surface charge and a local electrostatic potential are created at the interface of the solution

and the wall.[36] As shown in Figure 2.5., the inner walls of the nanochannel are negatively charged (surface charge). If the walls of the channel have an electric charge, the surface of the channel will exert an electrostatic force.[35] The ions in the solution are adsorbed to the wall. These immobile counter-ions form a layer, which is called Stern layer. The mobile diffuse layer is where the ions and water molecules can freely diffuse. The combination of these two layers is termed the electric double layer. The EDL is formed as the result of attraction of ions of opposite charge to the surface charge. The thickness of an EDL is around a few tens of nanometers and is given by the Debye length (λ_D).[36] Usually the radius of the channel is much larger than the Debye length (about 1 – 20 nm depends on the concentration).

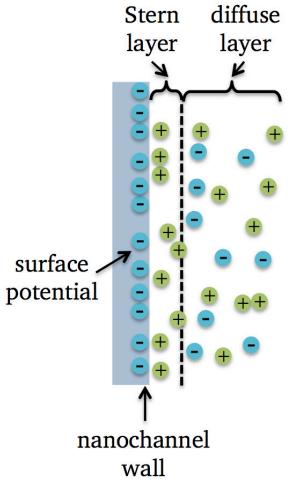

Figure 2.5. Schematic of an electrical double layer at a solid / liquid interface. The nanochannel wall has a net negative charge (surface potential), and the positive counter ions form an immobile Stern layer. The diffuse layer contains mobile ions. The strong electrostatic interaction between charged surface and the ions in the nanochannel form an electrical double layer. The positive and negative ions are represented as spheres.

Applying electric fields across these devices causes unbalanced ion flux, which results in ions being rapidly enriched at one end and depleted at the other end of the nanochannel.[36] This means that the co-ions (typically anions, as most device materials have negative surface charge) are excluded from the nanochannel and cations are transported through the nanochannel.[38] To keep the electrical neutrality in the channel, the number of cations at both ends is matched by the number of anions, which causes a salt concentration gradient in the diffusion boundary layers on both ends of the nanochannel.[36]

2.3 Deoxyribonucleic acid (DNA)

Genes carry biological information and DNA contains all the genetic information for cell functionality. *In vivo*, the DNA is located in the nucleus of eucaryotic cells. By cell division, this information must be accurately copied for transmission to the next generation. Many

genetic illnesses occur as a result of an incorrect replication of chromosome.[39, 40] If there is a mutation in the DNA, all the ribonucleic acid (RNA) coming from this part of the DNA will have the same defect, and so will all the proteins. As much as 98% of the human genome does not code for proteins, meaning that not all mutations are equally significant.[39] However, sometimes a mutation in the DNA can lead to irreversible problems and disease in a living body.

A DNA is a long-chain polymer molecule consists of two polynucleotide chains (strands). Polynucleotides are composed of simpler monomeric units called nucleotides. A nucleotide consists of a phosphate, a deoxyribose sugar, and a nitrogen base (Figure 2.6. (a)). The nucleotides are connected by phosphodiester bonds between the phosphate and sugars, leading to the formation of the "backbone".[41] The nucleotides are linked together covalently by phosphodiester bonds through the 3′-hydroxyl (-OH) group of one sugar and the 5′-phosphate (P) of the next.[41] The nucleotide backbone is composed of a five-carbon sugar (deoxyribose), which is attached to phosphate groups and a nitrogen-containing base.[41] The two DNA strands are in turn connected by hydrogen bonding between the nitrogen bases to create the double stranded helix, where A (adenine) base pairs with T (thymine) by forming two hydrogen bonds, and G (guanine) with C (cytosine), forming three bonds[41] (Figure 2.6. (c)). This *complementary base pairing* enables the base pairs to be packed in the energetically most favorable arrangement in a double helix,[41] where the two sugar-phosphate backbones wind around each other, with one complete turn every ten base pairs[41] (Figure 2.6. (d)). In principle, each strand of DNA contains a sequence of nucleotides that is exactly complementary to the nucleotide sequence of its partner strand. Therefore, each strand can act as a template, or mold, for the synthesis of a new complementary strand.[41] This feature is used in our technique to produce an optical map.

The way in which the nucleotide subunits are lined together gives a DNA strand a chemical polarity.[41] The polarity of one strand is oriented opposite to that of the other strand.[41]

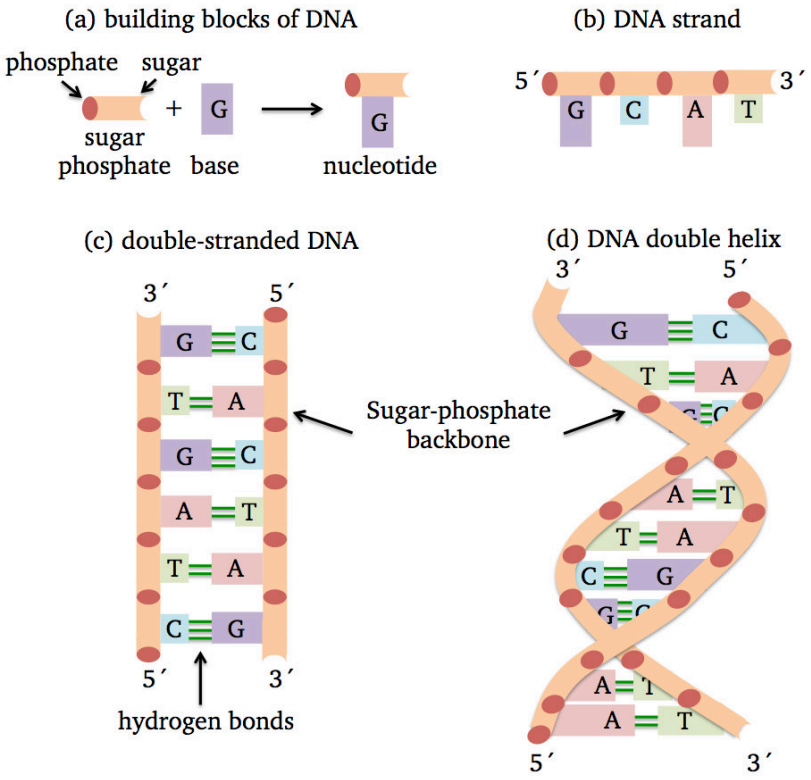

Figure 2.6. Schematic representation of a double stranded DNA and its building blocks. (a) a nucleotide contains a phosphate, a deoxyribose sugar, and a nitrogen base. (b) the sugar-phosphate backbone of DNA is linked to nitrogen-bases (A, C, G, and T) to form a strand. (c) a straighten DNA with complementary base pairing of A and T, G and C. The strands are held together by hydrogen bonds between the paired bases. Since AT base pairs are held together with two hydrogen bonds, and GC base pairs with three, it takes more energy (a higher temperature) to break a GC base pair apart. (d) helical arrangement of the two strands. The arrowheads at the ends of the DNA strands indicate the polarities of the two strands, which run antiparallel to each other in the DNA molecule. For simplicity, the schematic representation of straightened out DNA is used throughout this thesis.

Three different natural forms of DNA are known, namely A, B and Z. The most common helical form of the DNA within cells is the B form, which has an overall negative charge under physiological conditions. The DNA molecule is negatively charged due to the charges of electrons in the phosphate group.[42] This form of DNA displays a right-handed helix structure, with a twist angle of 36°, and a rise of 0.34 nm, per base pair (bp).[43] Its contour length is calculated by $L = Na$, where N is the number of base pairs, and a is the 0.34 nm distance between base pairs.

Double stranded DNA (dsDNA) does not have flexible bonds between individual monomers (units in a polymer) and is a better represented as a semi-flexible polymer (semi-rigid structure). This molecule is flexible on long length scales and stiff on short scales (curves smoothly as a result of thermal fluctuations). Consequently, it can be modeled using the "worm like chain" model that describes the DNA molecule as continuously flexible, as

illustrated in Figure 2.7. Despite its unusual high mechanical stiffness, this polymer molecule undergoes dramatic conformational changes in solution such as bending, twisting, and compression.[19, 44] The ability of DNA to change its three-dimensional structure is crucial for packing the extremely long molecule into chromosomes. However, the naturally folding properties of DNA structure can complicate mapping, sequencing, and other types of structural analysis.

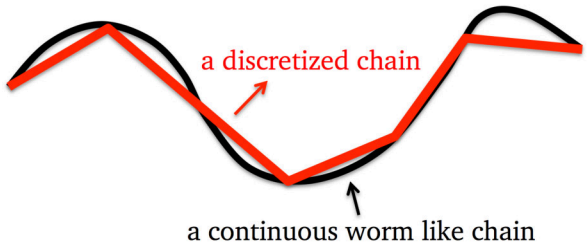

Figure 2.7. Discretization of a continuous worm like chain model of a DNA molecule, where it exhibits both local rigidity and long-range flexibility.

2.3.1 Confined DNA in the nanochannels

In this thesis, DNA molecules are confined and linearized using nanofluidics. Nanochannel confinement is a reproducible technique of DNA elongation,[25] with an application in DNA mapping experiments, such as restriction mapping, sequence specific fluorescent probes,[45, 46] or melting mapping.[47, 48]

Using the simplified model for a DNA chain in a nanochannel, the system can be described by four parameters:

(i) Persistence length P: is the bending stiffness and is roughly 50 nm[49, 50] in standard electrophoresis buffers.[51] It changes depending on the ionic strength of the experimental buffer[52] and increases with lower ionic strength[49, 53] due to intra-bead repulsion.[54] Staining with intercalating dye increases the persistence length.[43]

(ii) Effective chain width ω: The intrinsic physical width of the DNA double helix is approximately 2 nm,[50] but varies with ionic environment,[54] owing to electrostatic repulsion between DNA segments. It can be increased[52] at low salt concentrations.

(iii) Contour length L: end to end distance of the DNA when fully stretched, and calculated by multiplying the number of base pairs with their separation distance. The value depends on the number of base pairs in a specific DNA strand, usually calculated assuming 0.34 nm per base pair. For instance, the contour length of λ-DNA is approximately 16.3 μm.[55] Florescence labeling with intercalating dye increases the contour length.[52]

(iv) Dimension of the confining channel D: The nanochannel width / depth should be less than the radius of gyration of the molecule to elongate the molecule within the channel walls.

The elongation of DNA at high ionic concentrations does not significantly depend on the electrostatic interactions between the DNA and the nanochannel. However, electrostatic forces become more important when lowering the ionic strength of the solution. The extension of DNA in the nanochannels increases by reducing the ionic strength.[56] This is the result of the self-avoidance feature of DNA at low ionic strength.[56, 57] In addition, the repulsion from charged walls could lead to increase the stretching at low salt concentration.[26-28, 54, 58-60] As an example, the contour length of λ-DNA polymer, which is stretched within a nanochannel under low-ionic-strength conditions (0.05× and 0.01× TE) of Tris–EDTA is about 21.8 μm (in comparison to 16.3 µm).

Decreasing the salt concentration of the buffer has different advantages, but the molecules transportation by electrophoresis is more effective at a higher salt concentration.

A DNA molecule free in solution will coil in order to minimize its free energy. The size of the coiled DNA can be described by the radius of gyration (R_G), which is a measure of the root mean square distance of the segments to the center of the coil. Confinement restricts the DNA chain to reside within the confining geometry.[52]

In the classic Odijk regime, the channels have dimensions smaller than the persistence length (D < P).[61] Therefore, the DNA cannot coil up anymore and movement is restricted to only small undulations. Here, the effect of segments alignment by channel walls dominates, and all segments are strongly aligned and are unidirectional (Figure 2.8. (a)). When the bending energy is not strong enough to prohibit backfolding, the chain enters the backfolded Odijk regime (Figure 2.8. (b)). In the backfolded Odijk regime, all segments are aligned, but the segments are bidirectional because of backfolding. In the transition (partial alignment) regime, the segments close to walls are aligned, while segments further from the walls are randomly orientated (Figure 2.8. (c)). When the channel is wider, the chain gradually enters the coiled regime, where all segments can be considered as randomly orientated locally[52] (Figure 2.8. (d)). In the classic de Gennes regime, the channel dimensions are smaller than the radius of gyration, but still much larger than the persistence length ($P \ll D < R_G$), the DNA will be weakly confined and can be modeled as a series of non-interacting blobs with diameters similar to the cross section area.[62] In the coiled regime, the alignment effect is not significant locally, but it is significant on length scales larger than the channel size D (Figure 2.8. (e)). The coiled regime is separated into the classic and the extended de Gennes regimes due to the thermal energy. If the dimensions of the channels are larger than the radius of gyration ($R_G < D$), the DNA will act as when free in solution (Figure 2.8. (f)). These regimes are illustrated in Figure 2.8.

The de Gennes theory[43, 63] predicts the DNA extension r in the nanochannel with D in diameter as the following way:

$$r \cong L\left(\frac{\omega P}{D^2}\right)^{\frac{1}{3}} \qquad (1)$$

where P is the persistence length of the DNA molecule, ω is the effective chain width, L is the contour length of the DNA molecule, and D is the channel dimension.

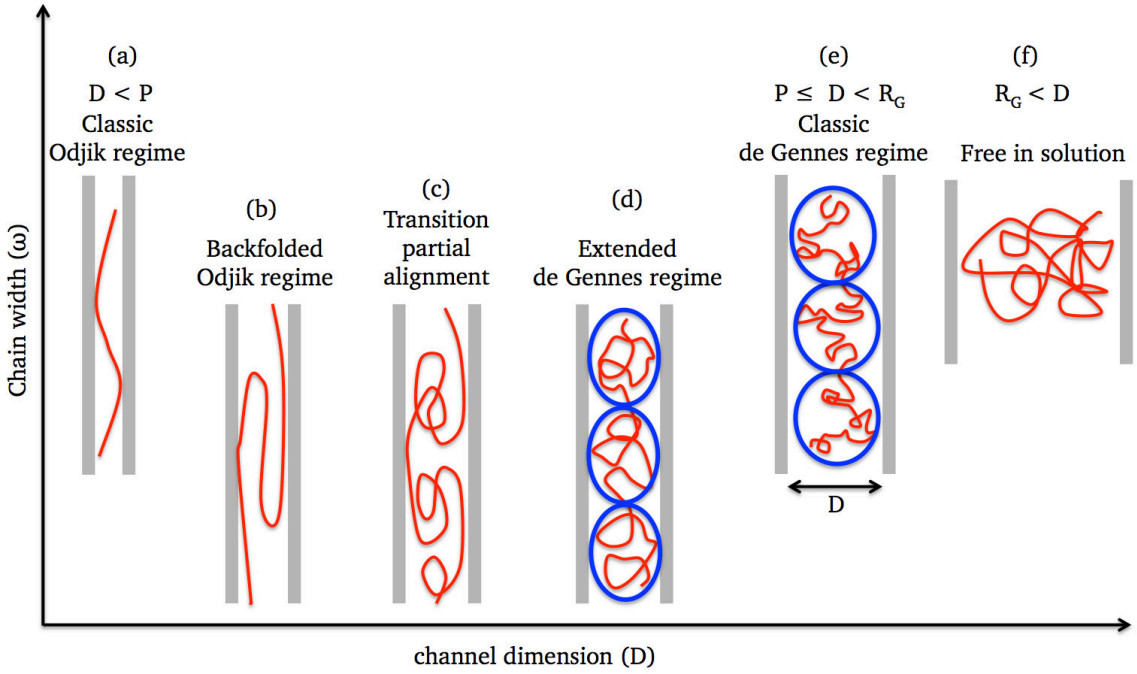

Figure 2.8. Illustration of different confinement regimes experienced by a long DNA molecule in a nanochannel when varying the channel size D and the chain width ω. The red curves indicate polymer chains (DNA), and the blue circles represent thermal blobs. R_G is the radius of gyration and P is the persistence length of the DNA molecule, while D is the average cross section of the confining environment. (a) the classic Odijk regime, where the channels dimensions is smaller than the persistence length. The DNA cannot coil up anymore and all segments are strongly aligned to the channel walls. (b) backfolded Odijk regime, where bending energy is not strong enough to prohibit backfolding. (c) transition is a crossover from the Odijk regimes to the de Gennes regimes, where the segments close to walls are aligned, while segments further from the walls are randomly orientated. (d) extended de Gennes regimes, where the segments are randomly orientated locally. (e) classic de Gennes regimes, where the channel dimensions are smaller than the radius of gyration, but still much larger than the persistence length. The DNA will be weakly confined. (f) free in solution, where the dimensions of the channels are larger than the radius of gyration and the molecule coiled up completely.

The possibility to increase the DNA elongation even in relatively large nanochannels by simply changing the surface charge and the ionic strength of the solution is useful for applications such as DNA mapping and barcoding, which require large elongation of

biomolecules during the analysis.[54] A lower concentration of ions in the solution will provide less shielding for the DNA from its own negatively charged backbone, increasing the stiffness, and thus increase the degree of extension.

2.3.2 DNA binding molecules

When studying DNA with fluorescence microscopy (Section 2.4), the DNA molecule is required to be stained with a dye in order to visualize them under the microscope. Cyanine dyes, such as YOYO, display favorable photophysical properties including high binding constants, high emission quantum yields (QY), and low background fluorescence.

The shape of the DNA double helix as it twists gives rise to small and large gaps, or minor and major 'grooves' that can accommodate various types of molecules.[14]

There are different binding modes with double-helical structure of DNA. Figure 2.9. shows four main ways that a ligand molecule can bind to the DNA: external binding, binding to the minor or major groove of the DNA helix, and intercalation between the DNA base pairs. External binding is facilitated by electrostatic interactions between a positively charged ligand and the negatively charged DNA backbone. Besides covalent binding, there are several classes of specific or unspecific non-covalent binding modes, such as intercalation between basepairs,[64] bis-intercalation,[65] minor groove binding,[66] and major groove binding.[67, 68] Some small molecules can sit in the gap between base pairs in what is known as an intercalating binding mode.[14] Intercalation is a process where a ligand inserts in the hydrophobic space in between the stacked DNA base pairs. It is a non-covalent stacking between adjacent basepairs via interaction with π-orbitals of these basepairs and often combined with hydrogen bonding.[64] Such binding ligands with no sequence specificity can change mechanical properties of the DNA strands. Intercalation extends and partially unwinds the DNA double strands, and affects the integrity of the DNA structure.[69]

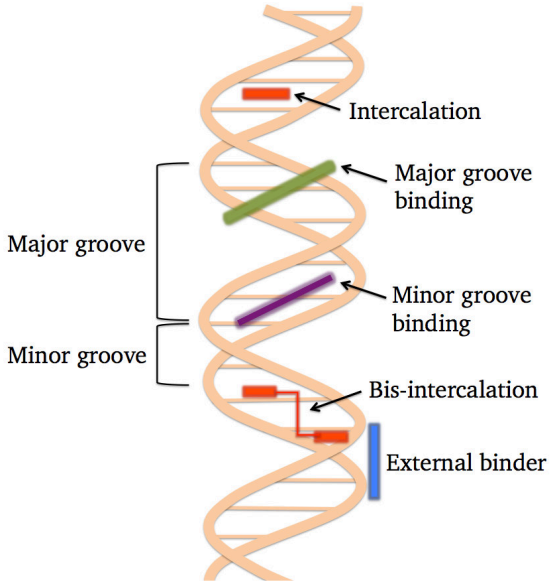

Figure 2.9. Schematic illustration of the four different binding modes to DNA molecule: major (green) and minor (purple) groove binding, external binding (blue) and intercalation (red). Minor groove binding mode is selective, such as binding of netropsin molecules which have a high affinity to AT-rich region of the DNA molecule. Intercalation is a non-covalent stacking between adjacent base pairs, with no sequence specificity. This binding mode extends and partially unwinds the DNA double strands. Upon binding of YOYO-1 bis-intercalation to DNA molecule, the contour and persistence lengths of the DNA molecule is extended. Electrostatic interactions between a positively charged ligand and the negatively charged DNA backbone allows for external binding. External binding to the DNA backbone has much lower binding affinities.

For the work presented in this thesis, three different DNA binding molecules, the bis-intercalating cyanine dye YOYO-1 and also TOTO-3, the AT-selective groove binder netropsin, and also external binding have been extensively used.

Rhodamine and the cyanines dyes are intercalators. Cyanines class of dyes has an additional interaction with the phosphate backbone of DNA.[70] Bis-interlacation is also observed for the TOTO and YOYO dimers, with the planar aromatic groups intercalating at different sites.[71] YOYO binds to DNA by inserting its two aromatic ring structures in between the base pairs. YOYO is practically non-fluorescent as a free molecule in solution, but it has extremely high affinity for nucleic acids. Therefore, once bound to double stranded DNA, fluorescence emission enhances more than 1000-fold, which makes YOYO ideal for high sensitivity epifluorescence measurements of single molecule studies. The maximum amount of YOYO bound to DNA, restricted by the nature of the binding mode, which is approximately one YOYO molecule every four base pairs. The binding of YOYO will also affect the structural properties of DNA. Upon binding of YOYO-1 bis-intercalation to DNA molecule, the contour (L) and persistence length (P) are increased by 30% at a saturating staining ratio of 1 dye molecule per 4 base pairs.

The persistence length increases due to a local mechanical increase in the double helix rigidity and also a reduction of the electrostatic interactions between segments of the negatively charged DNA backbone, due to the positive charge of YOYO-1. The positive charge of YOYO (two protonated amino and two protonated imino groups: +4) will reduce the average negative charge of DNA backbone.[54, 72] YOYO will alter the helical twist, unwinding the DNA helix by approximately 24 degrees. Overall, as changes in the properties are all less than an order of magnitude, the behavior of unstained DNA would be similar to the observed dynamics of the DNA/dye complex.

Netropsin is a non-fluorescent, natural antibiotic, which binds selectively to AT base pairs in the minor groove of the DNA helix. Netropsin has a site-specific binding which forms hydrogen bonds with adenine and thymine. The amino group in guanine hinders netropsin from forming hydrogen bonds to GC base pairs.

2.4 Fluorescence microscopy

It is almost impossible to discriminate biomolecules, for instance on the level of a cell, based on their natural photophysical contrast in optical microscopy. However, it is possible to artificially introduce contrast into the system by specifically labeling the sample using fluorescent dyes. Fluorophores are quite strong light sources. Fluorescent labeling (staining or tagging) increases a large contrast with a dark background, when excited using light (UV or visible).[14] Therefore, individual molecule detection is feasible for double-stranded DNA molecules by light microscopy methods.

Fluorescence microscopy is a light microcopy method which requires *fluorochromes* or *fluorophores*. Fluorophore absorbs light of a specific wavelength range, and re-emits it with lower energy (shifted to a longer wavelength).[14]

Some related fundamental concepts of emission of light and principles of a fluorescence are described in this section. The discussion is then coupled to a description of fluorescence microscope and its components as an imaging method in the thesis.

2.4.1 Principles of fluorescence

Fluorescence is the emitted light by an atom or molecule after absorption of electromagnetic energy (light).[73] Fluorescence arises usually from the transition of the excited species from its first excited electronic singlet level to its ground electronic level.[73] The excited state lifetime and the absorption time are in the sub-nano to nanosecond range.

When a photon is absorbed by a molecule, and its energy matches the energy gap between an electronically excited state of the molecule (S_n) and its ground state (S_0), the molecule raises to the excited state. After excitation to S_n, the molecule is rapidly relaxed to

the lowest vibrational energy of the first excited singlet state (S_1), via a combination of vibrational relaxation (non-radiative) and internal conversion (IC).[14] the relaxation of excited organic molecules can also happen via conversion to a triplet state, which may subsequently relax via phosphorescence, or by a secondary non-radiative relaxation step. A simplified Jablonski diagram illustrates the excitation and de-excitation processes of light-molecule interactions in Figure 2.10. Each electronic state is associated with a multitude of vibrational states. The wavelength of an emitted photon is longer than the excitation wavelength. The difference in wavelength and rapid relaxation from S_n to S_1 upon emission is called *Stokes shift*.[14]

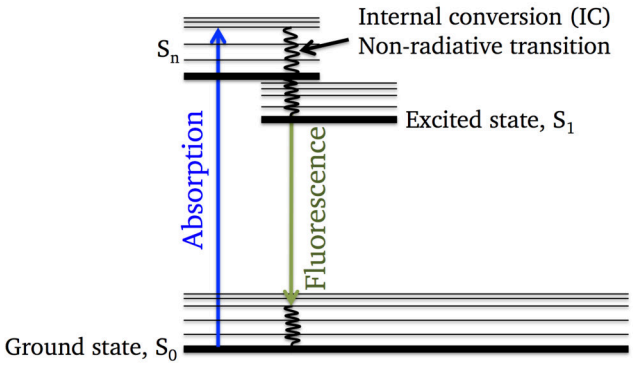

Figure 2.10. A simplified Jablonski diagram showing excitation and fluorescence emission of a fluorophore. Singlet (S_0, S_1 and S_n) states are shown with bold horizontal lines, with corresponding vibrational states as non-bold horizontal lines. Radiative processes, including absorption (blue), and fluorescence (green) are displayed as straight vertical arrows. The non-radiative processes internal conversion (IC) is shown as undulating arrows. After excitation to S_n, the molecule is rapidly relaxed to the lowest vibrational energy of the first excited singlet state (S_1) by internal conversion. The wavelength of an emitted photon is longer than the excitation wavelength.

Fluorescence emission from a single molecule usually occurs in a four step cycle: (1) electronic transition from the ground electronic state to an excited electronic state; (2) internal relaxation in the excited electronic state; (3) radiative or nonradiative decay from the excited state to the ground state as determined by the excited state lifetime; and (4) internal relaxation in the ground state.

2.4.2 Fluorophore

As mentioned, the molecules are required to be stained by fluorophores for visualization under fluorescence microscopes. The preferred properties of a fluorophore vary depending on the specific application. A large number of different dyes (fluorophores) with absorption from the UV to the near-infrared region are commercially available. Fluorophores can be small organic dyes, nanoparticles like semiconductor quantum dots, gold nanoparticles, or genetically encoded fluorescent proteins.[14] A suitable label should be sufficiently (photo)stable, conveniently excitable by the available light sources without producing

excessive fluorescence background, match the available excitation and detection equipment, and also be soluble in buffer solvents for biological applications.[14] The efficiency of the fluorescence emission is quantified by the fluorescence quantum yield. QY of a fluorophore is defined as the ratio between the number of emitted photons and the number of absorbed photons. The amount of emitted photons will depend on the ability of a molecule to absorb light, which is governed by the molar absorptivity (ε) at each wavelength. Thus, a bright fluorophore which has a high QY, and a high molar absorptivity is desirable. Furthermore, a distinct Stokes shift allows separation of excitation and emission more efficiently. For instance, the fluorophore YOYO, used in this thesis, has a QY of 0.52, molar absorptivity of 10^5 $M^{-1}cm^{-1}$ at 491 nm and an emission maximum at 509 nm, when bound to dsDNA.

There is always a small probability that fluorophores enter a long-lived state, and undergo a chemical reaction such as oxidation and become irreversibly nonfluorescent,[14] when fluorophores are illuminated, or while absorbing and re-emitting photons, or cycling between ground and higher singlet states. The loss of a dye's fluorescence (quenching) in a specimen is usually due to photo-oxidation, which is the oxidation of dye molecules in the presence of light.[14]

The other potential reason for the decrease in the signal is photobleaching of the fluorophore. Photobleaching or "fading" is an irreversible process of a gradual loss of fluorescence intensity of the specimen arising from interaction between the exciting light and the fluorescent compound. In this process, the fluorescence dye molecules are photochemically destroyed. As this loss of functional dyes occurs during the observation, photobleaching interferes with the collection of high-quality image data. Optimization of image recording parameters, especially the intensity of exciting light, can dramatically reduce the adverse effects of photobleaching. Photostability is the resistance to photobleaching, that is the ratio of the number of photobleached molecules to the total number of absorbed photons during the same time interval. Quantum dots are photostable but fluorescent dyes might have a limited stability, which means they photobleach, and then may produce phototoxic substances.[14] Phototoxicity and photobleaching can be minimized by reducing the excitation power and also by removing oxygen form the solution. Under favorable conditions, individual molecules can emit an average of 10^5–10^6 fluorescence photons before photobleaching.[14, 74]

The DNA flow measurements in this thesis are conducted in real time as the molecules pass through the nanochannels, and thus photobleaching is not an issue.

2.4.3 Main components of fluorescence microscope

Fluorescence microscopy utilizes emission of light to visualize a substrate. A fluorescence microscope allows excitation of fluorescence, subsequent separation of the relatively weak

emission from the strong exciting light, and the detection of the emitted fluorescence.

An epifluorescence microscope enables studies of live cells or DNA molecules in medium solution. With highly sensitive light detectors and cameras, detection and observation of single molecules behavior, such as blinking of quantum dots or the dynamics of individual DNA molecules is possible.

The main components of a fluorescence microscope include: an excitation light source, excitation and emission filters, an objective to focus the light onto the sample, as well as a detector to record the emitted photons. The light source can either be monochromatic, or contain a broad spectrum of wavelengths. A filter cube contains three components of excitation/emission filters as well as dichroic mirror, which can be changed in order to match the maximum excitation and emission wavelengths of the selected fluorophore. An efficient separation of the exciting wavelength and fluorescence emission bands by the filters is mandatory for a high image contrast (Figure 2.11). The light is sent through the excitation filter. The transmitted light is reflected on a dichroic mirror, which is positioned at 45° angle toward the incoming light, and focused through an objective before reaching the sample. The fluorophore of interest is excited by an excitation light source lamp, and emits at longer wavelength. The fluorescence is emitted in all directions, but only a selected light cone, which is a fraction of this fluorescence, is collected by the objective lens. The backscattered fluorescence emission is then collected through the same objective and transmitted through the dichroic mirror. The dichroic mirror reflects photons of a selected wavelength but allows the light of longer wavelengths to pass through the emission filter. The emitted light is detected via a sensitive camera, an electron multiplying charged coupled device (EMCCD). The principle of a filter cube in an inverted fluorescence microscope is sketched.

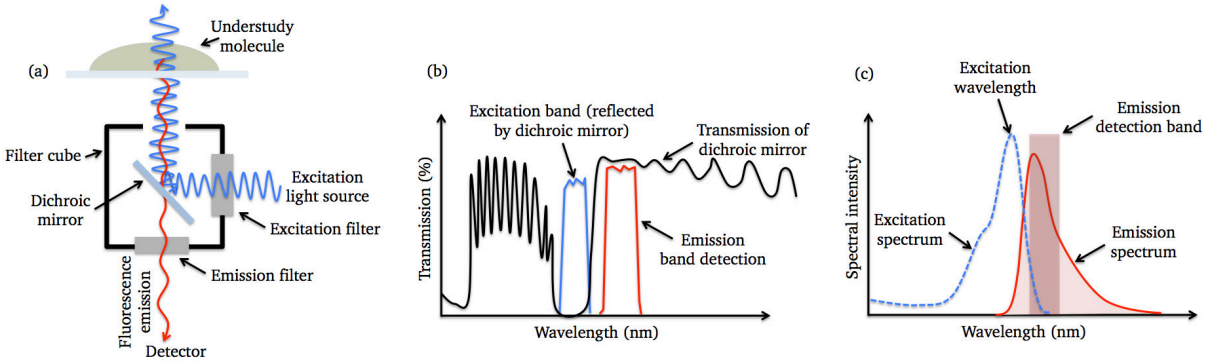

Figure 2.11. Schematic representation of a fluorescence microscope filter cube. (a) a filter cube containing an excitation filter, a dichroic mirror, and an emission filter. The exciting light is reflected by the dichroic mirror toward the specimen; the fluorescence emission, with a longer wavelength than the exciting light, is transmitted by a dichroic mirror toward the light detector. (b) a diagram of excitation and emission bands as well as transmission by dichroic mirror in a filter cube set. The excitation and emission filters are usually combined with a dichroic mirror, in such a way to reflect the excitation light and transmit the emitted light. (c) Schematic of spectral properties of a fluorophore. Emission wavelength is longer than excitation in fluorophores. An efficient separation of the exciting wavelength and fluorescence emission bands by filters is crucial for a high image contrast.

Sources of exciting light

A typical fluorescence microscope contains two sources of light. One, usually a halogen lamp, which is used for initial viewing of a specimen in a transmitted light mode or bright field illumination. The emission of photons occurs through the heating of a tungsten filament. The specimen is placed between the light source and the objective lens. The sample is illuminated and the diffracted light is collected by the objective lens.

Another and more important light source for fluorescence microscopy is often a mercury arc lamp, which is used for exciting fluorescence. A high-pressure mercury vapor arc-discharge lamp is a popular source of exciting light. Other sources of light can be Xenon or metal halide lamps.

Detection by electron multiplying charge-coupled device (EMCCD)

The weak fluorescence signal is detected with an EMCCD camera. A fast continuous read out at very low noise, high quantum efficiency, and high digital resolution are the features of this camera. An EMCCD camera uses an on-chip electron amplification before the fast read out, and it provides a low noise gain before the charge-to-voltage conversion. It offers sufficient sensitivity to detect single photons and observe single molecule behavior.

2.4.4 Optical resolution

It was believed that light travels in straight lines (rays). But, in the sixteenth century, it was discovered that light can "bend" around sharp edges (diffraction). This returns to the wave properties of light.[14] Since then, light is known for its wave and particle duality. Considering the wave nature of light, the origin of the limited microscopic resolution and image contrast can be explained.[14] The diffraction limit of light is defined by Abbe. The Abbe formula describes the parameters that influence the optical resolution in the plane of the specimen[14] in images with a negligible noise. The resolution refers to the level of detail that can be recognized in an image, such as small structures or the distance between closely neighbored small objects (Figure 2.12. (a)). This condition is named the "Rayleigh criterion". The Rayleigh criterion gives a minimum distance for which two light sources can be optically resolved.[75] The optical resolution, according to the Rayleigh criterion d_R, is therefore

$$d_R = \frac{0.61\lambda}{NA}, NA = n \sin \propto \qquad (2)^{14}$$

Where λ is the wavelength of illuminating light and *NA* is the numerical aperture of the optical system,[75] n is the refractive index of the medium between the lens and the object, and α is the maximum angle, in which an objective lens collects the emitted light.

Utilization of high NA objectives and immersion media with higher refractive indices such as water, or oil in combination with suitable objectives enhances the resolution further.[14] Biological samples which are often observed in an aqueous buffer solution, a water or oil immersion lenses are used, for which the refractive index of water is n_w=1.33[14] and n_{oil}=1.518.

The term d_R represents the center-to-center distance between two markers. The fluorophores are optically resolvable if d_R is greater than the radius of the marker's Airy disk[75] (Figure 2.12. (a)). Visible light is not a good candidate to resolve the two active neighboring labeled samples with fluorescent markers. Therefore, a shorter wavelength – ultraviolet (UV) or blue – provide a better resolution compared to long wavelengths, such as red or infrared. Each molecule produces a diffraction-limited signal, which is a bright circle of a diameter not smaller than approximately 250 nm in the plane of the specimen.[14] Using light microscopy, objects can be discriminated from each other when they are positioned at a distance of minimally about 250 nm from each other in the best configuration.[14]

In fluorescence microscopy, image noise is usually relatively high, while the signals are low and continue to decrease owing to photobleaching. In fact, under such conditions, it is the noise level that becomes the decisive factor defining spatial resolution (Figure 2.12 (b)).

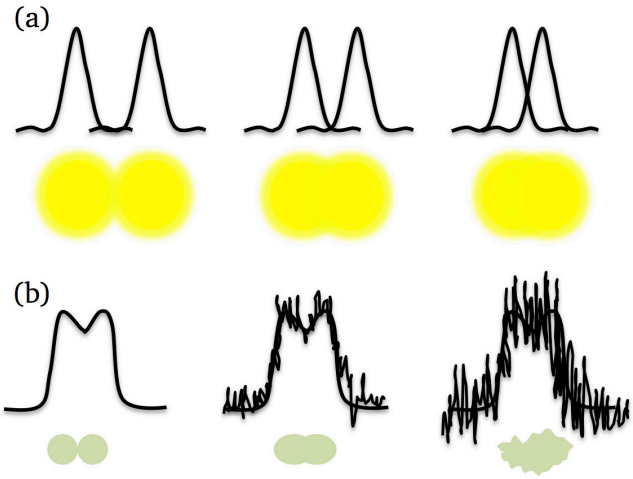

Figure 2.12. (a) The Rayleigh criterion - overlap of Airy functions defines the resolution. In order for two peaks to be resolved, they must be further apart than d_R. Left: the Airy disks do not overlap. Middle: the disks overlap slightly, but the peaks are separated by a distance greater than d_R; Right: the disks overlap and the peaks are separated by a distance smaller than d_R and are not resolvable. (b) signal-to-noise ratio affects the resolution. Two fluorescence signals that can be visually resolved when the signal-to-noise ratio is high in the Left diagram, but become visually unresolvable when the signal is weak in the Middle diagram, and comparable with the level of noise in the image Right diagram.

Therefore, two fluorophores should not be very close together, in order to be resolvable. We considered this issue in designing the fluorophores in the optical mapping.

2.4.5 Avalanche photodiode (APD)

An APD is a signal-amplifying device that uses the inner photoelectric effect. This photodiode is a semiconductor p–n (or p–i–n) junction. When a photon of sufficient energy hits the diode, it excites an electron, resulting in a free electron (and a positively charged electron hole). This, in turn, creates a flow of electrons (an avalanche) between the anode and the cathode. Accelerated electrons in the electric field collide with atoms in the crystalline silicone and induce more electron–hole pairs. Single-photon avalanche photodiodes are currently used as detectors in fluorescence lifetime imaging microscopy.

2.5 Optical DNA mapping

Next Generation Sequencing (NGS) is a technique for sequencing of the DNA molecules, which was developed after Sanger sequencing (First Generation Sequencing). NGS aims at increasing the sequencing speed and decreasing the cost, by performing parallel sequencing of short DNA fragments. To increase the sequencing speed, DNA molecules are fragmented into shorter strands (around 1000 base pairs). Then these short fragments are sequenced and afterwards stitched together. Assembling these fragments can form the overall sequence of the

genome. However, to avoid errors and to get the correct stitching of the different fragments, the same position (or fragment) might be read several times. Therefore, assembling and stitching of the small fragments in case of large-scale repetitions in the genome become very complicated; time consuming, and even contains errors.

Optical DNA mapping, pioneered by Schwartz,[76] has proven to be a versatile tool for extracting long range sequence information on individual DNA molecules at the kilo basepair (kbp) level (resolution).[9, 77] Optical mapping was first developed utilizing restriction enzymes, in which DNA clones are digested into smaller fragments using restriction enzymes, and the DNA molecules are cleaved at sequence-specific sites. The size of the resulting DNA fragments is then determined by gel electrophoresis.

In the modern techniques, the DNA molecules are not fragmented. Thus, reassembling of short fragments is not required, and the large scale information is not lost. Although optical mapping does not provide base pair resolution (due to optical light diffraction), it is capable of giving an overview of long strands DNA molecules that even modern NGS is not able to provide. In optical mapping, only specific sites of the long genome, known to encode for certain diseases, are inspected. Using optical mapping is only preferential, where verifying the existence of a specific genetic mutation is required. This means optical mapping of DNA cannot be used as a substitute for next generation sequencing, but as a complementary method, where optical mapping provides the big picture, and NGS contributes the resolution. A combination of these two techniques can potentially solve the problem regarding loss of large scale repetitions. This therefore, provides a faster, cheaper and longer range of information from an individual genome while avoiding averaging.

In general, optical maps of DNA are obtained by labeling the DNA in a sequence specific manner, elongating the molecules, and imaging them using a fluorescence microscope. The process of creating a barcode, stretching and detecting the maps are discussed in the following. The strategies for labeling and stretching of DNA molecules depend on applications, the imaging set up and the available techniques.

2.5.1 Creating a barcode

Particular sequences of interest are marked (barcoded) along the DNA length. These sequences can be viewed as genetic ‘barcodes’ that are embedded in all DNA molecules of the sample for identification of mutation. Labeling strategies can be divided into two main categories: enzyme based labeling, and affinity based labeling.

Enzyme based labeling methods include nick labeling, and Methyltransferase based labeling. In nick labeling, a nicking enzyme creates a single strand break (4 – 7 bp long) at its recognition site (a nick). Then, a new fluorescently labeled nucleotide is incorporated in that

location, in a DNA polymerase process. In methyltransferase based labeling, a fluorescently labeled methyl group is transferred to the DNA at a specific recognition site.

Affinity based methods are another barcoding technique, such as denaturation mapping, and labeling via competitive binding between the AT specific, or CG specific, using netropsin or actinomycin, accordingly. To create barcodes in the denaturation mapping method, the lower melting temperature of AT base pairs compared to CG base pairs is taken into the account. Stained DNA with intercalating fluorescent dye is melted by increasing the temperature carefully. Therefore, the broken AT regions bonds release their intercalating dyes, knowing the dyes prefers double stranded DNA over single stranded DNA. Thus, the sequences containing CG keep their fluorescent dyes and stay bright, while the AT region become dark, creating a bright and dark barcode.

A new labeling method is developed during this work with hybridization of fluorescent dyes attached to short probes whose sequence is complementary to the DNA molecules repeat units. Therefore, a unique barcode is created over the long DNA molecule. This new DNA sequence-specific fluorescent labeling technique is discussed in details in Chapter 4.

2.5.2 Linearization of barcoded-DNA molecules

Genetic information is stored along the length of DNA, but is difficult to “read out”, because of extensive folding. DNA stretching facilitates access to the barcodes for optical DNA mapping, in order to determine the positions (locations) of those barcoded sequences along the entire long DNA molecules.

Main techniques for extending DNA include molecular combing,[78, 79] where an immobilized DNA molecule is anchored and stretched on modified (silanized) glass surfaces, or using nanofluidic devices,[37] in which DNA is extended by the hydrodynamic forces exerted on the molecule by a moving meniscus. Since the molecular combing technique suffers from inhomogeneous stretching due to surface interactions, the latter technique which is flowing linearized and uniformly stretched fluorescent DNA molecules through nanochannels is a compelling alternative for mapping.

Our technique is based on fluorescent mapping in fluidic channels using lab-on-a-chip micro- and nanofluidic devices. Nanofluidic channels improve the consistency of DNA stretching and parallelism of several channels increases the throughput. These higher reliability reads of long single molecules eliminate the amplification of DNA short fragments.

2.5.3 Detection of optical maps

The direct reading of genomic maps with fluorescence microcopy is facilitated after linearization and extension of single barcoded-DNA molecules. The fluorescence of binding

sites and barcodes are excited, and their emissions are detected in the nanofluidic system. The signals are visualized (mapped) to prove the existence of specific sequences along the single molecules, as depicted in Figure 2.13.

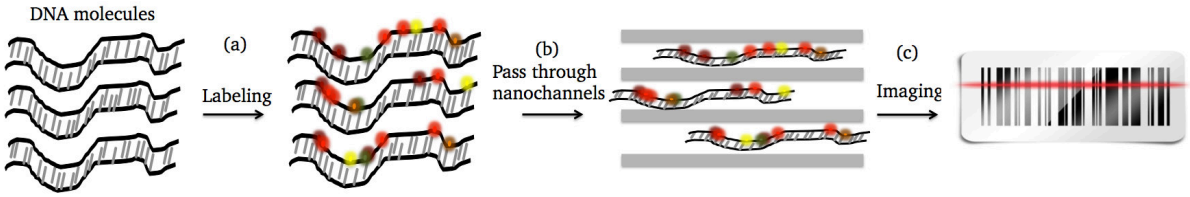

Figure. 2.13. Creating an optical map in 3 steps of barcoding the molecules, stretching and visualizing them. (a) creation of barcodes at specific sequences along the single DNA molecules. (b) linearization of the confined barcoded-DNA in nanochannels. (c) detection of the emitted fluorescence signal using a fluorescent microscopy and analysis to visualize the DNA barcode.

Chapter 3:

Device Fabrication

The ultimate goal of the lab-on-a-chip technology is to fabricate entire laboratory-scale analysis workflows onto a single compact chip with the capability of sample-in/answer-out for characterization of small test volumes. LOC devices are especially powerful candidates for the isolation of single-molecules, and on-chip analysis with the minimum user interaction, except for initialization.

The objective of this chapter is to establish a robust method for fabricating lab-on-a-chip micro- and nanofluidic devices that effectively and reproducibly confine genomic DNA.

To fabricate these micro- and nanofluidic devices, first a silicon master stamp is fabricated. The quality of silicon stamp structures has a large impact on the final device structures. In this thesis, microfluidic channels are patterned in a silicon stamp using standard photolithography and well-defined etching in the vertical direction. A large microchannels width is advantageous, because it yields a high flow rate, which results in ease of operation and guiding the molecules into the nano-region area. Large circular reservoirs are connected to the microchannels as liquid inputs. As described in Chapter 2, nanoconfinement-based DNA linearization requires the channels with dimensions on the nanoscale. The nanofluidic channels of the silicon stamp are fabricated either by EBL and RIE, or using direct FIB milling. For high throughput analysis, an array of parallel nanochannels is arranged perpendicular to the microchannels. E-beam lithography and RIE techniques provide square/rectangular cross-sectional profiles, while focused ion beam milling patterns V-shape channels. Very smooth squared nanochannels are considered to be better candidates for flow measurements of DNA molecules.

Fabrication of each device using FIB or EBL is, however, expensive and time-consuming,[35] especially when specifications such as different depths or 3D tapered transient inlets are required. Nanoimprint lithography, on the other hand, allows for affordable mass-production of polymeric devices, as it can be easily scaled-up to wafer scale[80-82] or parallelized. Therefore, we propose a smart combination of direct milling by FIB or EBL for high-resolution prototyping of silicon master stamps, and UV-NIL for cost-effective high throughput device fabrication.[83] This combination leads to a fast and simple “nano-sculpturing” of multilevel, multidimensional lab-on-a-chip devices for biomedical applications.

The fabrication process in this thesis is based on a duplication imprinting process as schematized in Figure 3.1. First, a silicon master stamp is fabricated by photolithography complemented by FIB or EBL. Then, a negative replica is made by UV-nanoimprint lithography as depicted in Figure 3.1. (a – c). Therefore, all micro- and nanofeatures of the silicon stamp are transferred onto the polymeric copy at once. Afterwards, this negative glass stamp is used as a working stamp to imprint the fluidic devices again by UV- NIL Figure 3.1. (d – f). This step (d – f) is repeated each time for the fabrication of micro- and nanofluidic circuitry in one single step, only in 2 minutes, prior to flow analysis. In this method, no

etching or lift-off process is needed after demolding.

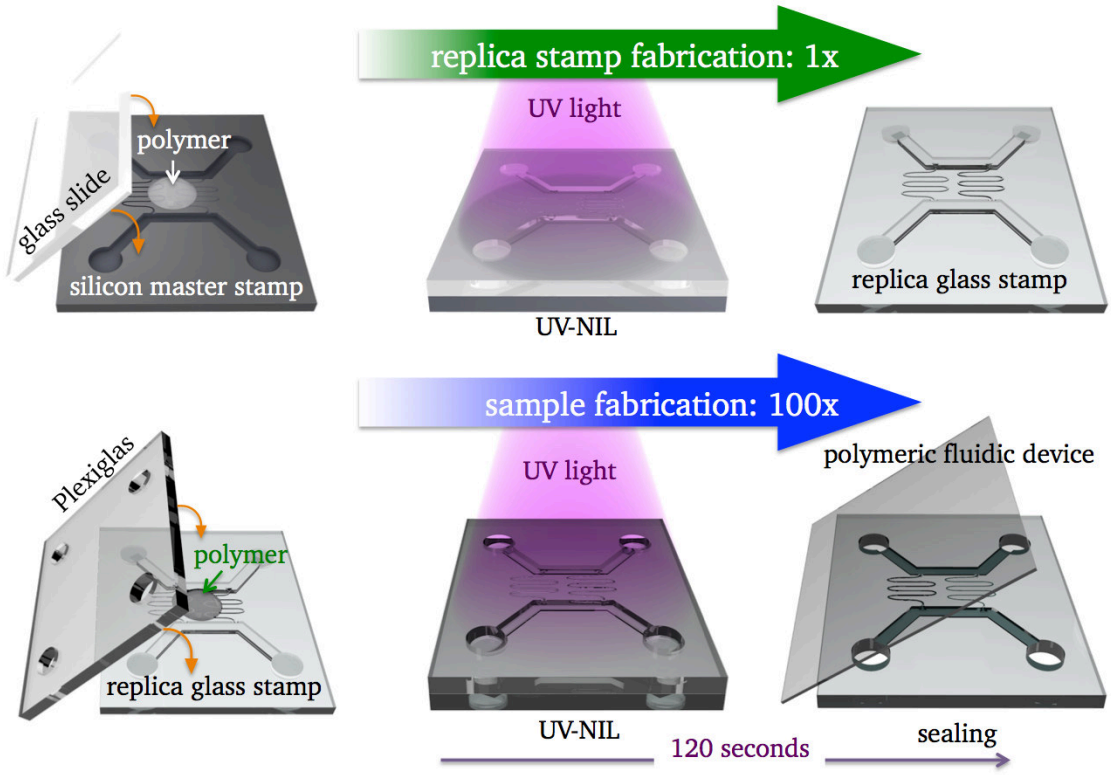

Figure 3.1. The complete micro- and nanofluidic system fabrication, from a silicon stamp to the final polymeric device by ultraviolet nanoimprint lithography (UV-NIL). (a – c) stamp fabrication: first a silicon master stamp is fabricated by photolithography, and EBL or FIB. A negative glass stamp with inverse shape of the silicon stamp is then fabricated by casting and curing of a polymer by UV-NIL. (d – f) sample fabrication: the same UV-NIL process is conducted on the glass stamp to fabricate a sample (polymeric device) for flow measurements. All pattern structures of the glass stamp are transferred to the sample. After separation of the glass stamp from the sample, the fluidic device is sealed on the top surface using a thin coverslip. The molds can be used again, and will produce an exact replica.

During this project several designs of nanochannels and inlet structures by means of EBL and FIB were fabricated and optimized. Different applications require different nanochannel configurations. For instance, nanochannels with V-shaped or triangular cross section confine nanoparticles more effectively, due to the higher particle-wall interaction, whereas the flow of DNA molecules is better in square/rectangular cross-sectional nanochannels. The V-shape of nanochannels is due to the Gaussian profile of the ion beam during the milling process.

Using EBL, silicon masters with nanochannels of short and long (5 μm to 158 μm), narrow and wide (50 nm to 300 nm), with depth of 80 nm to 100 nm are fabricated. Using FIB, linear and meander nanochannels with different width (120 nm to 300 nm) and depth (up to 410 nm), as well as 3D tapered inlets at the entrance of nanochannels were fabricated. Various types of inlets were studied to differentiate the flow and elongation characteristics in

Section 3.1.2. Finally in section 3.4., we proposed a configuration of bowties nanoantenna adjacent to the nanochannels, which allows for a highly enhanced localized electromagnetic field, concentrated in the nanochannels. This allows for a better control on the light-molecule interactions in the single-molecule range, overcoming the diffraction limit of light in the optical microscopic techniques.

The fabricated polymeric device in this chapter is used to study DNA translocation events during electrophoresis experiments, which will be described in chapter 4.

3.1 Silicon master stamp

The stamp fabrication is the most important process, as all its structures are replicated in the final device with the same quality. The stamps which were used in this thesis contain microfluidic as well as nanofluidic parts. The 20 μm wide and 1 μm deep microfluidic channels in all stamps are fabricated by photolithography and dry etching. However, the critical part of the stamp is the nanofluidic channels, as they are used to confine the molecules and elongate the DNA. We used EBL writing and direct FIB milling to pattern the nanochannels. The fabrication of nanochannels with different depths by e-beam lithography requires several steps, including alignment, exposure, development, etching, and resist stripping for each desired set of nanochannel depth or profile. In contrast, FIB allows for a straightforward, flexible prototyping, by fabricating new complex stamps with versatile structures and depths in a quick manner.

Using EBL or FIB, all silicon master stamps (mold) are fabricated in two steps: using EBL, the nanochannels are fabricated first and then the microchannels are aligned to the nanochannels. This is vice versa using FIB system. In all stamps, the microchannels are made by conventional photolithography. At the end, all stamps are coated with a monolayer of fluorosilane for an easy release, without damage.

One of the unique properties of stamps with FIB milled nanochannels is that they contain 3D transient inlets at the entrance of the nanochannels, which is fabricated in the same step as the nanochannels. This facilitates the flow and particularly pre-stretches the DNA molecules before entering the nanochannels. Patterning 3D funnel like with neck dimension is not easy with EBL, as the process of spin coating, exposure, developing and etching is required to be repeated several times, and the result is rather step like inlet than a smooth profile.

3.1.1 Fabrication of alignment marks and microchannels

The fabrication of nanofluidics using EBL requires alignment marks. This facilitates finding a suitable position for e-beam writing of the nanochannels, or optimizing the focus and astigmatism of the beam close to the area of exposing. This step can be avoided in FIB

milled nanochannels with the purpose of time efficiency. Since alignment marks and the microchannels are fabricated using photolithography, we patterned one photolithography mask containing both designs.

Photomask design

Alignment marks and microchannel patterns are drawn and generated in a computer aided design (CAD) program, as illustrated in Figure 3.2.

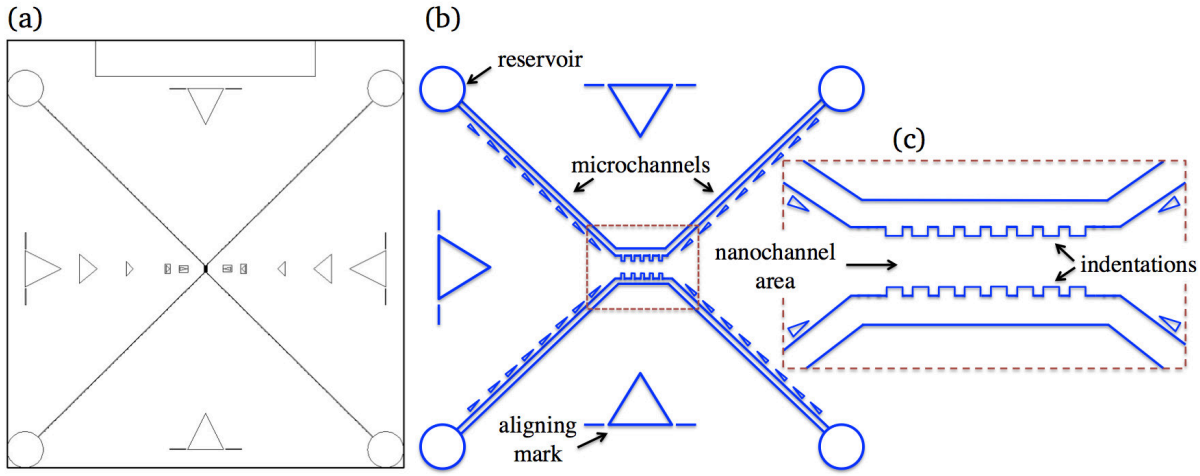

Figure 3.2. Alignment marks, the V-shaped microchannel structures, and the reservoirs. (a) two-dimensional CAD design layout of the alignment marks and V-shaped microchannels. (b) schematic overview of alignment marks and microchannel structures, with arrows along the channel to facilitate the guidance under a microscope for easy tracking of the nanochannels. Indentations, as shown in the inset (c), are designed at the entrance of the nanochannels to facilitate a smoother flow from microchannels to the nanochannels. The center-to-center distance between two neighboring reservoirs is 1 cm.

An opaque chromium layer is deposited on a UV transparent glass plate. A positive tone photoresist (Microposit S1813, Shiply Ltd.) is spun on the chromium at 3000 rpm for 1 minute. Then, it is baked at 90°C for 2 minutes on a hot plate. To pattern the mask, a laser writer (Heidelberg DWL 66+, Heidelberg Instruments Mikrotechnik GmbH) with a controllable laser beam (λ = 405 nm) is used. The resist is developed using MIF-319 (metal-ion-free, Shiply Ltd.) for 45 seconds and the process is immediately stopped by rinsing with deionized water (DI-water), and dried with purified nitrogen. Then, the chromium in the resist-free area is etched in a chromium etch solution (10% Veric ammonium nitrate, 4.25% perchlorid acid, 84.95% H_2O, MicroChemicals GmbH) for 50 seconds. The etched areas are UV transparent. Figure 3.3. illustrates the resulted photomask.

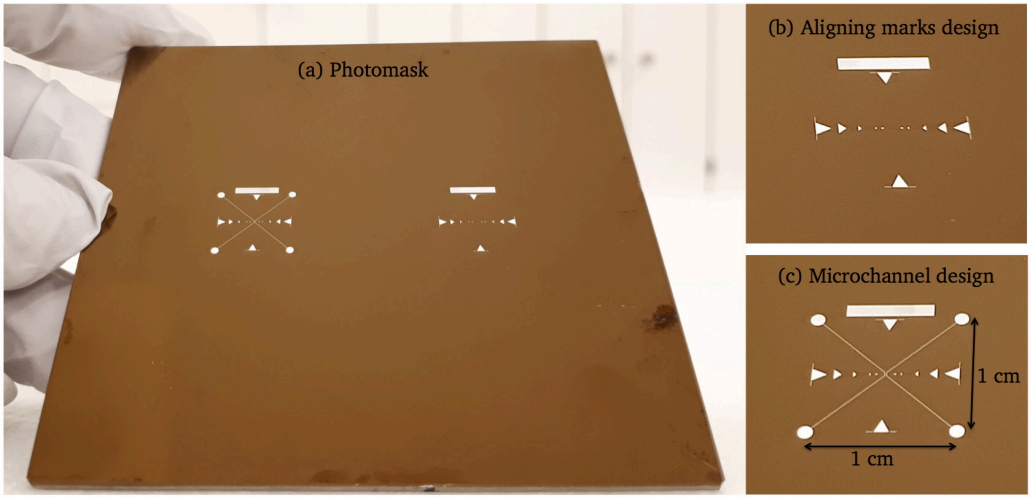

Figure 3.3. The photolithography mask with alignment marks, V-shaped microchannels and the reservoirs. (a) The CAD design in Figure 3.2 is transferred onto a chromium mask using a laser writer. (b) the alignment marks. (c) the microchannels, alignment marks, and the reservoirs. In the stamps with EBL nanochannels, the alignment marks are patterned on the silicon stamp, which is used as the guidance for e-beam exposing area. In the FIB direct milling, no alignment mark is required. The microchannels are aligned to the nanochannels after EBL.

Photolithography of alignment marks

The alignment marks are patterned using photolithography and metal deposition. These alignment marks assist the EBL process for fine optimization of focusing and astigmatism as well as the alignment of the nanochannels with the microchannels. The silicon wafer {100} is spun with the photosensitive chemical AR 300-80 at 4000 rpm for 1 minute, following a 1-minute bake step at 100°C. This layer is served as the adhesion layer. After cooling down, the photoresist S1813 is spun over the silicon wafer at 3000 rpm for 1 minute. Then, the silicon wafer is baked for 2 minutes at 90°C. This viscous photoresist is casted on the wafer using a filter and a syringe. The photomask is placed in contact with the resist coated silicon wafer in a Mask aligner MJB4 (SÜSS MicroTec) and exposed to a wavelength of 365 nm with the power of 13 $mWcm^{-2}$ for 10 seconds. The photolithography process parameters of alignment marks are summarized in Table 3.1. After exposure, the patterns are developed in MF 319 for 45 seconds, followed by a DI-water rinse and drying with purified nitrogen gas.

Table 3.1. The photolithography process parameters of alignment marks

Alignment marks	Material	Parameter	Time
Spin coating	AR 300-80	4000 rpm	1 min
Bake		100°C	1 min
Spin coating	S1813	3000 rpm	1 min
Bake		90°C	2 min
Exposure	Wavelength (nm)	Power ($mWcm^{-2}$)	Time
	365	13	10 s
Develop	MF 319		45 s

The resist acts as a shadow mask with structures for the next step, which is sputtering gold palladium (AuPd). AuPd is sputtered on the whole wafer from a target by bombardment with energetic ions for 3 min at 20 mA. The sputter method is preferred if a large area needs to be covered uniformly in a single step. This results in a thickness of 60 nm metal layer. After the lift-off process in acetone with ultrasonication, the samples with metallic alignment marks are cleaned in isopropanol and dried with purified nitrogen gas. This fabrication of alignment marks can be omitted in the stamps with FIB milled nanochannels.

Photolithography of microchannels

In stamps with FIB-milled nanochannels, the patterning of the microchannel inlets and outlets has to be performed prior to the milling. In stamps containing nanochannels patterned by EBL, however, microchannels are patterned after the nanochannel production.

The photolithography process of microchannels is similar to the alignment marks process. However, instead of metal evaporation, a dry etching process of Si/SiO_2 is performed after photolithography.

The 1 cm × 1 cm microchannel layout of two V-shaped microchannels (Figure 3.3.) is transferred to the silicon stamp in this process. In the area where the nanochannels will be placed, indentations are designed which results in a smoother flow from the microstructures into the nanostructures. In a photolithographic process, the positive resist AZ4562 (MicroChemicals GmbH) is spun at 4000 rpm for 30 seconds onto a silicon substrate. The substrate is stored for 1 min exposed to air at room temperature, followed by two baking steps at 60°C for 1 minute, and then at 100°C for 6 minutes, subsequently. This results in a 6.5 µm thick layer. Then the silicon stamp is stored in air at room temperature for 10 minutes before being exposed with a mercury vapor light source with a wavelength of 365 nm and the power of 13 $mWcm^{-2}$ for 15 seconds in the mask aligner MJB4 with a mask containing

microchannel patterns. Afterwards, the photoresist is developed for 2 minutes and 30 seconds in AZ 826 MIF (metal-ion-free, MicroChemicals GmbH) and rinsed in DI-water to stop the develop process, followed by purified nitrogen flux to dry the substrate. The details of this process are given in Table 3.2.

Table 3.2. The photolithography process parameters of microchannels

Microchannels	Material	Parameter	Time
Spin coating	AZ4562	4000 rpm	30 s
Stored		room temperature	1 min
Bake #1		60°C	1 min
Bake #2		100°C	6 min
Stored		room temperature	10 min
Exposure	Wavelength (nm)	Power ($mWcm^{-2}$)	Time
	365	13	15 s
Develop	AZ 826 MIF		2 min + 30 seconds

Then, the microchannels are etched into the silicon with an inductively coupled plasma reactive-ion etching tool (ICP-RIE SI 500, SENTECH Instruments GmbH). We use a gas mixture of SF_6, C_4F_8 and O_2 and follow the recipe with the parameters listed in Table 3.3. Under these conditions, an etching time of 120 seconds leads to ~1000 ± 30 nm deep microchannels, as measured by profilometer (DektakXT, Bruker). Afterwards, the resist is removed by sonication in acetone, rinsing with isopropanol and drying with purified nitrogen.

Table 3.3. Dry etching of microchannels into silicon master stamp with a reactive ion etching machine. This recipe results in ~1000 ± 30 nm deep microchannels.

Parameters	Value
ICP power	400 W
HF power	15 W
Temperature	0°C
Chamber pressure	1 Pa
Time	120 seconds
Gas	Flow (sccm)
SF_6	50
C_4F_8	70
O_2	5

Figure 3.4. displays the SEM images of two facing microchannels, which are etched into the silicon. The nanochannels are later aligned to the indentations on the microchannels for a smoother flow.

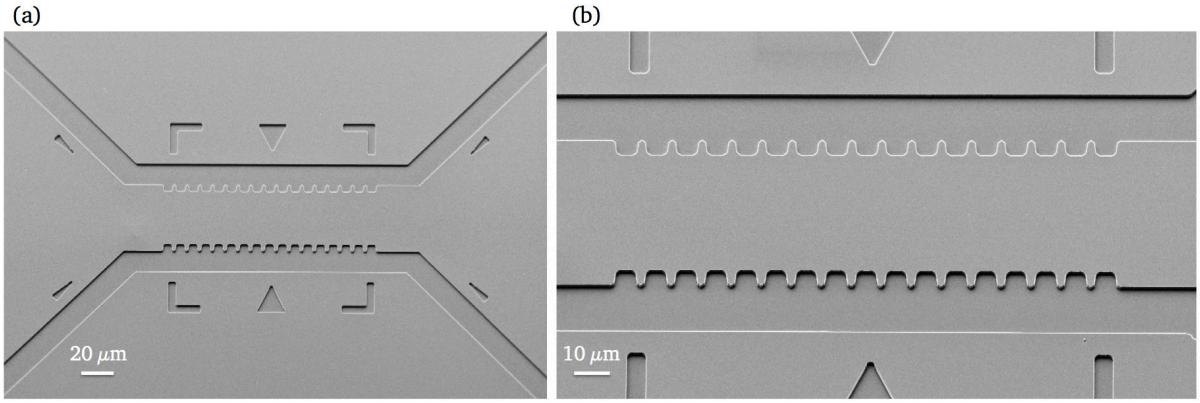

Figure 3.4. (a, b) SEM images of the microchannels with indentations, fabricated by photolithography and reactive ion etching. The microchannels are ~20 μm wide and ~1 μm deep.

Two different sets of microchannels are designed in this thesis. The gap between two parallel microchannels is 40 μm or 100 μm, based on the applications. The photolithography and etching process are the same in both cases.

3.1.2 Fabrication of nanochannels by EBL and FIB

In Chapter 2, it has been pointed out that nanochannels allow confinement of different particles and elongation of DNA molecules. The feature size of structures patterned by standard UV-lithography is limited by diffraction of light and practically the best resolution of this technique is limited to approximately 1 μm. In order to produce nanoscale channels, other nanopatterning techniques, using a beam of electrons or ions can potentially fabricate channels with a width of a few nanometers.

A beam of electrons or ions corresponds to a much smaller wavelength (picometer range) than UV light in conventional photolithography. This allows to achieve features of sub-10 nm are possible using EBL or FIB.[5, 84]

In the following section, the patterning process of nanochannels using e-beam and focused ion beam lithography is described. Nanochannels with different width from 50 nm to 300 nm, and different depth from 80 nm to 410 nm are fabricated. Some of the stamps contain short nanochannels such as 5 μm or 38 μm, while meandering nanochannels with 158 μm are patterned to visualize very longer DNA molecules in one single frame view of a camera. At the entrance of some nanochannels, short and/or long 3D transient inlets are fabricated to facilitate the flow from the micro- to nanochannels and the pre-stretching of the DNA molecules.

Nanochannels and inlets by FIB

When the FIB is operated with a proper beam size, beam current, and energy during a milling process, incoming ions introduce a cascade of collisions. Ions can provide enough energy for target atoms to overcome surface binding and escape from the substrate, which results in a nanoscale trench. This drilling process is called direct FIB milling. Direct FIB milling enables maskless[85] and resist-free fabrication of nanostructures, and 3D patterns with different cross sections and depth levels, all in one step. The ability of simultaneous monitoring of the milling process in real time leads to a quick and easy quality control during parameter optimization.

One of the main drawbacks of FIB is the slow speed of the milling process. However, we show that it is possible to pattern functional stamps within few minutes using higher Ga^+ beam currents. Higher beam currents provide a faster milling process for quick prototyping of structures. Lower milling currents provide a smaller beam diameter and lead to a smoother surface roughness at the nanochannels walls.

Here, we demonstrate how FIB allows simple patterning of stamps with multiple levels and 3D structures within a short time for fast prototyping. We fabricated three different types of silicon stamps with long and short arrays of linear or meander nanochannels with different profiles and/or depths, combined with 3D transient inlets. The stamps are categorized as: two stamps with long linear nanochannels; two stamps with meander nanochannels; one stamp with short/long linear nanochannels as well as different types of inlets. All the nanochannels in this section are milled through the silicon substrate using a focused gallium (Ga^+) ion beam of a ZEISS Crossbeam 550.

In this approach, first the microchannels are patterned on the silicon substrate as schematized in Figure 3.5. (a). Then the 3D nanofunnels transient inlets (b), and the nanochannel (c) are patterned.

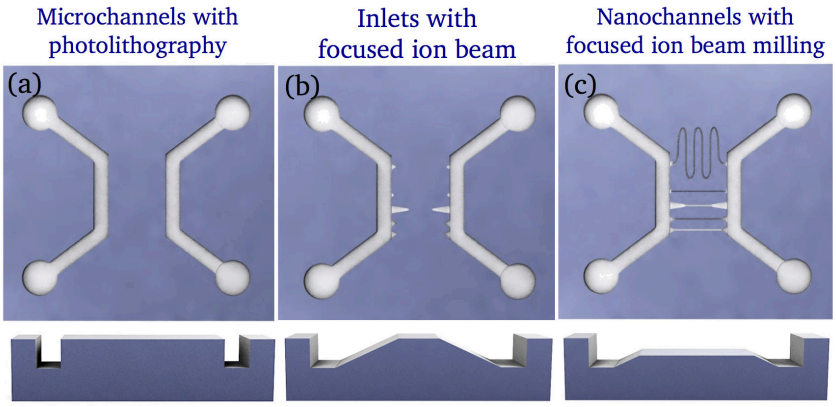

Figure 3.5. Schematic overview of a stamp fabrication using focused ion beam milling for nanochannel patterning. (a) two microchannels and four liquid inlet holes are fabricated by photolithography and reactive ion etching. (b) different types of nanofunnels transient inlets and (c) nanochannels with different depths and cross sections are milled into silicon by focused ion beam milling.

Fabrication of 3D transient inlets

The size mismatch between the micro- and nanoscale channels hinders the flow and the delivery of the molecules. In addition, long DNA molecules often entangle at the entrance of nanochannels due to an abrupt transition.[86] A smooth transition from the microchannels to the nanochannels facilitates the introduction of the molecule into the nanochannel, since the change in entropy for the molecule is less abrupt and especially less damaging to the DNA strands. In addition to the indentations at the entrance of each nanochannel, we have designed 3D nanofunnels that act as transient inlets at both ends of the nanochannel. Such inlets facilitate the flow, avoid clogging, and pre-stretch the DNA molecules[87, 88] before entering into the nanochannels. Structures with gradually decreasing width and depth are easily fabricated by FIB, in contrast to other techniques, where 3D and multi-level patterning requires multiple steps.[89]

After optimization of the ion beam, test structures are milled few micrometers away from the region of interest, assuming a linear relationship between pixel intensity and milling depth. The varying nanofunnel width causes deviation from a linear milling rate, due to the dependence of sputtering yield on the beam angle of incidence, and the impact of feature dimensions on material redeposition. Smooth 3D inlets are achieved by patterning a triangle or trapezoid with a homogeneous dose in one (or two) uni-directional passes, from triangle tip to bottom. This leads to material re-deposition on the exposed parts, which create the desired gradient depth. Figure 3.6. shows the re-deposition of ejected atoms while scanning with ions.

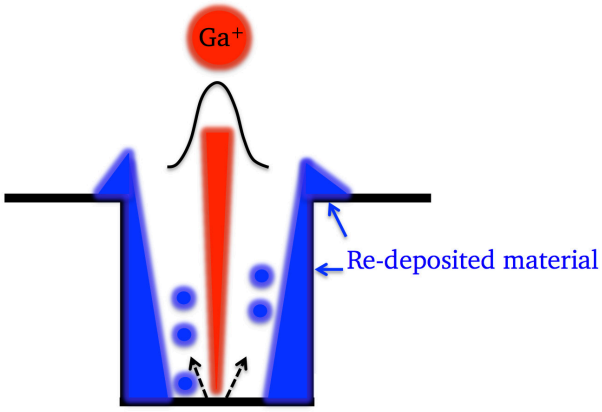

Figure 3.6. Schematized re-deposition effect during the FIB milling. This effect is used in our favor to fabricate 3D funnel-like transient inlets for a smooth transition between the micro- and nanostructures and minimize the entropic barrier. Its Application is shown in Figure 3.7.

An acceleration voltage of 30 kV has been used to obtain highest possible lateral resolution and sputtering yield. Figure 3.7. illustrates a 3D funnel-like tapered inlet, milled with a 300 pA beam current and a dose of 200 mC/cm^2, in two cycles with unidirectional scanning mode, in 40 seconds, starting at the triangle tip.

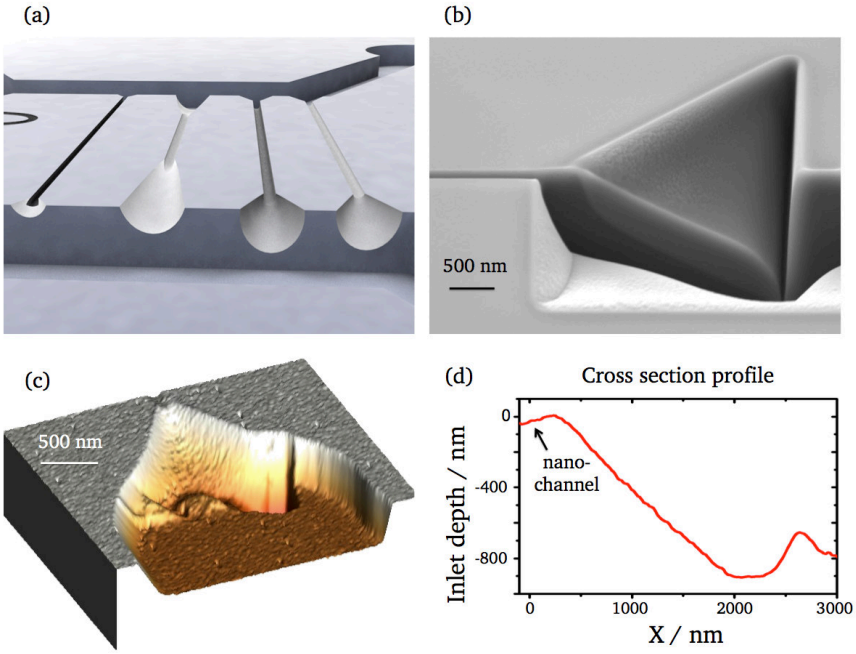

Figure 3.7. A smooth 3D funnel-like tapered inlets as a result of re-deposition in FIB milling fabrication. (a) schematic of different types of inlets (short/long with different depth profiles). (b) SEM image of the cross section of a short triangular inlet. (c) 3D AFM profile of a short triangular transient inlet. (d) the slope and low surface roughness of an AFM cross section profile. The milling time for fabrication of this triangular inlet is 40 seconds.

The transient inlets can have different shapes. Figure 3.8 shows a fabricated silicon stamp with 17 nanochannels and different types of transient inlets. The stamp contains three identical blocks, with 5 different inlets in each block. The 3D inlets have different geometries and configurations, from left to right: long trapezoidal inlets; short trapezoidal inlets; a combination of short trapezoidal and rectangular inlet; two sets of narrow and wide rectangular transient inlets; the most right is a combination of trapezoidal and two set of narrow/wide rectangular inlets. Furthermore, the stamp has two long nanochannels, 270 nm and 420 nm wide, which are directly connected to the indentations / microchannels. The imprinted devices obtained from this stamp are used to evaluate the influence of the different transient inlets on the DNA flow, in particular to study the flow throughput, and to control the stretching factor, and translocation speed.

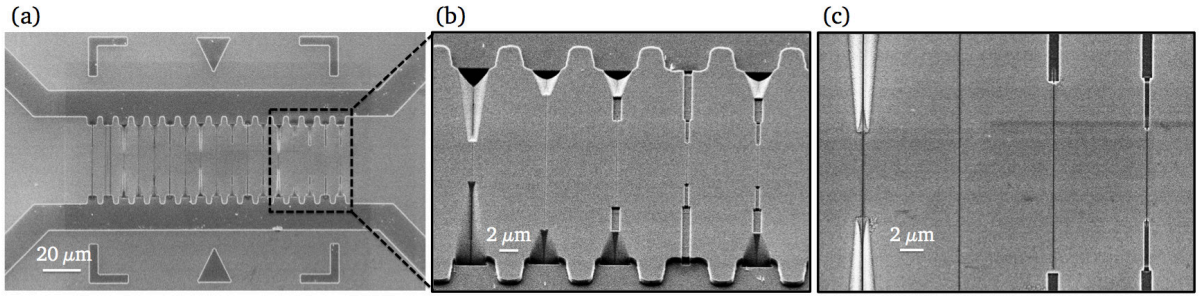

Figure 3.8. Graded Inlets silicon stamp with different rectangular and trapezoidal inlet configurations. (a) one block out of three repeat blocks. Gallium liquid ion source FIB is used to fabricate facing funnel like transient inlets, and the nanochannels. (b) and (c) different types and configuration of graded transient inlets. Different configuration of inlets has an influence on the translocation speed and flow throughput of the device.

Long linear nanochannels with short triangular inlets

Short triangular transient inlets and long straight lines are milled perpendicularly to the microchannels. Figure 3.9. shows a silicon stamp with an array of ~38.5 µm long linear nanochannels. The stamp has 17 different nanochannels, with lateral dimensions, ranging between 120 nm and 245 nm. The total milling time of inlets and nanochannels is 27 minutes.

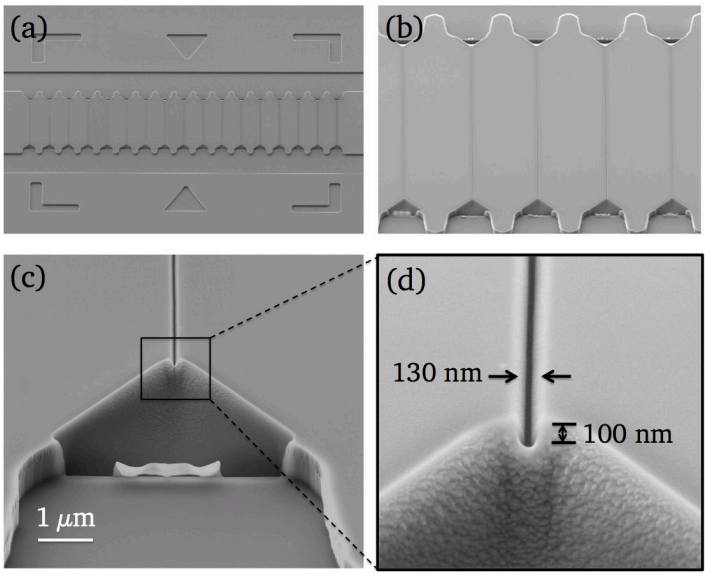

Figure 3.9. SEM images of a silicon stamp with an array of ~38.5 µm long linear nanochannels and short 3D triangular inlets, fabricated by direct FIB milling. (a, b) the 17 nanochannels in this stamp have widths between 120 nm and 245 nm. (c, d) details of the smooth, 3D triangular tapered inlet, used to facilitate the flow of biomolecules in the nanochannels. The total milling time of inlets and nanochannels is 27 minutes.

Roughness at the bottom and sides of the nanochannels are most likely the reason for DNA sticking. To reduce channel roughness, a lower ion beam current is used, which prevents fast re-deposition and sputtering by incoming gallium ions.[31]

By tuning the milling parameters, we can tailor the profile of the nanochannels, as shown in Figure 3.10. (b, c). As can be seen in the SEM image of Figure 3.10 (c), two linear nanochannels with different cross sections and depths are easily milled one after the other within the same stamp. The deeper nanochannel on the left has a rectangular cross section. The right nanochannel is wider and has a V- shaped profile. To obtain different cross sections and depths, the left nanochannel is milled with three times higher Ga^+ ion beam current and dose than the right nanochannel. The parameters of 300 pA and 240 mC/cm^2 for the left nanochannel is used in comparison to 100 pA and 80 mC/cm^2 for the right nanochannel. All other parameters are the same in both channels, including the milling time.

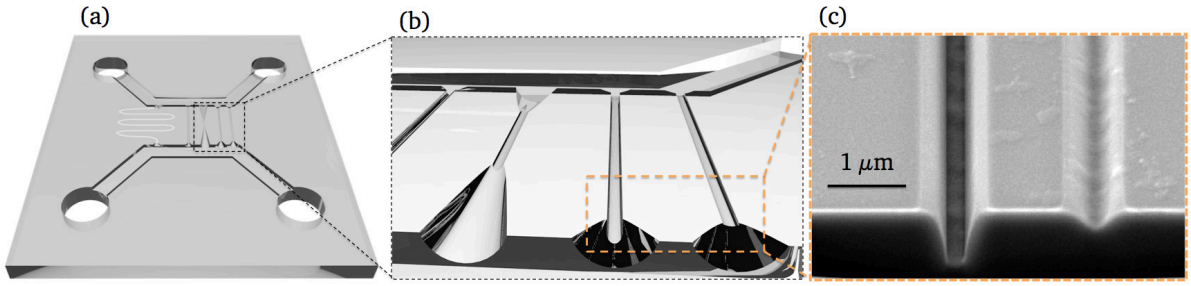

Figure 3.10. Nanochannels with different profiles and depths. (a, b) 3D schematic of nanochannels with different lengths, depths and cross sections. (c) SEM image of the cross section of two nanochannels with different depths and profiles. The deeper, U- shaped nanochannel profile on the left is milled with a three times higher current than the shallower V-shaped nanochannel on the right. 300 pA and a dose of 240 mC/cm^2 for the left nanochannel in comparison to a channel milled with 100 pA probe current, with a dose of 80 mC/cm^2 for the right one. All other milling parameters are the same for both trenches, including the milling time.

Meander nanochannels

Two stamps with different widths and depths of meander nanochannels are fabricated. Meander nanochannels are useful to observe the long DNA molecules within one single field of view of the camera.

A stamp with an array of four similar meander nanochannels, ~158 µm long, ~350 nm wide, and ~150 nm deep is shown in Figure 3.11. The total milling time for this stamp, including the nanochannels and inlets is less than 8 minutes. All four nanochannels of this stamp are milled with a high Ga^+ ion beam current (300 pA) in one cycle with a dose of 10 mC/cm^2, in 10 seconds. The full width at half maximum (FWHM) obtains by atomic force microscopy (AFM, Dimension 3100, Digital Instruments–Veeco) compares the results. The mentioned parameters resulted in nanochannels with 350 nm FWHM, and a depth of 150 nm.

The nanochannels in the second meander stamp are milled with a low current (10 pA), with a dose of 100 mC/cm^2 in 30 cycles (bidirectional scanning) in 1 hour. This set of milling parameters resulted in nanochannels with 400 nm FWHM, and a depth of 410 nm, as confirms by AFM profiles. Figure 3.11 compares two different working nanochannels milled with different ion beam currents for different milling throughput: very fast (left graph), using high probe current for rapid prototyping of nanochannels in only few seconds; and slow (right graph), with low ion beam current, for high quality patterning of nanochannels within an hour.

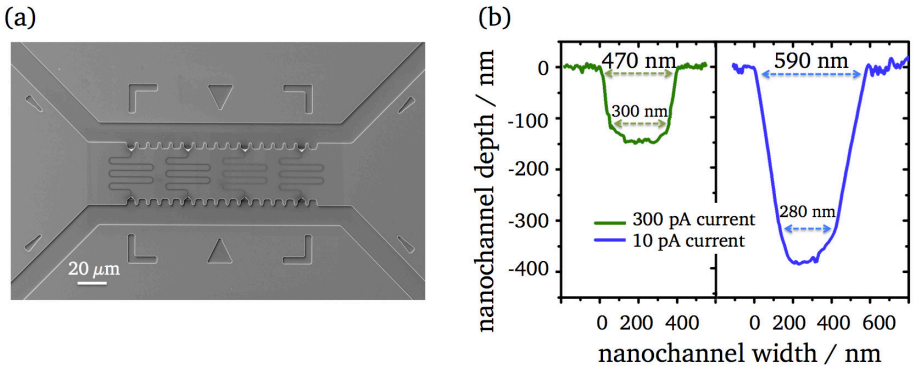

Figure 3.11. Silicon stamp with four similar meander nanochannels. (a) SEM image of the silicon stamp with nanochannels of ~350 nm wide, ~150 nm deep, and ~158 µm long. (b) comparison of two stamps with meander nanochannels based on their AFM profiles. Fast milling: the milled nanochannels in 10 seconds with high current and low dose are compared with slow milling: the right nanochannel profile, milled in 1 hour with low current and higher dose. The FWHM of left profile is 350 nm with a 150 nm depth. Right profile has a FWHM of 400 nm and is 410 nm deep. The sidewall angle of the left nanochannel is 85°, and it is 73° for the right one. The AFM data in tapping mode is taken from the negative polymeric replica, so the nanochannels are protruded. This minimizes the tip convolution, and ensures the accuracy of measured height/depth. Then the profiles are inverted.

In order to have a clean and smooth stamp, a sonication in acetone for 3 minutes, and a 10-min plasma-cleaning step is conducted. Before replication of the silicon stamps into the final micro- and nanofluidic device, a monolayer of fluorosilane is deposited on the surface, which is explained in detail in section 3.1.4.

Nanochannels by EBL and RIE

As mentioned before, the nanochannels patterned by e-beam lithography are fabricated after alignment marks. The microchannels are later aligned to the pre-patterned nanochannels by photolithography.

The e-beam resist (a positive or negative resist) is chosen in the conceptual design phase to comply with the requirements of the subsequent fabrication steps. We used a positive resist. After exposure and developing the resist, those silicon regions that are not covered by the resist are etched away with a fluorine-based reactive ion etchant. After etching, the rest resist on top of the silicon substrate is removed, and the surface is coated with a monolayer of fluorosilane.

In the following, the fabrication of three different silicon stamps with square or rectangular nanochannel cross sectional profiles is described. For the fabrication of all three stamps, the beam current is measured with a faraday cup. The beam current defines how many electrons are impinging on the sample per second. Its value affects the maximum obtainable resolution, as high currents tend to result in wider beams. Another important

parameter, which affects the resolution, is the "writing field size". Writing field is the largest area exposed without moving the stage, where the beam deflects to pattern the structures. A smaller field size allows for obtaining a better resolution.

Before deposition of the resist on the silicon stamps, the substrate is sonicated in a petri dish of acetone for 5 min, and then rinsed with isopropyl alcohol (IPA), following the dry process with purified nitrogen. Polymethyl methacrylate (PMMA) is the resist used in fabrication of all stamps using EBL. The resist is spun onto the silicon sample and baked. The solubility of PMMA is enhanced in the exposed parts, so that after the development, these areas can be etched into the silicon, forming the nanochannels. When electrons hit the resist with high energy, some electrons are reflected from the substrate and backscatter (large angle scattering) with micrometer range. Due to proximity effects and backscattered electrons, the neighboring features should not be tightly spaced. Despite the very small beam spot size (0.5 - 2 nm), the exposed areas are enlarged, with the possibility of merging the structures after etching. The optimization of resists thickness, and beam dose results in a reduced proximity effect. These proximity effects are much smaller in FIB milling.

Short nanochannels with long triangular inlets

This silicon stamp contains nanochannels of 5 μm long. Figure 3.12. illustrates the ELPHY CAD design of short nanochannels with long triangular inlets. These inlets will be as deep as the nanochannels, as they will be etched into the silicon in the same step. Therefore, these inlets are less effective in a flow throughput than the 3D inlets which are patterned using FIB.

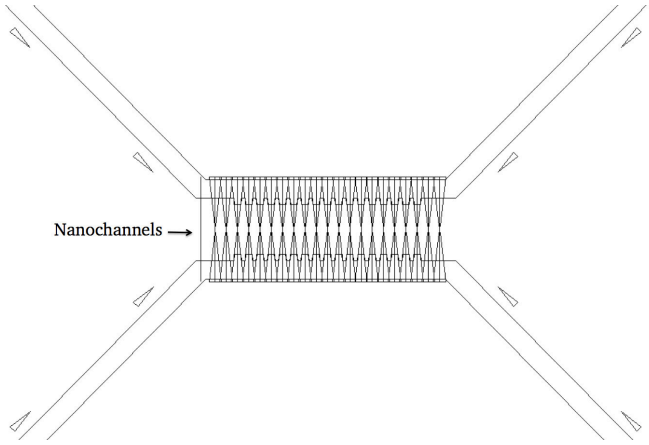

Figure 3.12. CAD design of short nanochannel and their long triangular inlets. The inlets will have the same depth as the nanochannels after etching into the silicon substrate simultaneously. The nanochannels are 5 μm long. The gap size between the facing microchannels is 40 μm.

A layer of PMMA 950-A4 polymer (MicroChem. Corp.) is spun onto the substrate with 6000 rpm for 1 min, and heated up at 160°C for 2 min (layer thickness of 150 nm).

For exposure of the nanochannels and inlets, a SEM (Quanta FEG, FEI company) in connection with NPGS runs at 20 kV with spot size of 2 nm and a beam current of 29 pC with a writing field of 200 μm. After exposure, the resist is developed with AR 600-56 for 2 min. Table 3.4. summarizes the parameters.

Table 3.4. Fabrication of nanochannels and inlets using electron beam lithography for silicon stamp with short nanochannels.

Nanochannel	Material	Parameter	Time
Spin coating	PMMA 950-A4	6000 rpm	1 min
Bake		160°C	2 min
Exposure to electron beam (EBL)			
Develop	AR 600-56		2 min

After developing the resist, the structures are etched into the silicon using the RIE tool. The depth of the open nanochannels can be precisely controlled by RIE, due to its slow etching rate. Etching parameters are summarized in table 3.5.

Table 3.5. Dry etching parameters of nanochannels for the silicon master stamp. This recipe results in 110 nm deep nanochannels.

Parameters	Value
ICP power	150 W
HF power	10 W
Temperature	0°C
Chamber pressure	0.5 Pa
Time	30 seconds
Gas	Flow (sccm)
SF_6	10
C_4F_8	22
O_2	5

After the etching step, the resist is removed by sonication in acetone, followed by rinsing with isopropanol and drying by purified nitrogen. The SEM image in Figure 3.13. displays the silicon stamp with 5 μm long nanochannels fabricated by the mentioned parameters. The microchannels are then patterned using photolithography as discussed in section 3.1.1.

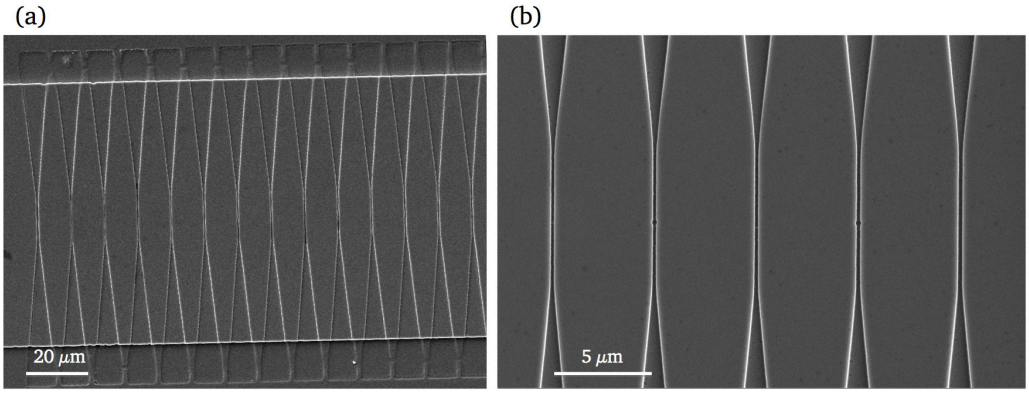

Figure 3.13. SEM images of the silicon stamp with nanochannels ranging from 240 nm to 340 nm wide, 110 nm deep and 5 μm long. The nanochannels are fabricated by EBL and RIE. The microchannels of 20 μm wide and 1 μm deep are patterned by photolithography.

Nanochannels with bowties

This silicon stamp contains nanochannels of 50 nm wide and 90 ± 10 nm deep as well as bowties, which will act as nanoantenna when coated with gold. The bowties are in close proximity to the nanochannels, in the same plane, and well-aligned to them. To achieve 50 nm wide nanochannels, PMMA 950-A4 resist has to be diluted in Anisole with the ratio of 1:1 (PMMA A2) and the rotation speed of spin coating is modified to 2000 rpm in order to reduce the thickness of the PMMA. After spin coating of the resist for 1 minute, the silicon substrate is baked at 160°C for 2 minutes. This result in a 70 nm thick resist, which allows for structuring narrower nanochannels after dry etching. The EBL is performed using a SEM (Supra 55, ZEISS) combined with a RAITH pattern generator. Triangular inlets are designed at both ends of the nanochannels. An acceleration voltage of 20 kV, a beam current of 11.3 pA, 7.5 μm aperture, a writing field of 200 μm (patterning area 200 ×200 μm^2) are chosen for the exposure. The energy density area dose for triangles and bowties is 150 $\mu C/cm^2$ and the main dose for lines (nanochannels) is 300 pC/cm. A dose factor will be assigned to each line. The area dose factor is 1 for all. The line dose factor of 2 to 2.5 resulted in nanochannels with 50 ± 3 nm wide. The nominal bowtie tip-to-tip distance (gap) is designed between 50 nm and 100 nm. The step size and line spacing of 3 nm is one pixel. To avoid thermal drift in long exposures, the triangle, lines and bowties are ordered one after the other in ELPHY CAD design. About 30 minutes (using this beam current) after launching the exposure, the silicon stamp is ready for develop in a solution of AR 600-56 for 1 minute, and the process stops by rinsing isopropanol and drying with nitrogen flux. Table 3.6 summarized the parameters of nanochannel fabrication of this stamp.

Table 3.6. Fabrication of the nanochannels and the inlets using electron beam lithography for the silicon stamp with bowties.

Nanochannel	Material	Parameter	Time
Spin coating	PMMA A2 (A4 is diluted in Anisole with 1:1)	2000 rpm	1 min
Bake		160°C	2 min
Exposure to electron beam (EBL)			
Develop	AR 600-56		1 min

Then the nanochannels are etched using a reactive-ion etching tool for 120 seconds, which results in of 90 ± 10 nm deep nanochannels, and smooth vertical sidewalls. The etching parameters are given in table 3.7.

Table 3.7. Dry etching of nanochannels with bowties. This recipe results in 90 ± 10 nm deep nanochannels.

Parameters	Value
ICP power	150 W
HF power	10 W
Temperature	0°C
Chamber pressure	0.5 Pa
Time	120 seconds
Gas	Flow (sccm)
SF_6	10
C_4F_8	22
O_2	5

After the anisotropic etching of the nanochannels, the residual resist is removed by sonication in acetone, following rinsing with isopropanol. The stamp is dried by purified nitrogen and the microchannels are then fabricated perpendicular to the nanochannels.

This stamp provides nanochannels of width below the persistence length of native DNA (50 nm) with well-defined squared cross section profiles. The SEM image of the nanochannels with bowties is displayed in Figure 3.14.

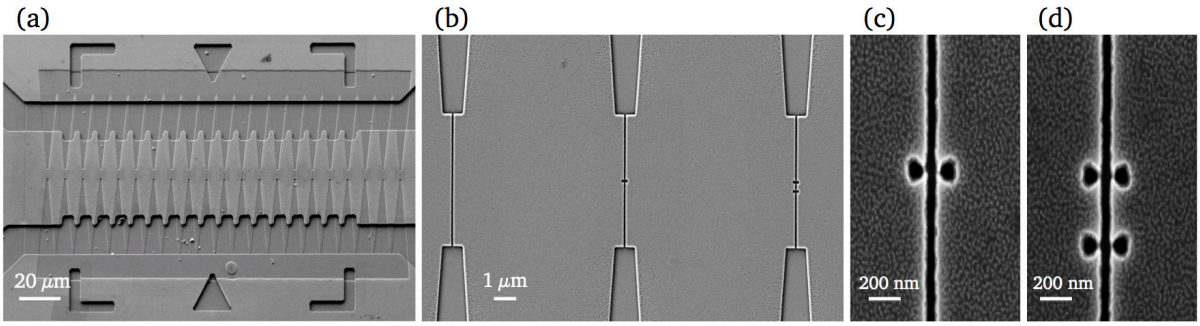

Figure 3.14. SEM images of a silicon stamp with short nanochannels and triangular bowties in close proximity to the nanochannels. (a) SEM image of a series of 22 nanofluidic channels, each 50 nm wide, 90 ±10 nm deep, and 5 μm long, written by EBL on a silicon wafer (100). A reference line with four double pairs of bowties in designed at the left side of the stamp. (b) the stamp contains groups of 3 nanochannels with the same design. Each group has one nanochannel without bowties, one nanochannel with one pair of bowties, and one nanochannel with double pair of bowties. (c) SEM image of the nanochannels with pairs of bowties. The distance between neighboring bowties in double pair bowties is 225 nm. This stamp is patterned based on the parameters given in Table 3.6 and Table 3.7.

Variations of the cross section are minimized due to the low edge roughness of the EBL pattern and RIE etching. The crystalline anisotropic etching removes the sidewall edge roughness (to achieve atomic smoothness), and the conformal edge definition guarantees the channel width uniformity. This stamp has the nanochannels comparable to the persistence length of the DNA molecules (50 nm). Decreasing the nanochannel dimensions reduces the conformational degree of freedom, and the DNA molecules can be elongated to their full contour length.

After patterning the microchannels, the silicon stamp surface is silanized for an easy release of replicated samples.

3.1.3 Anti-adhesive coatings by fluorosilanization

When the fabrication process of a silicon stamp is completed, a negative replica of the silicon stamp is fabricated. The mold surfaces (silicon stamp or negative glass stamp surfaces) should allow for an easy separation from the sample. In order to facilitate the release, and also to prolong the stamp lifetime, an anti-sticking film layer of fluorosilane is deposited onto the silicon master stamp surface via chemical vapor deposition (CVD), before replication of molds into sample. Damage to the molded structure during demolding is highly dependent on the quality of the anti-adhesive layer. Fluorinated chlorosilanes with different carbon chain lengths are commonly used due to their low surface energy, high surface reactivity, and high resistance to the temperature and the pressure.[34]

The structured silicon master stamp is sonicated in a beaker of acetone for 3 minutes,

rinsed with isopropanol and dried with purified nitrogen. The master stamp is then transferred into an UV-Ozone cleaner (Model 144AX Series, Jelight Company, Inc.) for 2 minutes. This allows formation of hydroxyl group on th surface which will interact and make bounds to the silane molecules. The sample is then loaded into a vacuum oven with a liquid drop of the fluorosilane (1H, 1H, 2H, 2H-Perfluorodecyltrichlorosilane, Alfa Aesar) for 30 minutes at 400 mbar, and at 80°C. This process results in the deposition of a self-assembled monolayer of fluorosilane on the stamp surface. The silane binds covalently to the silicon oxide of the stamp surface. The fluorosilane layer decreases the surface energy and makes it hydrophobic, allowing a clean and easy separation of the stamp and the imprint. The measured contact angle of silicon after surface coating with the fluorosilane is 105°.

3.1.4 Comparison of EBL with FIB

The costs of acquisition, maintenance and running nanolithography equipment is higher than for micro scale lithography techniques such as photolithography.

Using EBL and RIE allows only for inlets with a constant depth from the microchannels to the nanochannels. In order to facilitates a smoother from and overcome the entropic barrier due to the size mismatch between the micro and nanochannels, 3D transition inlets with a slope in depth can be fabricated using FIB. Furthermore, the proximity effect is less using FIB for patterning the structures.

In the following, the production time of a silicon stamp using FIB and EBL is compared. FIB is often classified as a slow technique, but the throughput can be largely improved with the appropriate parameters (i.e., ion probe current). In the previous sections, we demonstrated patterning of the functional nanochannels and the transient inlets within a few minutes. Patterning by FIB allows for direct milling of different sizes, depths and levels within the same step, and thus avoids time-consuming pre- and post-production steps needed in EBL, such as spin coating, exposure, developing, and resist stripping. Particularly, when different depths of structures are required, all the mentioned steps are repeated each time.

Table 3.8. summarizes the typical times required for each processing steps of both method. As can be seen, the total time required for the fabrication of a stamp by EBL or FIB is rather similar (between 1 h and 1.5 h). However, in case of more than one EBL step (like tapered inlets), the total time is doubled/tripled, while patterning another depth level by FIB can be performed with a minor effort within the same step.

Table 3.8. Comparison of the total processing time for a silicon stamp patterned by EBL and FIB.

		EBL	FIB
Process	Steps	Duration	Duration
Pattern writing	Spin coat resist	5 min	--
	Tool alignment and calibration	15 min	30 min
	Exposure / milling	20 min	30 min
	Develop	5 min	--
Pattern transfer	RIE cooling down	30 min	--
	RIE etching	2 min	--
	Resist stripping	10 min	--
	TOTAL TIME	**87 min**	**60 min**
Alignment marks	Spin coat photoresist	5 min	--
	UV lithography	5 min	--
	Metal sputtering	20 min	--
	Lift-off	20 min	--
	TOTAL TIME	**50 min**	**--**

3.2 Fabrication of glass stamp by NIL

In order to improve the fabrication throughput by minimizing the nanolithography time per chip, the fluidic devices are imprinted using nanoimprint lithography. This technique provides parallel printing in a short time (seconds to few minutes). Imprint lithography is a standard, simple, quick and easily repeatable method. It abandons the use of an energetic beam of electrons, photons, or ions. As a result, it eliminates many factors that limit the resolution of the conventional lithography techniques, such as the wave diffraction, scattering in the resist, backscattering from the substrates, and the chemistry of the resists and developers.[80] This low cost technique is capable of transferring all the micro- and nanostructures as well as the 3D features in a polymer resist, with no further etching processes. It can also print a large area at once (i.e. in wafer scale) at room temperature, offering a high throughput. This technique requires inexpensive materials and employs non-specialized equipment.

As mentioned in Chapter 2, this technique uses compression molding to replicate the structure of the mold on a resist, usually a polymer. If the master stamp is made of silicon, the negative stamp which is its replication has to be transparent to UV light, so that the squeezed polymer between the two substrates is cured. A glass substrate is first treated in UV-Ozone cleaner for 2 minutes. Afterwards, an adhesion promoter (OrmoPrime08, micro resist

technology GmbH) is spun on the substrate at 4000 rpm for 1 minute, and then baked at 150°C for 5 minutes. This results in a film thickness of ~130 nm, as measured by profilometry. The promoter enhances the adhesion to glass, so the durability of the stamp is increased. We used OrmoStamp (micro resist technology GmbH) as UV curable resist for the imprinting process. OrmoStamp is a silicon-containing glass-like inorganic-organic hybrid polymer. It is solvent-free, and shows minimal shrinkage after curing. Once the silicon stamp is fabricated, a small drop of this viscous liquid polymer is casted on the silicon master stamp, and a glass slide – treated in UV-Ozone for 2 minutes – is placed on the droplet. Without applying any additional pressure, the polymer spreads between master stamp and the glass slide substrate and fills the trenches and cavities by capillary action (where surface energy controls the wetting and spreading of the viscous material). When the polymer is fully spread, the viscous molding material is hardened by exposing to UV light with Hg lamp (365 nm wavelength) with power of 13 $mWcm^{-2}$ for 2 minutes. Curing by UV exposure is used for cross-linking of the polymer to make it durable for demolding. Then the silicon master stamp and the replicated structures on the glass slide are separated. The resulting topography is a negative replica of the original silicon master stamp which has reversed topography of the original mold. This process is schematized in the Figure 3.1. (a – c). The glass stamp can be used repeatedly to quickly generate nanoscale features to make the fluidic devices for flow measurements.

The large contact area between this transparent negative stamp and the resist on the fluidic device gives rise to great adhesion forces, which leads residual of hardened resist on the stamp after each printing process. For an easy release of the glass stamp from the final device (which will be discussed in next section), a thin anti-adhesive layer coating is applied on the mold (section 3.1.4). This anti-adhesive coating is chemically inert, hydrophobic, and at the same time allows the filling of the mold cavities when the polymer is in its viscous state.[34] The adhesion layer (Ormoprime) and the silanization allow reusing the negative stamp for tens /hundreds of imprints without affecting the quality of the replicated micro and nanostructures. The stamp is replicated 4 times in the glass slides using OrmoStamp polymer to remove any residuals on the surface of the mold. The fifth replication of each new stamp (silicon or glass) can be used for the purpose. Using stamp copies instead of the original stamp is a way to enhance the lifetime of the original stamp, simply because the original is preserved undamaged for the copying process.

3.3 Fabrication of polymer devices by NIL

The fluidic samples are also made by direct UV-NIL, in a quick (two minutes long) step, and do not require any post-processing. The fluidic devices can be fabricated on a variety of substrates including silicon, glass, quartz, plastic or metals. In this thesis, we used 2 mm thick Plexiglas plates as substrates, since Plexiglas can easily be cut into different sizes depending

on the device requirements. Additionally, drilling holes for liquid input is simple as compared to glass or other hard/brittle materials. The samples are made of 7.5 cm × 2.5 cm Plexiglas pieces, to emulate the dimensions of a typical microscope glass slide, and facilitate the optical characterization. Four holes (3 mm in diameter, 1 cm apart) are drilled through the Plexiglas, as liquid reservoirs. Then, the micro- and nanostructures are patterned by UV-NIL as schematized in Figure 3.1 (d – f). Figure 3.15. depicts the SEM images of a silicon master stamp, a negative glass stamp and the final polymeric fluidic device.

The Plexiglas substrate with holes is treated in UV-Ozone cleaner for 2 minutes. A drop of OrmoStamp polymer is casted on the transparent stamp surface. Plexiglas is placed on top, and gently pressed against the stamp. The spread out polymer is cured for 2 minutes under a UV lamp with 365 nm wavelength, with the power of 13 $mWcm^{-2}$, and then the sample is released from the negative glass stamp. All multilevel, micro- and nanostructures of the stamp are imprinted into the polymer at once.

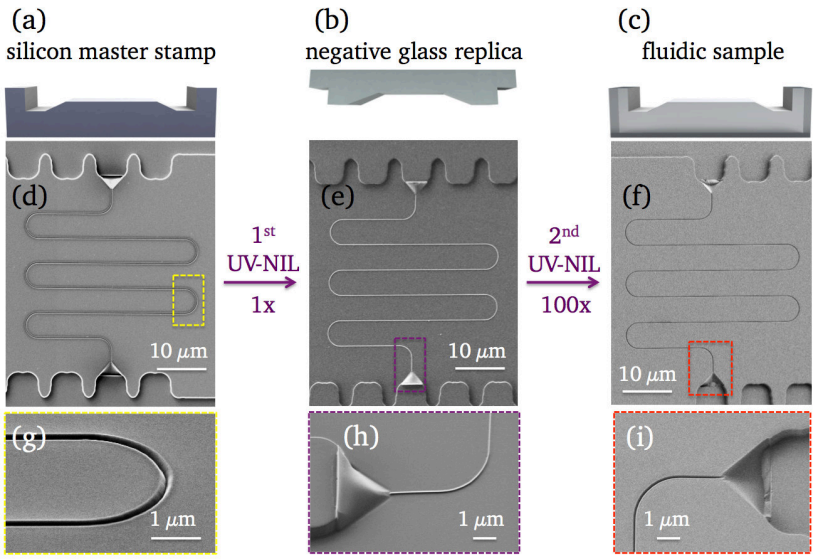

Figure 3.15. Double UV-nanoimprint lithography replication process of a meander nanochannel. (a – c) a sketch of the (a) silicon master stamp, (b) the negative glass replica and (c) final polymeric fluidic device. (d, g) the nanochannels of the silicon master stamp, (e, h) the nanochannel of a transparent negative glass stamp, made by UV-NIL process. The protrusion of inlets and nanochannel is visible. (f, i) the nanochannel in the polymeric fluidic device, imprinted by second UV-NIL process using the stamp in (e). The SEM images are taken using charge compensation; with no metal coating.[102] The first replication of silicon master stamp into the negative glass replica is performed only once. The second UV_NIL process is repeated every time prior to the flow measurements, with no need to repeat the first UV-NIL process.

To perform flow measurements on the final fluidic device, the sample needs to be sealed. A glass coverslip and the sample (Plexiglas with imprinted structures) are treated in UV-Ozone cleaner for 2 minutes. This improves the polymer adhesion and makes the surface

hydrophilic as wetting the fluidic system can pose a difficulty depending on the internal dimensions and hydrophobic nature of the substrate. Then the coverslip is brought into contact with the sample, and sealed just by pushing them together. The rigid polymer seals the hollow channels without collapsing. A defect free and flat surface is crucial for the final bonding of the device. The quality and smoothness of the imprinted micro- and nanostructures is replicated from the original silicon stamp across the different samples.

The thin sealing material (coverslip) is transparent to permit the optical characterization inside the channels and facilitate the further use of these devices for single-molecule and particle detection in the transmission and reflection modes in an epifluorescence microscope. Such disposable nanofluidic devices for DNA stretching are fabricated in the polymer at low cost and high throughput in a single imprint process.

Both of the silicon stamp and the negative stamp can be reused several times to fabricate hundreds of copies as schematized in Figure 3.16. To increase the throughput even more, the nanofluidic devices can be produced in parallel.

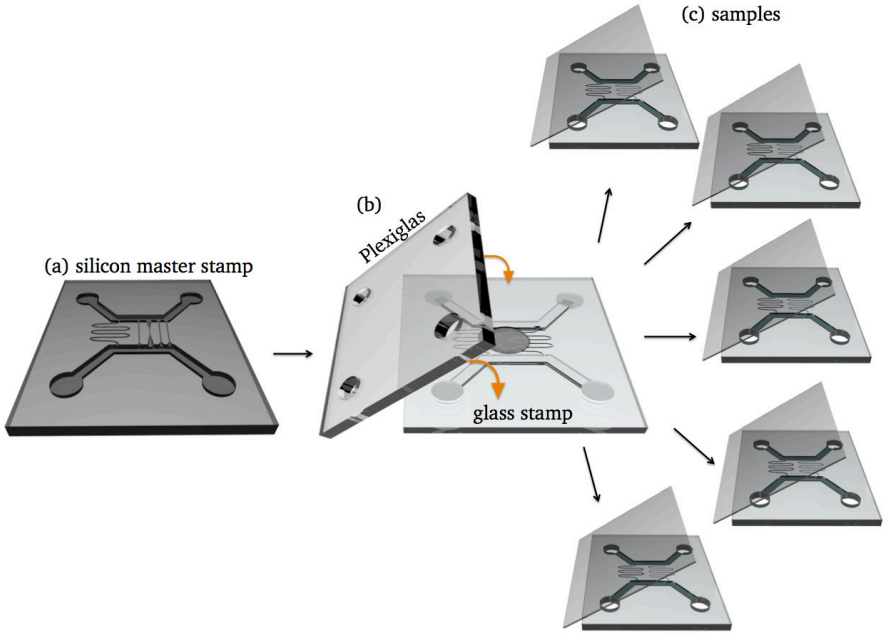

Figure 3.16. Batch processing of nanofluidic devices in parallel using UV-NIL to reduce fabrication time of final sample. Once the silicon master stamp is fabricated (a), a negative transparent polymeric replica is made (b). This negative stamp is used to imprint the several polymeric fluidic device (c).

Imaging with charge compensation function

To ensure that the intended design is consistent from silicon master to glass stamp and polymeric device, all parts were imaged at several occasions. SEM images are obtained using charge compensation, enabling to characterize even the most insulating samples (nanostructures imprinted on a thick polymer onto a glass or Plexiglas substrate) in a non-destructive way. A common method of avoiding surface charging, due to ion implantation and secondary electrons generation, is the deposition of a thin metal film, like Au and Cr, or

conductive polymer on the sample surface. However, this permanent coating will render the samples unusable. Activation of local surface charge compensation and charge neutralization allows direct inspection of the glass stamp and the fluidic sample with no metal coating. For this, dry nitrogen is injected locally through a nozzle towards the sample, resulting in ionization of the nitrogen gas by the electrons, and local neutralization of negative charges by positive ions on the sample. Figure 3.17. shows the charge compensation function.

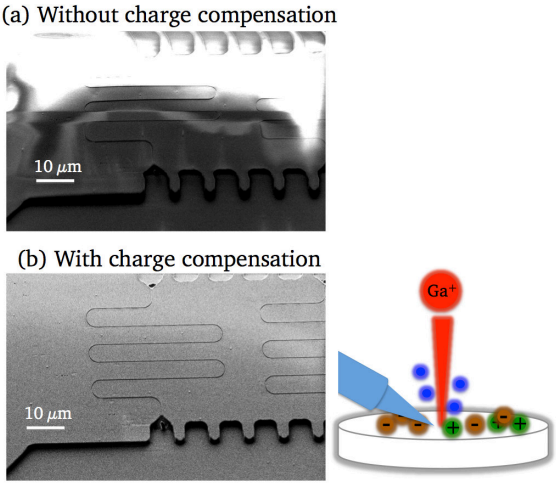

Figure 3.17. Comparison of scanning an insulating substrate with and without charge compensation function. Both samples are not coated with metal. (a) without charge compensation: strong charging even at very low acceleration voltage. (b) with charge compensation: partially compensation of electron charges on the surface. Ionization of the nitrogen gas by the electrons and local neutralization of negative charges by positive ions on the sample allow for the direct inspection of the sample without metal coating. The acceleration voltage in both cases is 1 kV.

3.4 Fabrication of the plasmonic bowtie nanoantenna

The resolution provided by all optical microscopes is diffraction limited. However, the DNA molecules or quantum dots are in the range of only few nanometer scales. In addition, increasing the signal-to-noise ratio and reducing the background signal by shrinking the optical spot size improve the sensitivity of the measurements. To overcome the mismatch between the optical wavelengths and the nanoscale objects, a plasmonic bowtie nanoantenna can be integrated adjacent to the nanofluidic channels for ultra-high sensitive measurements. The goal in this section is to fabricate a biosensor device that improves the resolution for the single-molecule detection. The bowtie antenna creates ultra-intense fields by strong plasmonic coupling between the pairs[90] of small metallic triangles as depicted in Figure 3.18.

The bowtie shape is chosen, since the excitation of surface charge or plasmons in sharp tips produces enhanced optical fields, which are locally confined to the regions approximating the radius of curvature of the tip.[90] Bowtie antenna consists of two metallic triangles facing tip to tip that are separated by a small gap. The local field enhancement is highly dependent on

the bowtie gap size, so that smaller gaps have higher local field strengths than the larger gap bowties or the single triangles.[90] The facing triangles combine the electromagnetic properties of the sharp metal tips with those of coupled plasmon resonant nanoparticle pairs.[90] Maximum field enhancement occurs between the two triangle tips, which are called hot spot. The confined and localized optical field in a nanometer region allows for sensing the experiments at higher resolution, below the diffraction limit.

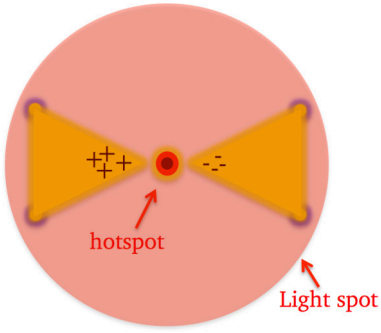

Figure 3.18. Schematic of a plasmonic gold bowtie nanoantenna and charge distribution under resonant conditions. The maximum field confinement in the gap, due to the excitation of surface plasmons in sharp tips is called hot spot. The smaller gap provides a more intense field concentration and enhancement.

A process combining nanofabrication steps of pattern definition by EBL, shadow evaporation of metal, and lift-off process, was used to fabricate the gold bowties on Plexiglas samples. The EBL fabrication of such bowties is discussed in section 3.1.2. and the Figure 3.14. In the following section, the gold evaporation in the samples is described.

3.4.1 Metal evaporation and the lift-off process

The evaporation of metals is performed by physical vapor deposition (PVD, PLS 500, Balzers-Pfeiffer). PVD provides a smoother film, compared to the sputtering process.In this technique, solid materials are vaporized by an electron beam, transported through the vacuum, and condensed on a substrate surface. The PVD process is typically performed in high vacuum, where molecules travel in straight ballistic lines (free molecular flow regime).

As shown in the Figure 3.14 the nanochannels of 50 nm wide, and the bowties tip-to-tip gap of about 55 nm is fabricated. Bowties are perfectly aligned along the nanochannels. Nanochannels are served to deliver the liquid to the hot spot where the field is maximized.

A 25 nm thick chromium layer as sacrificial layer is deposited by shadow evaporation on pre-patterned Plexiglas substrate, followed by a 20 nm gold thick, as illustrated in Figure 3.19. Afterwards, the samples are sonicated in chromium etch for the lift-off process. The samples are then rinsed with DI-water, and dried using nitrogen flux. No adhesion layer is used in the fabrication of bowties, as it quenches the plasmonic properties.

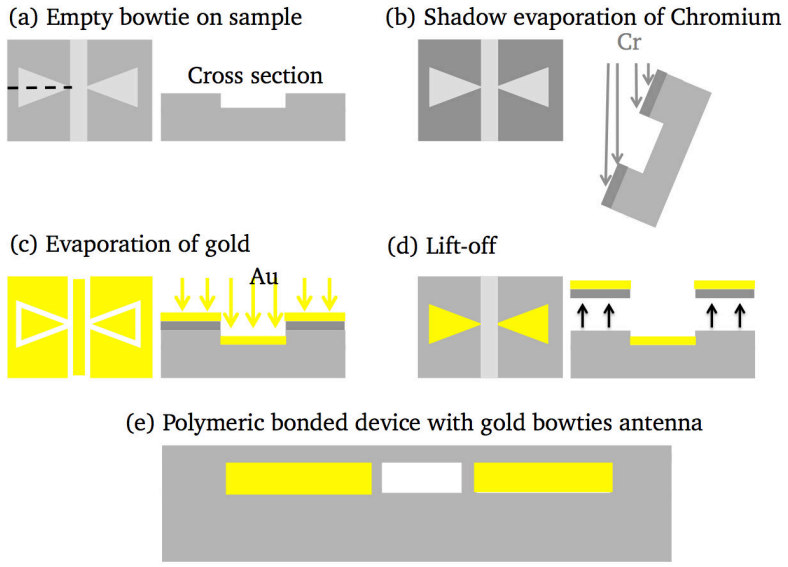

Figure 3.19. Schematic of metal evaporation and the lift-off process of bowties nanoantenna integrated adjacent to the nanochannel. (a) schematic of the cross section of an empty bowtie in a pre-patterned Plexiglas. (b) 25 nm chromium thick is deposited on the sample as sacrificial layer by shadow evaporation. (c) 20 nm thick gold is deposited on chromium. (d) lift-off process by chromium etchant using sonication. The area with sacrificial layer is lifted-off, and the gold remains only in the bowties. No adhesion layer is used in this process as it quenches the plasmonic properties. (e) cross section of a sealed device with a hollow nanochannel and pair of gold bowties.

The plasmon resonance of the metal, the laser source, and the fluorophore for staining DNA molecules have been matched for the optimum system. Gold was selected for filling the bowties antenna, since Au nanoparticles resonate in the range of 700 nm – 800 nm wavelength. To resonate the gold bowtie antenna, a He:Ne laser (633 nm) laser is focused to a diffraction-limited spot (around 1 μm) on the bowtie. This laser wavelength is matched with our fluorophore used for staining the DNA molecules in our experiments. As the result, the emission luminescence intensity signal of the molecule is enhanced. Figure 3.20. illustrates SEM images of fabricated gold bowties nanoantenna. Scanned pairs of bowties under illumination of a He:Ne laser confirm the existence of gold nanoparticles in the bowties. Using this system, the read out resolution is about 50 nm (the gap size) instead of hundreds of nanometer which is the light diffraction limit.

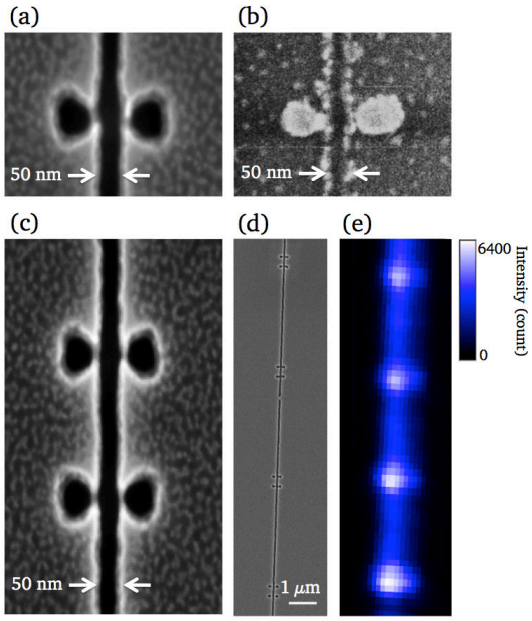

Figure 3.20. SEM images of gold plasmonics bowties nanoantenna. (a) SEM image of a pair of bowties before gold evaporation. Bowties are adjacent to the nanochannel. (b) SEM image of the bowties coated with gold in shadow evaporation of chromium, followed by the lift-off process. (c) SEM image of a double pair of bowties in close proximity to the nanochannels. (d) SEM image of a long nanochannel with 4 pairs of double bowties. (e) scanned pairs of gold bowties under illumination of a laser (633 nm wavelength) and detected by an avalanche photodiode. The gold bowties are scanned using a piezoelectric stage and a custom-made LabVIEW software. This image confirms the existence of gold nanoparticles in the bowties and allows for detecting the exact location of the hot spot before the flow measurements.

This bowtie antenna can create a 50 nm × 50 nm hot spot inside the channel, where the field is confined beyond diffraction and greatly increased. This allows to read the optical signal, and probe the nanochannel with sub-diffraction resolution in real time.

Chapter 4:

Flow Measurements

In this chapter, we present the flow measurement results on the fabricated polymeric biochips for investigating the statics and dynamics of the confined DNA molecules in the nanochannels. The biochips have been fabricated in a fast and inexpensive manner based on a double replica molding process as shown in chapter 3 (Device Fabrication). As described, two microchannels and four reservoirs were patterned on a silicon master stamp by standard lithographic techniques, and an array of nanochannels was produced by electron beam lithography, or focused ion beam milling. Then, the OrmoStamp polymer was used to replicate the pattern into the polymeric material using ultra-violet nanoimprint lithography. Finally, the polymeric fluidic device was treated in UV-Ozone and bonded to a glass coverslip in order to seal the device. A 2-minute UV-Ozone treatment makes the walls hydrophilic for a better sealing, and more importantly for a smooth flow in the channels. The liquid polymer (OrmoStamp) as the active material shows a good biocompatibility, homogeneity, chemical inertness and durability. These disposable devices are directly used for flow measurements after fabrication, without further post-processing requirements. Polymeric sample patterns have smooth vertical sidewalls to optimize the flow experiments.

In this chapter, the flow experiments of different liquids are described to evaluate the device, and validate the sealing quality, the liquid confinement, as well as studying single quantum dots by microspectroscopy. Samples from different silicon stamps are produced for different applications in this thesis. These molecules were observed to undergo several configurationally transitions, and their behavior varied depending on whether they were free in solution, in the microchannels or in the nanochannels. Elongation and linearization of electrokinetically-driven double stranded λ-DNA and kaposi's sarcoma-associated herpesvirus (KSHV) molecules across the nanochannels are studied. These fluorescently labeled single-molecules in the rectangular nanochannels made by e-beam lithography, and also triangular-shape nanochannels made by focused ion beam milling are imaged using inverted epifluorescence. We studied the effects of different types of multi-level transient inlets on the flow throughput, the pre-stretching and the translocation speed of the DNA molecules in the nanochannels. Having 3D nanofunnels at the entrance of the nanochannels allows for reducing the electric field over the nanochannels and to achieve a higher device throughput, providing a better transport control in the nanofluidic analysis platforms.

Since imagining the molecules with optical microscopes suffer from the diffraction limits of light, fluorescence microscopy coupled with a laser beam and a high-efficiency photodiode detection system to directly observe the diffusive movement and the emission process of individual fluorescent molecules in real time. In this technique, the fluorescently labeled molecules are passing through the nanochannels under a point-light source and their photoluminescence intensity signals is guided through a 100 μm-diameter pinhole before detecting by the photodiode, which eliminates the out-of-focus signal to increase the signal-to-noise ratio. Real-time measurements show the single-molecule fluorescence records with a

time spread that corresponds to the actual transition of a particular molecule. The high detection sensitivity achieved by an avalanche photodiode at fast data acquisition speeds allows the real time observation and counting of single-molecule fluorescence without statistical analysis or averaging. Monitoring of real-time measurements of single molecules using this technique is rapid (seconds to minutes) and practical.

The goal of this thesis is to optically map the barcoded DNA molecules in real time, which can be a complimentary technique to the DNA sequencing. As discussed, sequencing of DNA molecules is time-consuming and expensive ($1,500 for high-quality 'draft' whole human genome sequence in late 2015). Therefore, researchers are looking for alternative methods such as optical mapping of DNA molecules, as a quick and efficient technique to obtain the long-range information of the DNA molecules. Optical mapping has a limited resolution caused by the optical setup and the used wavelength. Therefore, it cannot provide basepair resolution of the DNA sequencing, but it can handle the DNA strands with sizes in the mega basepair regime, making it easy to identify the large scale information.

In this thesis, we proposed the real time optical mapping of the barcoded KSHV-DNA and λ-DNA molecules in the lab-on-a-chip micro- and nanofluidic devices, as a rapid and high-resolution characterization technique for mapping of the binding sites. These simple but sensitive and cost-effective technique have the capability to rapidly determine the spatial location of the genetic information along the long DNA molecules, without amplification steps, with a minimum volume of reagents. The individual DNA molecules are barcoded (tagged) and linearized into the nanochannels and their emission intensity profiles along time are visualized.

In this chapter, two barcoding techniques will be discussed: using organic dye probes which are the complimentary sites of the KSHV-DNA repeat units, as well as the barcoded λ-DNA molecule with netropsin molecules. Netropsin is a non-fluorescent molecule which has a high affinity to AT-rich regions of the DNA to prevent the intercalating dye to attach, thus creating a fluorescence map of AT versus GC-rich regions on the DNA molecule. All the measurements were performed in the ambient-temperature solutions at room temperature (300K).

4.1 Optical setup

An inverted epifluorescence microscope configuration (ECLIPSE Ti- U, Nikon) with a multiple input and output ports is equipped with suitable systems for light detection, image digitization, and recording. The output signal is derived to an EMCCD camera for imaging or recording the videos, or is directed into an interchangeable 100 μm-diameter pinhole for obtaining photoluminescence signals by avalanche photodiode or to a spectrometer for wavelength analysis. A cooled, high-quantum-yield camera charge-coupled device (EMCCD Evolve® 512 Delta, PHOTOMETRICS) is used to achieve highly sensitive detection of very low intensity signals and the observation of the single-molecule in the fluidic samples. The ImageJ software is used to identify the single molecule traces. An overview of the optical setup is schematized in Figure 4.1.

The excitation source is a metal halide lamp (Intensilight, Nikon). Fluorescent filter cubes are used for fluorescent imaging. A set of several filter cube cassettes, prepared for used fluorescent dyes in this thesis is mounted on a filter wheel. This allows for a rapid change of excitation and emission ranges for the multi-wavelength excitation and analysis. The dichroic mirror is positioned at 45° angle toward the incoming light to reflects the exciting wavelengths and transmit the corresponding emission bands. Our in-house assembled filter wheel contains custom-made filter sets in an empty filter block (holder) to spectrally filter with the appropriate optical filters and reduce the background. It allows optimization for the source of exciting light and for our specific applications. It is also used to cut the excitation signal for spectroscopy.

Two laser beams are used in this study, 532 nm (Ar^+) and 633 nm (He:Ne) wavelengths. The laser beam is brought to its diffraction-limited focus using a low autofluorescence 100× oil-immersion, high-numerical–aperture objective (NA $\sim$ 1.45). The diffraction-limited radius of the Gaussian laser beam is $\sim$1 μm in experiment. The laser excitation allows for observing the DNA molecules as they flow in the nanofluidic devices, and obtain the photoluminescence time scans in the same set up. This makes it possible to simultaneously excite and observe several fluorophores. Additional filter cube cassette with a dichroic mirror reflects the laser light to the objective and so allows the two beams directed toward the sample at the same time. In order to control the intensity of exciting light, a neutral density filter wheel is placed in the light path directly before entering the laser light in the microscope.

A small pinhole (100 µm in diameter) is placed at the image plane to reject the light from out-of-focus regions. The collected fluorescence emission passed through an emission filter. One end of the fiber is connected to the output of the microscope and the other end to a single photon counting module (COUNT-100C-FC, Laser Components GmbH). In this configuration, the fluorescence signal passes through the pinhole before striking a photon-counting system. This results in a better signal than the diffraction-limited resolution image,

as this approach has important advantages: real-time imaging and recording the long molecules. This supersensitive single-photon avalanche diode provides a quantum detection efficiency of more than 70% and a dark count of less than 100 counts/s.

A piezoelectric stage which is controlled by a home-made LabVIEW software can scan the sample in X and Y directions. It also allows an accurate placement of the laser excitation spot at the desired position. This is particularly crucial in obtaining a good photoluminescence signal of DNA molecules, which are stretched in the nanochannels or for comparison of QDs blinking which are confined in a nanoscale channel. A spectrometer is coupled at one of the microscope output ports, for photoluminescence spectroscopy. The transmission tower can hold a condenser for dark field spectroscopy of bowtie antenna.

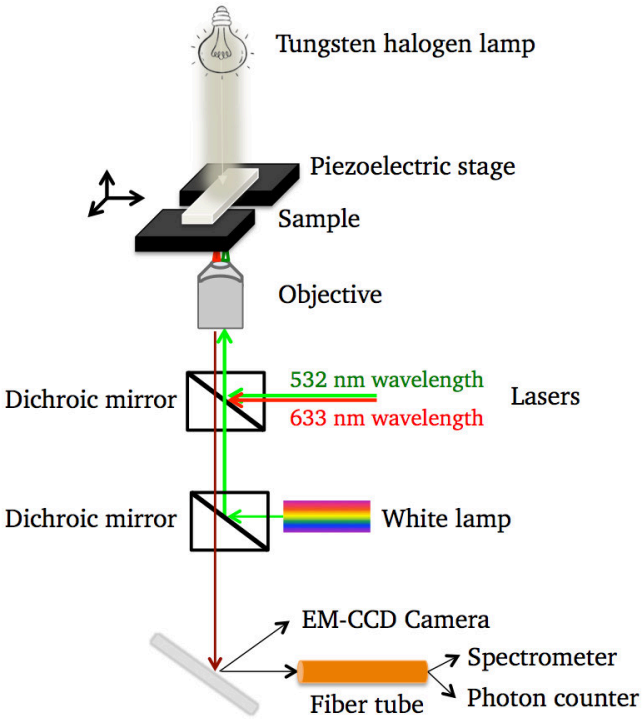

Figure 4.1. Schematic configuration of an inverted epifluorescence microscope with multiple input and output ports, used for this study. The output signal is derived to an EMCCD camera for recording the videos, or an interchangeable pinhole for obtaining photoluminescence signals by avalanche photodiode, or to a spectrometer for wavelength analysis. A set of several filter cube cassettes for various fluorescent dyes is mounted on our in-house assembled filter wheel. Additional filter cube cassette with a dichroic mirror reflects the laser light to the objective. The transmission tower holds a condenser for dark field microspectroscopy. This system is equipped with two lasers of 532 nm and 633 nm wavelengths.

4.2 Device validation by rhodamine and quantum dot flow

The validation and the reliability of the imprinted lab-on-a-chip micro- and nanofluidic devices is observed by continuity of the channels, the liquid confinements, and discarding the

leaks or clogging. Fabrication of such narrow channels might induce area defects. For instance, FIB milling can sometimes lead to non-uniform and rough surfaces, due to the material re-deposition. The performance of the fluidic system and the continuity of the nanochannels are evaluated by the flow tests over the entire length of the channels, using colored rhodamine and quantum dots. This study is performed using a fluorescence microspectroscopy.

Rhodamine B diluted in isopropanol, and QDs in toluene are flown in the nanochannels for quality check of the different fluidic components, and to proof their potential applications for visualization of the single nanoparticles detection.[102] Rhodamine dyes are chosen for evaluation of the devices due to their insensitivity to pH, their high photostability, and the low background level (high signal-to-noise ratio). QDs are also bright and remarkably photostable, which allows a prolonged illumination at high light intensity.

We ensured that the fluorescent signal is detectable, and the nanochannel is continuous along the entire channel. A drop of 5 µL diluted rhodamine B in isopropanol is loaded into one of the reservoirs. The liquid fills up the upstream microchannel immediately by capillary action.[102] Then the liquid passes through the nanochannels to fill the opposite microchannel (downstream). Figure 4.2. (a) illustrates the fluorescence image of diluted rhodamine along a meander nanochannel. To check the liquid confinement and discard the leaks, we performed photoluminescence microspectroscopy.[102] A laser (532 nm wavelength, matching the absorption of rhodamine) is focused down to a sub-micrometer spot, and centered on the nanochannel. The emitted photoluminescence (PL) signal is recorded with the spectrometer. Figure 4.2. (b) compares the photoluminescence signals obtained by focusing the laser spot in the microchannel (μch, blue line), in the nanochannel (nch, red line), and on the polymer surface in-between fluidic structures (green line) as the background signal.[102] The position of the excitation spot is controlled with a piezoelectric stage. Comparing the fluorescence signals evidences the liquid confinement in the nanochannels, and discards the leaks.

Semiconductor QDs seem to be the most toxic to the live specimens, on the basis of their chemical composition.[14] However, as long as the toxic nanocrystalline core is well shielded from its surroundings by a chemically stable shell, the toxicity is not an issue. Semiconductor core–shell QDs, Zn-Cu-In-S core / ZnS shell (PlasmaChem GmbH), is used in this study. The quantum dots with ZnS shells are typically synthesized in an organic solvent (coated with hydrophobic organic ligands) and thus initially insoluble in the aqueous solution.[14] These non-toxic luminescent nanocrystals with a radii of 4 – 5 nm with an emission maxima at λ_{max} = ~700 ± 25 nm are suspended in toluene. The emission peak width (FWHM) is rather narrow (ca. 100 nm) and symmetric.

Confined QDs in a meander nanochannel are displayed in Figure 4.2. (c – i).[102] Quantum dots suspended in toluene are flown into the device. Figure 4.2. (c) shows an epifluorescence

image of confined QDs in the whole meander nanochannel. After evaporation of the solvent within few minutes, the immobilized nanocrystals (static) can be observed individually (Figure 4.2. (d)). The image in (d) was obtained from a photoluminescence movie, by plotting the maximum intensity of each pixel, so all the quantum dots can be seen at the same time.[102] The PL intensity signals of different quantum dots along time are shown in Figure 4.2. (e – h), corresponding to the spots marked in (d). They can be seen "blinking" or "flickering" as the photoluminescence signal goes ON and OFF in the intensity plots along time. The stepped signal (ON and OFF states) confirms that the luminescence is obtained from the single particles. This is also reflected in the histogram of Figure 4.2. (i), which corresponds to the PL signal shown in (h). Here, the distribution of the ON/OFF emission states can be seen and compared to the background. All signals obtained from quantum dots are compared against the background.

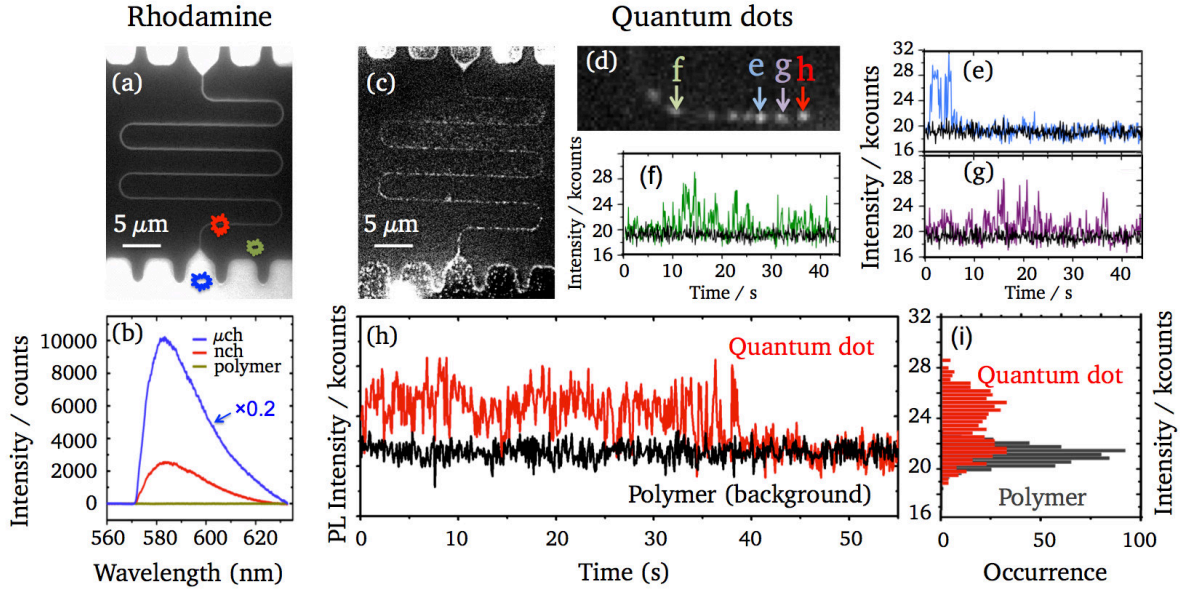

Figure 4.2. Device validation by rhodamine and quantum dot flow for nanochannel patency and the particle confinement. (a, b) diluted rhodamine B in isopropanol. (a) epifluorescence microscopy image of rhodamine B flown in a meander nanochannel. The exposure time is 100 ms. (b) PL emission spectra of the liquid in the microchannel (μch, blue line), in a nanochannel (nch, red line) and on the polymer (background, green line). The spectra are taken with a 532 nm laser excitation wavelength. The microchannel spectrum is divided by 5 to aid the comparison. (c – i) diluted Zn-Cu-In-S / ZnS quantum dots in toluene are flown in a meander nanochannel. (c) epifluorescence microcopy image of QDs with an exposure time of 100 ms, which is magnified in (d). This image is obtained by plotting the maximum intensity of each pixel from a 43 second long movie. (e – h) time traces of individual quantum dots, marked in (d), where the emitted photoluminescence intensity is plotted along the time. All PL signals are compared to the background (flat polymer in-between nanochannels). (i) The histogram of ON and OFF emission states of the quantum dot, corresponding to the PL plot in (h).[102]

4.3 DNA flow in the micro- and nanofluidic devices

After establishing a robust fabrication procedure that produces the smooth channel walls, the next step would be to load the DNA molecules into the micro- and nanostructures.

DNA molecules have typically a coiled conformation in the solution. When they are forced to flow through a nanofluidic channel, it is energetically more favorable for them to be in an elongated state. In this case, the coiling of the molecule to form a loop would cost an energy much higher than the thermal energy. Therefore, the nanofluidic channels can be used to reliably stretch the DNA, allowing to study the structure and the dynamics of confined single-molecules,[91, 92] or for quick optical mapping in few seconds.[93, 94]

In this thesis, we developed a device with an array of nanochannels for ultrasensitive and rapid read out of individual DNA molecules in real-time. In this section, our approach to elongate and monitor the single fluorescently labeled DNA molecules crossing a focused laser beam and recording their translocation events along time is described.

Filling the channels of a nanofluidic device is not trivial. Surface wettability is determined by a force balanced between adhesive and cohesive forces. Due to the high surface/volume ratio of a nanochannel, surface forces dominate the fluid behavior. The buffer solution of the DNA molecules is usually water-based. Therefore, the hydrophilic surfaces are desired, where water tries to maximize the contact with the surface. In this work, the surface wetting properties of the polymer nanochannel walls and the coverslips are modified by surface treating/activating in UV-Ozone cleaner or in an oxygen plasma before sealing the devices. This improves the hydrophilicity of the surfaces which are exposed to the fluid.

Background signal

After filling the micro- and nanochannels, an excitation beam source is focused on the nanochannel to record the translocation events. However, the excitation light illuminates a relatively large area of the specimen in the plane of focus, as well as the regions above and below this plane. Both the exciting light and the emitted fluorescence are scattered in this region. This causes substantial out-of-focus light, which is detected as the background.

In addition, even in the absence of any fluorescence in the sample, the detector sensors still generate certain read out values that are greater than zero. These weak unwanted signals that do not represent the fluorescence are generally called background or noise. The photon noise or the shot noise results from the quantum nature of light.

A low background and high signal-to-noise ratio are ideal conditions for the measurements of the stretched single molecules. In order to improve the signal-to-noise ratio,

the background fluorescence signal should be reduced or efficiently rejected. In this study, we used two ways to improve the signal-to-noise ratio.

First, ultra-small volumes and efficient optical filters are effective ways in reducing the background signal. Limiting the size of the excited volume by confinement of the molecules in the nanoscale channels, the background from scattering or the intrinsic fluorescence of the unlabeled species in the excitation volume is decreased.

The second way is photobleaching of the auto-fluorescence materials prior the flow experiments. Low autofluorescence materials are ideal for the fluorescent experiments. However, glass and polymer display autofluorescence. Polymers typically exhibit a broad band fluorescence under the illumination (auto-fluorescence) which can limit the signal-to-noise ratio of the fluorescence imaging. Since our whole device is made of polymer, reducing the amount of polymer in the optical path is not an option. However, by illuminating the sample under a light excitation source for few minutes, reduced the autofluorescence of the polymer. We also experienced that new samples show a higher auto-luminescence.

4.3.1 DNA sample preparation and the staining protocol

We used double stranded DNA from λ-bacteriophage (Thermo Fisher Scientific), 48502 base pairs long, and also the ds KSHV-DNA molecules (Heinrich Pette Institute, Leibniz Institute for Experimental Virology), ~150-180 kbp.

Fluorophores that binds to the DNA are selected based on the specific application. YOYO-1 and TOTO-3 Iodide (Thermo Fisher Scientific) are the fluorescent bis-intercalating dyes which are used to label the DNA molecules in this thesis. YOYO-1 is the brightest intercalating dye in this category, and TOTO-3 emission wavelength range is in the resonance range of the gold bowties nanoantenna. Intercalating dyes insert themselves between the planar surfaces of the DNA base pairs. YOYO-1 is a cyanine, a green fluorescence with the excitation and maximum emission wavelengths of 491 nm and 509 nm, respectively. TOTO-3 Iodide has the excitation wavelength at 642 nm and the maximum emission at 660 nm. These dyes exhibit a strong binding affinity towards the double stranded DNA.

The stained DNA molecules with fluorophores are diluted in a buffer solution. However, the intercalated DNA molecules are rapidly photobleached in water or the conventional buffers. The presence of oxygen radicals is one of the main causes of photobleaching and the photoscission. When exposing the fluorophore to the light in the presence of oxygen, oxygen radicals will be formed; capable of producing the single strand breaks on the DNA, a process referred to as photonicking. Degasing of the buffer avoids the photonicking of the stained molecules in presence of oxygen and also minimizes the formation of air bubbles in the microchannels while performing the flow measurements. To ease the filling of the microchannels and reduce the degree of photonicking, diluted 0.5× TBE is degassed for ~45

minutes, just prior to the experiments.

Double-stranded DNA molecules were fluorescently stained with the intercalating dyes at a ratio of 1:5 dye/base pairs. The stained DNA molecules are diluted in a freshly degased 0.5× Tris-Borate- EDTA (TBE, 10 mM Tris, 10 mM borate, and 1 mM EDTA, pH 8.3, Sigma-Aldrich) aqueous buffer. This buffer is good for the electrophoresis experiments. A small droplet (0.1 µL) of Triton X-100 (Sigma-Aldrich) is added at 0.5% (v/v) to the loading buffer (degassed TBE) to prevent sticking of the DNA to the polymer surface.

4.3.2 Capillary and electrophoretically flow

Before each flow measurements, the Brownian motion of the stained DNA molecules was observed. A 5 μl of the solution containing λ-phage DNA molecules which were stained with YOYO-1 was pipetted on a glass slide and a coverslip was placed immediately on top. The test solution was examined under the fluorescence microscope, indicating partially supercoiled state of the DNA in the solution.

Then the polymer chip is positioned and fastened on the stage of the microscope during the experiments, to avoid any drift on the oil-immersion objective. Before conducting experiments on the polymer chip, the autofluorescence of the device is quenched by exposing the chip to the white light at high intensity. Along with lowering the general background signal, this procedure also helps acquiring a constant background signal over the entire nanochannel throughout the experiments.

5 µL of liquid is injected into one reservoir (access hole). The negatively charged DNA is driven and transported along the microchannels by the capillary action and breaking the diffusion. The hydrophilic nature of the material promotes the wetting of the channels, once the DNA and the buffer are added to the chip. When the upstream microchannel is fully wet (after ~10 minutes), the downstream microchannel (opposite side) is filled with the degassed buffer (no DNA). Our detection scheme for measuring the DNA in a confined fluidic system is an inverted epifluorescence microscope. The stained DNA is illuminated at the dye's excitation wavelength, and the resulting fluorescent emission is measured with an EMCCD camera. The DNA transport in the microfluidic structures and translation of the confined stretched DNA molecules along the nanochannels is shown in Figure 4.3. This semi-flexible self-avoiding heteropolymer is stretched in the confinement of a nanochannel due to the self repulsion and self-exclusion of the charged polymer backbone. Optical detection of a single-molecule in a liquid relies on the repetitive emission of photons by a fluorescently labeled single molecule.

The major advantage of the nanoconfinement over traditional linearization techniques is that the entire confined DNA molecule is theoretically exposed to the same confinement force, allowing a uniform stretch. This contrasts with the traditional linearization techniques, which exert a high stretching force at the anchored ends of the molecules for elongation.

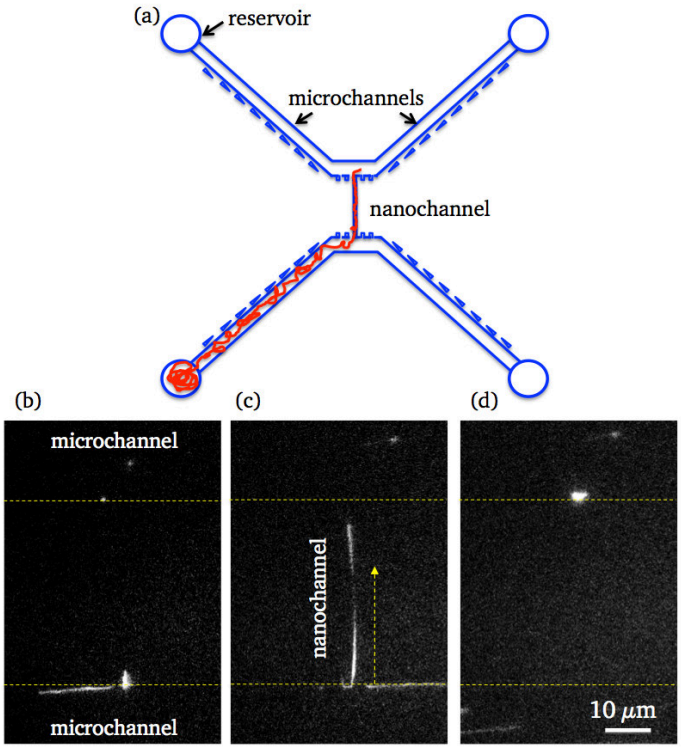

Figure 4.3. Observation of the coil-stretch transition of the λ-DNA from microchannel to the nanochannel. (a) schematic of DNA flow in the V-shape microchannels and the perpendicular nanochannels. (b – d) epifluorescence microscopic images of a fluorescently labeled single DNA molecule confined and elongated by a nanochannel. The DNA molecule is labeled with YOYO-1 at the 1:5 ratio (dye:base pair) and stretched by the capillary flow. The exposure time is 100 ms.

In general, capillary filling is the preferred method for filling of the nanofluidic channels. However, the capillary filling is slow, unreliable, and not appropriate for a flow-through system. The capillary filling is also dependent on the viscosity and the wetting behavior of the filling liquid. The transport of the DNA molecules through the nanoscale channels is most often achieved by applying an electric field between the opposite sides of the microchannels, which induces an electrostatic force on the negatively charged DNA and pulls it into the nanochannel. This force must be sufficient to overcome the free-energy barrier to the DNA entry into a nanochannel that results from the reduced conformational entropy of the confined macromolecule. Electrophoresis is one of the primary kinds of the electrokinetic phenomena in the micro- and nanofluidic systems. Electrophoresis is defined as the movement of charged particles relative to the stationary fluid. Electrical contact was made with platinum electrodes inserted into the reservoirs as shown in Figure 4.4. The electric potential or the applied voltage generates electric fields to drive the flow in the micro- or nanoscale channels. Once a positive bias is applied, the negatively charged DNA molecules are forced to move towards the positive electrode passing through the nanochannel, and these translocation events are then detected.

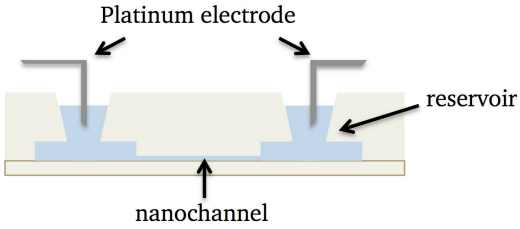

Figure 4.4. A side view schematic representation of an optically transparent micro- and nanofluidic device with two reservoirs. DNA molecules are loaded into the fluidic reservoirs and the platinum electrodes are inserted in the reservoirs for electrophoretically driving of the DNA molecules across the nanochannels.

However, introducing DNA molecule into a nanochannel by electrophoresis induces a considerable stress on the molecule.[95] Therefore, the electric field must be limited to avoid the damage on the long DNA molecules. When a molecule is pulled into a nanochannel, the force induced by the high field strength is opposed by the drag of the molecule's trailing end. This causes significant extension of the DNA molecule when it is pulled into the nanochannel.

The velocity of the DNA (V_{DNA}) during the electrokinetic transfer is given by $V_{DNA} = \mu E$, where μ is the electrophoretic mobility of the DNA and E is the electric field.

4.3.3 Single DNA molecule in the FIB nanochannels

The nanostructures patterned on a silicon master stamp by FIB in section 3.1.2. and imprinted (section 3.3) are used for the flow measurements.

As discussed before, it is thermodynamically unfavorable for the DNA molecules to spontaneously enter the nanochannels. In addition to electrophoresis, the transient inlets at the entrance of the nanochannels facilitate the entry of molecules into the nanochannels. These funnel like transient inlets are designed to overcome the size mismatch between the micro- and nanochannels, and also to pre-stretch the molecules. It is preferable if the DNA strand is already partly stretched out, before entering the nanochannel.

3D transient inlets

An entropic barrier can be produced by the transition from a low to high confinement such as the transition from a microchannel (where the DNA is allowed to recoil) to a nanochannel. Entropic effect can arise when biopolymers are forced (e.g., by an electric stimulus or a pressure gradient) to interface with the nanostructures with different size or topology.[54] The DNA molecules accumulate at the entrance of the entropic trap array at low electrophoretic force. When the electrophoretic force (respectively hydrodynamic drag) is suddenly increased, the DNA enters the nanochannel. This is schematized in Figure 4.5. The DNA molecules have a worm like behavior when entering through the restricted media in an

extended configuration, and alternatively contract and lengthen as they move. The force gradients experienced by a DNA molecule as it is electrokinetically driven from a microchannel into a nanochannel are highly dependent on the geometry at the nanochannel entrance that defines how abruptly or gradually a DNA molecule experiences the increased confinement.[96] When the DNA molecules are forced to enter a confined area abruptly, they are often trapped and become hooked in a U-shape at the entrance of the nanochannels or the obstacles, and show an elastic behavior. This is schematized in Figure 4.5. (a). The DNA molecule acts upon by the three forces indicated in this Figure.

The electrohydrodynamic force, is the sum of the electrostatic force, acting on the DNA molecule, and the hydrodynamic force induced by the fluid flow in the direction opposite to the DNA migration. The walls of the funnel suppress the fluid backflow around the molecule (Figure 4.5.(b)). The entropic force results from the reduction of conformational degrees of freedom of the DNA molecule as it moves deeper into the nanofunnels inlet. Resisting of the molecule against stretching (due to molecule's elasticity) is another contributor to the entropic force. For each segment of the molecule, the opposing electrohydrodynamic and the entropic forces are unbalanced. This imbalance results in a molecular compression, a dense molecule, and the repulsion increase within the molecule.[96] The magnitudes of the electrohydrodynamic and the entropic forces are dependent upon a molecule's position within the funnel, and thus the molecule is denser at some positions of the inlet more than the other.[96] This concentration gradient results in an osmotic pressure gradient along the longitudinal inlet axis and an osmotic gradient force.[96]

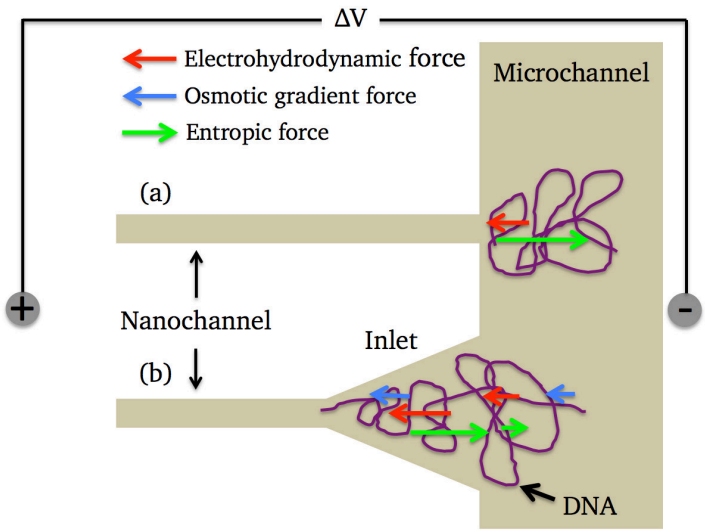

Figure 4.5. Effect of a 3D transient inlet on DNA threading into a nanochannel. (a) without transient inlet. The electrohydrodynamic (red arrow) and entropic (green arrow) forces affecting the leading portion of the DNA molecule, as it is electrophoretically pulled into a nanochannel abruptly under an applied bias, ΔV. Entropic force is greater than the electrohydrodynamic, and DNA accumulates at the entrance of the entropic trap (b) with transient inlet. The mentioned forces and an additional osmotic gradient force (blue arrows) act on the entire DNA molecule as a result of the extended high electric field region and the confining effects of the transient inlet (in contrast to the smaller portion of segments affected in (a)). At the wide entrance to the inlet (its mouth), the electrohydrodynamic force is greater than the entropic force. A smooth transition to the nanochannel is provided.

The gradual and smooth transition from microscale to the nanoscale confinement within our FIB-milled nanofunnels avoids clogging the nanochannel entrance, facilitating a smooth DNA entry into the nanochannels. Beside the indentations, which were fabricated by photolithography, a smooth 3D nanofunnel with a depth decrease to the nanochannel entrance is designed to gradually increase the confinement. As the force acting on the DNA molecule within the nanofunnel drives it towards the nanochannel entrance, the increasing confinement partially extends the DNA molecule, reducing its conformational entropy, as discussed in Figure 4.5. (b). By incorporating a 3D nanofunnel at the nanochannel entrance, the DNA can be more efficiently introduced into the nanochannel without an increase in the electric field strength threshold.

Evaluation of different inlets

The imprinted samples with 3D graded inlets evaluate the DNA molecules behavior in the nanochannels. Figure 4.6. (a) displays a sketch of the linear nanochannels and the inlet configurations of one section of this device. This device has different types of inlets, connecting the microchannel to the nanochannels. Most of the nanochannels in this section are 250 nm wide, except for one of the long nanochannels (channel 2), which is 420 nm

wide, and the most right one (channel 8), which is 210 nm wide. Bacteriophage λ-DNA molecules are stained with YOYO-1 and introduced into the nanofunnels. These entropic traps partly confine the DNA molecules. Platinum electrodes are immersed in the filled reservoirs, and a voltage drop is applied. The DNA molecules are electrokinetically driven into the nanochannels by sweeping the voltage in the range of 30 - 60 V cm^{-1}. Smaller nanochannels require higher voltage drops, since the field strength should be high to avoid the diffusion and the entropic recoil. Videomicroscopy captured the continuous motion of fluorescently stained DNA molecules in their extended state after introduction to the nanochannels or during their driven transport through a nanochannel. The individual hybridized molecules were imaged with an EMCCD camera with 100 ms exposure time.

The individual molecules are imaged while translocation from the inlets towards the nanochannel. When the molecules overcome the entropic barrier, the entire molecule is pulled into the nanochannel. Figure 4.6. (b) shows a fluorescence image of the DNA molecules flowing across the nanochannels sketched in (a). The fluorescence image is obtained by plotting the maximum intensity of each pixel in the 1000 frames of a 100 second long video.[102] This image is a clear overview of the DNA flow in the different inlets and the nanochannels. The time sequences variations of the single molecules passing through the different inlets and the nanochannels are visualized in Figure 4.6. (c – f). The long 3D trapezoidal structure inlet configuration could slow down the DNA molecules at most, as shown in the channel 3 (Figure 4.6 (f)).

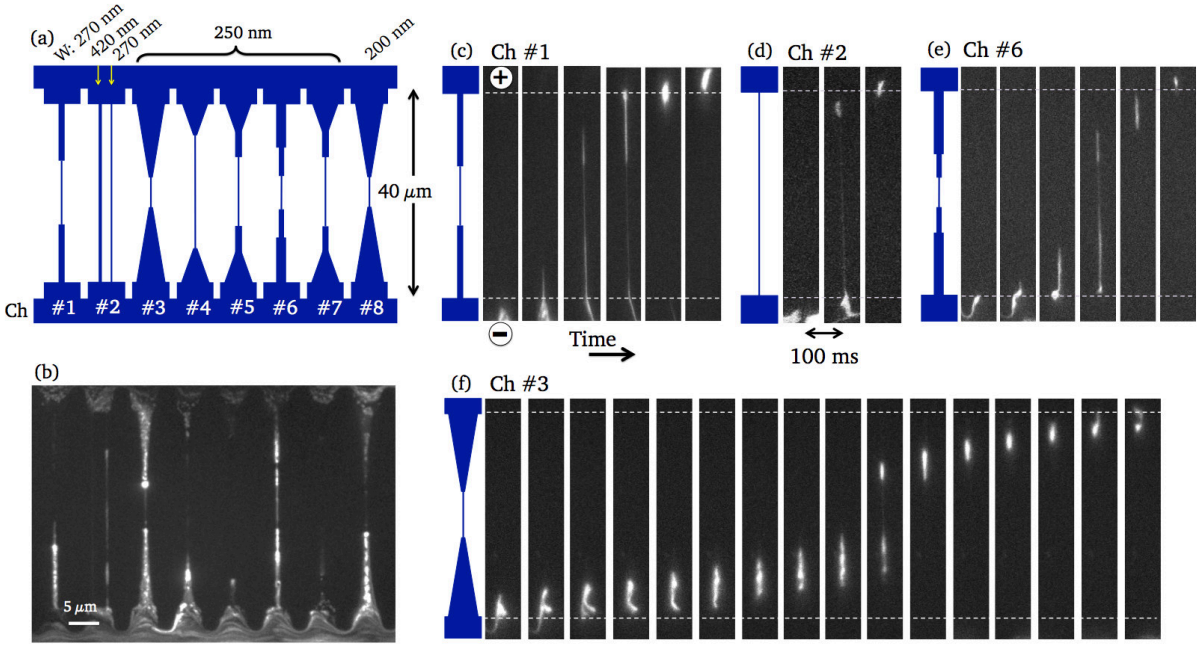

Figure 4.6. Transport of fluorescently labeled λ-DNA molecules within the 3D graded inlets and the nanochannels. (a) the sketch of different inlet configurations and the nanochannels. This section is repeated 3 times within the device with different nanochannel widths. (b) an averaged fluorescence image of the λ-DNA molecules flowing across the nanochannels. The fluorescence image is obtained by plotting the maximum intensity of each pixel from the 1000 frames of a 100-seconds long video. (c – f) recorded frames of a long videomicroscopy representing the position and the conformation of a λ-DNA molecule at various time points as it is electrokinetically driven upwards through a nanofunnel and into the associated nanochannel. The left panel of each category is a sketch showing the position of the nanofunnels, thenanochannel, and the voltage polarity applied across the nanofunnel–nanochannel device. The frames are sequenced from left to right. Inlets with different topographical configurations: (c) one rectangular shape inlet, (d) no inlet, (e) a combination of two rectangular inlets, and (f) long smooth trapezoidal inlet. The translocation times from bottom microchannel to the upward microchannel are very different depending on the inlet configuration (listed in Table 4.1.). DNA molecules are stained with YOYO-1 at the ratio of 1:5 (dye/base pair) at concentration of 0.6 ng/μL. Image frames are captured at 100-ms exposure time.[102]

Pre-stretching effect

We also observed the pre-stretching effects on the molecules passing through the inlets. The comparison of Figure 4.6. (c), (e) and (f) containing an inlet configurations, and (d) with no inlet depicts the pre-stretching influence of the inlets. The translocation time along the entire nanochannel for a given molecule into the channel 1 or 6 with the rectangular inlets is about 0.4 seconds (Figure 4.6. (c, e)). This duration time is extended to 1.5 seconds having the trapezoidal inlet at both ends of the channel 3 (Figure 4.6. (f)). Having no inlets speed up the translocation event along the whole nanochannel to less than 0.1 seconds (Figure 4.6. (d)). As a result of the direct comparison of these structures, we conclude that transient inlets

with gradually decreasing the width and depth improve the flow rate, pre-stretch the molecules and help to smoothen the transition from the micro- to nanochannels. Slowing down the molecules using inlets allows for a better control on the molecule while analyzing them in real time.

Flow throughput in the nanochannels with 3D inlets

The flow throughput along different nanochannels with 3D trapezoidal and rectangular inlets is characterized on several samples. The total number of molecules that passed through each nanochannel in each device for a given amount of time is detailed along with the total flow throughput in the Table 4.1.[102] The flow throughput is defined as the number of the DNA molecules that transit through each nanochannel per minute. The translocation of λ-DNA was recorded in four fluidic devices. The results in Table 4.1. indicate an obvious improve in the flow throughput using a smooth transition from microchannel to the nanochannel, either the rectangular, the trapezoidal inlets or their combination.[102] In addition, the effect of nanochannels dimensions can be directly compared. For instance, channel 3 and 8 have exactly the same inlet configurations, but different channel widths (250 nm and 210 nm, respectively). This leads a 1.3 times greater number of the DNA flow rate across the nanochannel 3, than the channel 8. This is due to a 1.2 times larger cross section of the channel 3, in comparison to the channel 8.[102] The nanochannel 2b is the longest nanochannel without any inlet. We observed a significantly lower number of transitions across this nanochannel. The channel 2a has the same length, but a much greater cross section, which leads in a higher throughput.[102]

Table 4.1. Flow throughput and the translocation time of λ-DNA molecules across different nanochannels with the different inlet configuration. The throughput for each nanochannel has been calculated by counting the number of the DNA molecules that flows through the nanochannels for a certain time interval. This table contains the characterization of four devices.[102]

Channel # (refer to Figure 4.6)	Channel width (nm)	Translocation time (s)	Flow throughput		
			Total molecule	Total time	Molecule/min
1	270	0.4	347	1248	17
2a	420	<0.1	534	1136	28
2b	270	<0.1	42	997	3
3	250	1.5	177	1387	8
6	250	0.4	278	1387	12
8	210	1.5	49	475	6

DNA flow in the meander nanochannels

As discussed in the chapter 3, we have fabricated different types of devices using FIB milling: devices with short linear nanochannels (between 5 and 38 µm long), and with very long (158 µm) meander nanochannels. The folded channels allow the visualization of four times longer molecules, compared to the linear ones. For long DNA molecules, linear nanochannels allow the visualization of only some fragments of the molecules in one frame of the camera. To visualize the entire/or greater fragments of the molecule in one field-of-view, the nanochannels can be folded to form meander patterns.[97] For a smooth transition from the micro- to nanochannels, short triangular inlets are also designed at the both ends of the nanochannels.

In the device validation section, meander nanochannels are verified by the flow measurements of rhodamine B and also the diluted quantum dots. Figure 4.7. shows the translocation of fluorescently labeled λ-DNA molecules through a 400 nm wide, 410 nm deep and 158 µm long meander nanochannel, driven by a voltage drop of about 40 V cm^{-1} across the nanochannel. The molecule enters the nanochannel from the left microchannel, flows along the meandering structures, and exits on the microchannel at right side. The background has been subtracted to facilitate the visualization.[102]

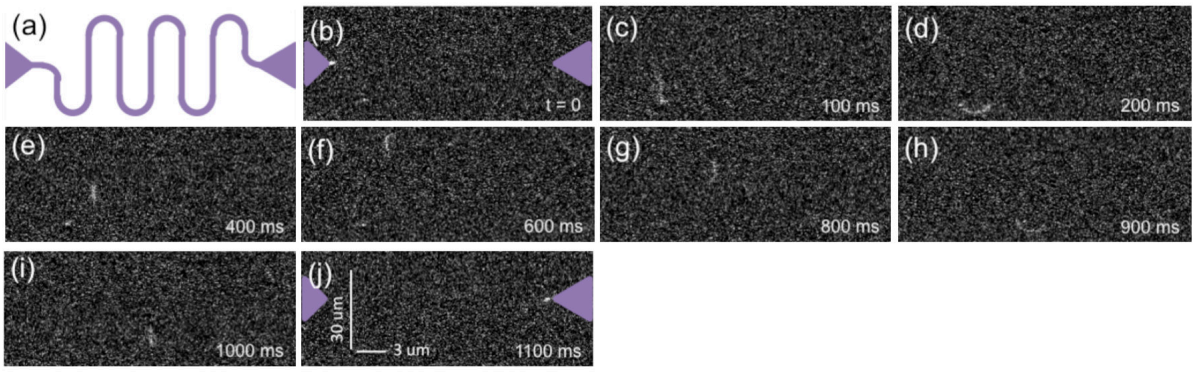

Figure 4.7. Dynamic translocation of an electrophoretically-driven λ-DNA molecule through a long meander nanochannel. Different frames of a movie are extracted to proof the nanochannel continuity. The molecule enters the nanochannel in the microchannel on the left side, is stretched by physical confinement, flipped along the curves, and exit into the microchannel on the right. The exposure time for each image is 100 ms. The images have been elongated along the horizontal axis and the background has been subtracted to facilitate the visualization. The DNA molecules are stained with YOYO-1 at the ratio of 1:5 (dye/base pair).[102]

4.3.4 Single DNA molecule in the EBL nanochannels

The nanochannels fabricated by e-beam lithography have well-defined squared cross sections, produced by an isotropic dry etching. The imprinted devices contain triangular

inlets, but due to the limitation of the resist, they have a constant depth as with the nanochannels, in comparison to multi-level transient inlets made by FIB.

The sub-100 nm wide nanochannels were defined by EBL in PMMA, followed by RIE etching on the silicon wafer as described in section 3.1.2. The linearized DNA molecules are then imaged using an EMCCD camera in an inverted epifluorescence microscopy with a 100×/1.45 NA oil immersion objective. This provides a sequence of frames (videos) for analysis of the DNA stretching. In addition to the imaging by microscopy, the real time measurement using a photon counter will be described, facilitating the single-molecule analysis without any photo-induced damage.

Real time measurements

Here we demonstrate a method to dynamically elongate, rapidly detect, and carefully analyze the single DNA molecules in a nanofluidic channel.

Prolonged illuminating and exciting the fluorescence molecules by an epifluorescence microcopy can induce damages on the molecules. In addition, the noise as a result of thermal drift and the molecule diffusion in imaging by an optical microscope can limit a good signal-to-noise ratio, especially in imaging of the single-molecules. By real time read out measurements of the elongated DNA molecules under a focused laser spot, a photoluminescence intensity signal is achieved along the time, instead of imaging the molecules with a microscope. This improves the resolution as instead of a 1-μm light spot, the focused laser spot is confined in a 100-μm diameter pinhole before striking on the APD. Furthermore, a laser light is monochromatic and, thus, provides a single wavelength in spectral region, whereas the lamps are polychromatic, so that only a small fraction of the light is emitted in the required spectral region. Moreover, this method allows the rapid analysis of a large number of the molecules, for instance, counting the molecules. In this technique, the ultrasensitive detection of the individual molecules is also not limited by the length of the molecule. The PL signal is recorded along the time, as the molecules are dynamically transported in the nanochannels. On-chip detection in real time is a new technology which is possible, due to the improvements in the photon-counting system. This technique has a greater sensitivity to collect more emitted photons from the single-molecules. For fluorescence dyes with nanosecond excited state lifetimes, a single-molecule will need to stay in a laser beam for approximately 10 to 50 µs to generate about 20 photon counts (at 5% overall photon detection efficiency).

Our inverted epifluorescence microscope is equipped with diffraction-limited laser excitations (633 nm and 532 nm), and a high-efficiency single-photon avalanche diode for detection of the single molecules. Figure 4.8. schematized the real time measurement of confined DNA molecules in the nanochannel under a point light source (laser spot).

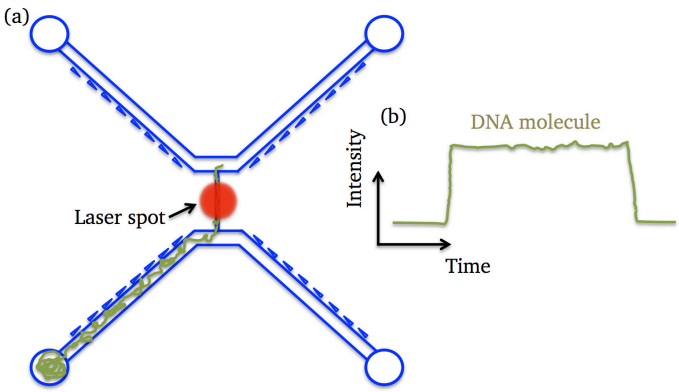

Figure 4.8. Schematic of the real time measurement of the DNA molecules which are dynamically elongated due to the physical confinement in the nanochannel. A focused laser is placed on the nanochannel, where the DNA molecule is linearized. The fluorescence intensity profiles are recorded along the time to illustrate the DNA molecule fluctuations.

The λ-DNA was labeled with TOTO-3 fluorescent dye at the ratio of 1 dye molecule per every 5 base pairs. The red-emitting labels (TOTO-3) have a lower resolution than the blue-emitting ones (YOYO-1). An image of an elongated DNA molecule in a nanochannel and its real time detection is illustrated in Figure 4.9. (a, b). Several signal spikes are recorded as the single molecules enter and then exit under the laser spot in real time (Figure 4.9. (b)). Each spike corresponds to one molecule. By magnifying a single spike, it is clear that the signals have a step-like shape (Figure 4.9. (c)) with a time duration (Δt) which is associated with the total time that the molecule needs to transit the laser spot, as well as an amplitude (ΔI). The lower signal intensity associates with a higher degree of elongation. A costume made software using LabVIEW has been developed for signal analysis of the photon counter module. To calculate the peak duration, the starting point of the event is set as the first point before the intensity rises, and the ending point as the first point after the intensity drop back to the noise level.

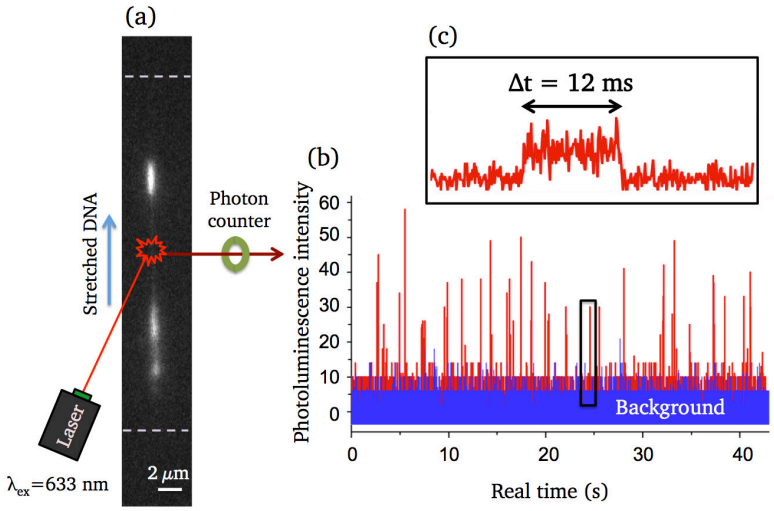

Figure 4.9. In-line real time translocation read out of the λ-DNA molecules confined in a nanochannel. (a) epifluorescence microscopy image of an elongated DNA molecule. Exposure time is 100 ms. (b) the laser spot is focused in the nanochannel where the DNA is elongated and the photoluminescence intensity time traces of the DNA molecules is recorded in real time. Each spike corresponds to one molecule. (c) magnified signal of one molecule. Each step-like signal has a time duration (Δt) which is associated with the total time that the molecule needs to transit the laser spot, and also an amplitude (ΔI). The 633 nm laser wavelength (He:Ne) excited fluorescently labeled DNA by TOTO-3 (1:5 dye/base pair) (λ_{ex}=640 nm, λ_{em}=660 nm), and the molecules are electrophoretically driven along the nanochannel.

To ensure that we have measured single DNA molecules, the measured peak time durations are compared. Single-molecule transit times are significantly long, which means aggregated molecules and artifacts are excluded. The spikes or peaks with short transit times are excluded in the statistics. The frequency or number of detected fluorescence signals depends linearly on the concentration, but the signal intensities remain the same. This is another proof of principle that the molecules are elongated similarly. The signal intensity (ΔI) should show saturation as expected for the stretched single-molecule, discarding the hairpins or backfolding. The PL signal provides a valuable information on the mechanical properties by observation of the thermal fluctuations of the confined DNA. DNA molecules in the nanochannels are free to oscillate under the thermal noise. The oscillations are readily visible as fluctuations of the intensity along the molecule, due to the underlying fluctuations of the density of base pairs. These large amplitude motions are caused by the dynamic structural changes of the DNA molecule, its elasticity of the DNA chain, and the intramolecular forces (i.e., the superhelical formation). In addition, the surface charges on the nanochannel walls affect the conformation of semi-flexible DNA in an aqueous solution at the physiological pH. The negative surface charge has a repulsion effect which repels the molecules and force them to elongate. Photobleaching can be neglected as the molecules pass through the nanochannels only in the range of milliseconds.

Different lengths of DNA molecules

The achieved sensitivity by real time measurements permits detection of different sizes of the single molecules with the respect to the possible application to high throughput screening of substances in the media. A unique approach of this technique for the characterization of particles or other biomolecules is counting the individual molecules as they trnsit an interrogation region. By counting the appeared spikes, the events are quantified. Furthermore, the real time measurement allows characterizing different length of the molecules, such as various DNA molecules. To show the sensitivity of this technique, a mixture of λ-DNA (48.5 kbp) and kaposi's sarcoma-associated herpesvirus (~150 kbp) DNA molecules are fluorescently labeled by TOTO-3 at the ratio of 1:5 (dye/base pair) in a freshly degassed TBE buffer solution. The length distribution of observed fragments is provided in Figure 4.10. KSHV-DNA molecules are three times longer than the λ-DNA, which is clearly in the agreement with the time duration in Figure 4.10. (b), and also statistically in the histogram (c). The three times longer molecules required three times longer time to pass under the laser spot, creating longer step-like peaks in time. The translocation speed is almost constant for both short and long DNA molecules, with a slight increase only for the short fragments.

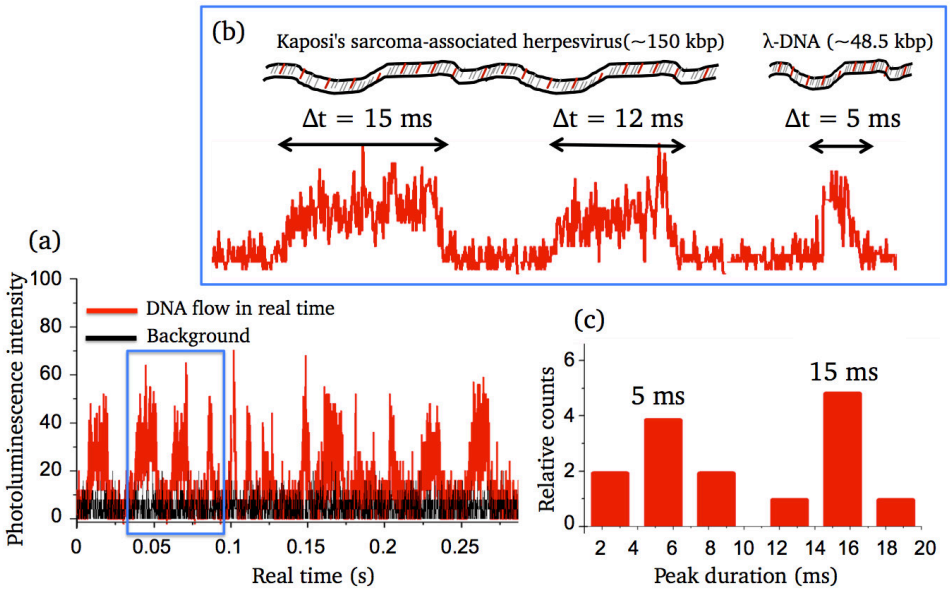

Figure 4.10. Sensitivity evaluation of the real time translocation event measurements of short and long DNA molecules. (a) photoluminescence intensity time traces of a mixture of λ-DNA molecules (48.5 kbp) and kaposi's sarcoma-associated herpesvirus DNA (~150 kbp) fragment molecules in real time. (b) the length of KSHV-DNA molecules is 3 times longer than the λ- DNA molecules. (c) histogram of peak durations (Δt) for both types of the molecules. KSHV-DNA molecules which are 3 times longer in length are statistically shown to have 3 times longer peaks in time. The average Δt for λ-DNA is 5 ms in comparison to 15 ms for KSHV-DNA. The molecules labeled by TOTO-3 at the ratio of 1:5 (dye/base pair), and electrophoretically driven into the nanochannel. A 633 nm laser wavelength (He:Ne) is used.

Backfolding or hairpins formation

The technique of plotting fluorescence intensity along the channel axis over time is a powerful tool for investigating the conformation of DNA molecules inside the nanochannels. In an epifluorescence microscope, the brighter signal of some DNA fragments evidence of folding of the molecules. However, much greater sensitivity even for very small knots is easily observable using the real time measurements. Knowing that the semi-stable stretched DNA molecules are rather relaxed to their equilibrium length inside the nanochannels, they might experience some backfolding or hairpins formations. The molecules exhibit partial folding, which is evidenced by the heightened values in their fluorescence intensity profiles. As depicted in Figure 4.11., some molecules might enter the nanochannels with some folding degrees. Figure 4.11. (b) illustrates the different situations, where (1) the DNA is elongated without folding; (2) the DNA molecule shows some degree of front end folding; (3) the spike like peak shows a folded DNA molecule.

Increasing the applied bias and the electric field will stretch the molecules further. However, the increased difference in the electric field strength between the microchannel and the nanochannel in the device can likely cause for this increased front end folding. A large electric field gradient leads to the random entrance of any part of the DNA molecule that comes close enough to the nanochannel firstly, as looped or folded or hairpin. The high speeds of the molecules in these experiments can increase the probability of the front end folding. The hydrodynamic effects or the interactions with the channel surface may also lead to a compression of the leading strand end.[98]

Folding could be the result of increased hydrodynamic interactions between the parallel strands of the folded molecules. A slight speed increase is observed for molecules with some degrees of folding. Such molecules have smaller ratio of apparent length than the real length. A schematic of the most probable folding situations are given in Figure 4.11.

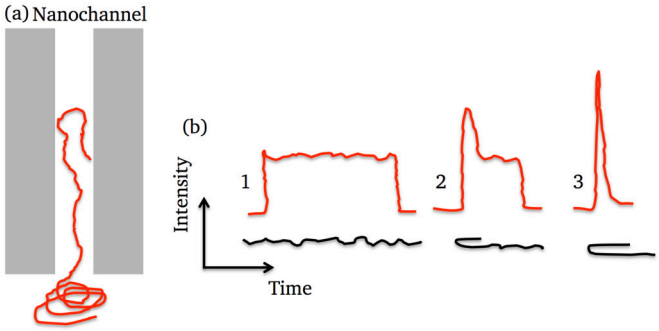

Figure 4.11. Schematic representation of backfolding or hairpin formation on the single molecule level. (a) the DNA molecule enters randomly into the nanochannel, due to its high speed which is the result of the large electric field gradient across the micro- and nanochannel. Hydrodynamic effects or the interactions with the channel surface may also lead to a compression of the leading strand end. (b) different types of intensity time trace signals of (1) the fully stretched DNA molecule; (2) partially folded molecules. Partial increase in the fluorescence intensity profile is an evidence of front end folding. (3) folded molecules. Such spike signals are excluded in the statistics when counting the elongated molecules.

To avoid errors, we concentrated on the molecules, which have almost similar PL intensity that indicates a similar elongation. The lengths of the molecules are measured directly from PL intensity signals.

4.4 Optical mapping

A variety of methods have been employed to manipulate and study the structure of the DNA molecules. A few commercial instruments dedicated to the single DNA sequencing or the sequence mapping are available today. BionanoGENOMICS[103] provides commercial nanofluidics-based single DNA stretching instrument for single molecule mapping. OpGEN[104] creates the whole genome mapping by restriction mapping of the surface tethered DNA using microscopy automation. For sequencing technologies, Oxford Nanopore Technologies[105] commercialized nanopore sequencers. Pacific Biosciences[106] have demonstrated single molecule sequencing based on fluorescence detection of base-by-base incorporation using a sub-diffraction limit optical detection (zero- mode waveguides[99]). Recently, Pacific Biosciences commercialized a single molecule, real time sequencer (SMRT)[107] where 500 kbp fragments are sequenced in parallel at a high accuracy in a shorter time (1 day).

DNA sequencing usually provides a high amount of information through base-by-base sequencing. Even with one of the last commercialized techniques[107] (SMRT from Pacific Biosciences), the DNA molecules are fragmented, and therefore, the long-range information is lost. Amplification of short pieces and reassembling them afterwards to obtain the whole sequence is slow, and sometimes inaccurate, where binding events originate in different genomes is lost.

We studied optical mapping of the DNA barcodes, which can be used directly or facilitate the assembly of short DNA sequences,[52] as a complementary technique to the DNA sequencing. Optical mapping is a simple, high-throughput, and inexpensive method, in which the DNA molecules are not cut, and so the long-range information is preserved to provide the missing contextual information lacking in the sequencing. Optical mapping delivers single-molecule analysis of the genome at the kilobase pair level.

Mapping consists of determining the location of a known short sequence along the DNA molecule in a rapid, repeatable, and reliable fashion. To obtain optical maps, the DNA molecules are barcoded at specific binding sites. DNA barcoding is a method for the quick and accurate identification of any species using one or few short DNA sequences ((400-800 bp)[100] taken from a standard and universally agreed portion of the genome, called DNA barcodes. These specific identification tags are compared to the reference libraries or the databases (sequence matching). The barcodes should be short enough to be quickly sequenced and they should be easily identified in all species of the organisms for rapid discrimination. It is important that they should be long/variable enough to provide a unique sequence for each species.

The process of optical mapping entails two basic steps: (1) building the DNA barcode based on the known information, and (2) elongating and visualizing the DNA molecules in real time, and comparing the signal to the known barcode location for identification.

In this thesis, we generated a unique fluorescent pattern along the genome, using sequence-dependent fluorescent tags to study and identify the DNA molecules. Using this method, a specific mutation or a genetic code configuration is rapidly identified. This section entails optical mapping of the individual barcoded KSHV- and λ-DNA molecules. Circular KSHV-DNA is selectively cleaved by a restriction enzyme, barcoded, stained with an intercalating dye, and stretched in the nanofluidic channels to visualize the presence of the targeted genes. In addition, the λ-DNA molecules are barcoded with netropsin in a competitive binding with intercalating dyes.

The fabricated devices and the proposed techniques in this thesis showed a great potential as the first step of single DNA molecule characterization in the POC diagnostics. The real time measurements of the DNA molecules allows for obtaining a higher resolution optical maps. Especially for the long DNA molecules where stitching of the frames together takes several days of analysis and even induces random errors. By measuring in the real time, the diffusion of fluorophores, the photobleaching and the drifting out of focus can be neglected.

4.4.1 Barcoded kaposi's sarcoma-associated herpesvirus molecules

In the first method, organic dyes are used for tagging the DNA molecules. Organic fluorophores are not as bright and photostable as the quantum dots but are smaller. Their small size will not limit the high density labeling and have a weaker effect on the physiological activity of their biological targets. However, the largest possible number of fluorophores is not used, since such dyes are prone for self-quenching at high densities.[14] DNA molecules are fluorescently labeled at specific sequence locations with sequence-dependent color tags to create an optical pattern resembling a barcode. This unique barcode allows for identifying the DNA fragment.

Barcoding protocol

Kaposi's sarcoma-associated herpesvirus is a herpesvirus, and has a large double-stranded DNA virus. KSHV has a genome of about 150 Kbp in length. This virus which exists as a circular piece. This molecule has several terminal repeat units (each 801 base pair in length). Knowing the sequence of the repeat units, we designed complimentary site probes for those repeat units to barcode the DNA with fluorophores (AT647 and Cy5, eurogins Genomics). Because phototoxicity and the light scattering are reduced at long wavelengths, fluorophores with excitation/emission maxima in the near infrared are preferred for live-cell imaging.[14] We designed two different probes, which their sequences are the complementary sites of those repeat unit terminals. The probes contain a fluorophore for visualization (used as barcodes on those specific binding sites). Based on the molecule map in Figure 4.12., TR probes (containing ATTO dye) have the complimentary sequences of the repeat units which are repeated 40 times, and DR4 probes (containing Cy5 dye) are the complimentary of 2 repeat units.

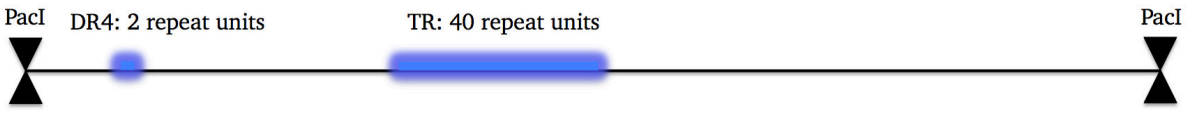

Figure 4.12. Linearized KSHV molecule with the terminal repeat units (each 801 bp). We selected the repeat units, which are repeated 2 times and also 40 times. The designed probes contain the complementary sequences of these repeat units.

9 μL of circular viral genome KSHV containing Bacmid constructs with the concentration of 340 ng/uL is cleaved by PacI restriction enzyme to obtain a linearized molecule. The recognition sequence by this restriction enzyme is 5′-TTAATTAA-3′. Then, 1 μL of DNA was diluted in 4 μL of 1x M-MuLV Reverse Transcriptase reaction buffer supplemented with 1 μL of dNTPs, 1 μL of H_2O, 12 μL of the labeled probes and a mixture of unlabeled random 6-14mer oligonucleotides (details in Table 4.2).

Table 4.2. The mixture reaction vial for barcoding of the KSHV molecules. The probes with fluorophore, and random oligonucleotides are hybridized on their complimentary site of the single stranded molecule to make a barcoded double stranded DNA molecule.

Sequence element	Probe to label (5')	Number of bases	Number of repeat units
DR4	CTGAGGGCTCGCAGTTTCACACAGAAGTTC	30	2
TR	CGCCCTCTCTCTACTGTGCGAGGAGTCTG	29	40

Quantity	Elements
1 μL	340 ng/μL circular DNA
2 μL	random 6
2 μL	random 8
2 μL	random 10
2 μL	random 12
2 μL	random 14
1 μL	DR4 with Cy5 fluorophore
1 μL	TR with ATTO 647 fluorophore
4 μL	Buffer M/ MuLV
1 μL	enzyme
1 μL	dNTP
1 μL	H_2O

Dilution should prevent rehybridization after the denaturation. The mixture was denatured at 95°C for 5 minutes in a thermocycler, and incubated at 60°C for 30 seconds to allow the probes to bind their complementary sites (Figure 4.13). Subsequently the reaction was set to 37°C for 10 minutes to allow the random oligonucleotides to bind. Digestion enzyme M-MuLV RT (Cat-600084-51) was added to fill in the gaps between the probes and the random oligomers. This enzyme does not have an exonuclease activity. This step should result in mainly double stranded DNA with the single strand nicks, which should be suitable to prevent the rehybridization of the virus genome and the formation of partially hybridized aggregates. To remove the unbound probes and the oligonucleotides, the reaction mixture of 80 μL of TE is added, following by centrifuging at 12200 with steps of 2 minutes, 5 minutes, 5 minutes and then 10 minutes respectively, with 500 μL of TE. The last purification is done using Microcon filter device (Millipore).

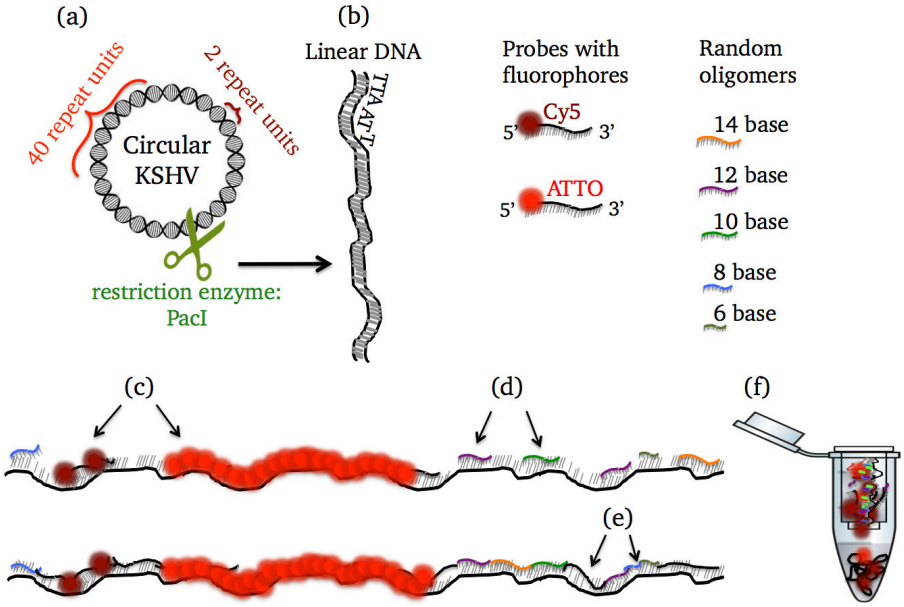

Figure 4.13. Schematics of barcoding KSHV-DNA molecules at its terminal repeat units (each 801 base pairs). TR probes (containing AT647 dye) are the complimentary sites of the 40 terminal repeat units and, DR4 probes (containing Cy5 dye) are complimentary sites of the 2 repeat units. (a) circular viral genome is linearized by a restriction enzyme (PacI). (b) the linearized DNA, the mixture of reaction buffer, the designed probes, and the unlabeled random oligonucleotides for hybridization process is denatured at 95°C for 5 minutes. Double stranded DNA becomes two single stranded. (c) an incubation process at 60°C for 30 seconds allows binding of the probes to their complimentary sequences (sites) on the single stranded DNA. (d) adding another enzyme at 37°C for 10 minutes allows binding of the random oligonucleotides. (e) adding the digestion enzyme fills the gaps in between the probes and random oligomers. This process results in a double stranded DNA molecule. (f) cleaning and purification process: removing the unbound probes and oligonucleotides by centrifuging and using filter devices.

We will stain the backbone of the DNA molecules with intercalating dyes to confirm the presence of the DNA while measuring in real time. Since TOTO-3 has a high affinity of the double stranded DNA, we intentionally created the double stranded at the end of the barcoding process.

Detection of photoluminescence signal of the barcoded DNA

After barcoding a deterministic optical pattern along the molecule, the DNA molecules are stretched out to identify the position of those patterns on the genome. The backbone of double stranded KSHV-DNA molecule is counterstained with the bis-intercalator TOTO-3, which is served as the reference to confirm the presence of the molecule and avoid fake signals. It also shows the beginning and end of the molecule, i.e. length of the molecule. Increasing the PL intensity signal from the noise level evidences the beginning of the molecule, and the intensity drops determines the end of the DNA molecule.

A 633 nm laser wavelength is selected to detect specific fluorophore tags of the intercalated DNA. The excitation and the emission wavelength of all fluorophores are in the range of the chosen laser wavelength ($\lambda_{ex}/\lambda_{em}$ of TOTO-3: 642 nm/660 nm, ATTO 647: 643 nm/664 nm, Cy5: 646 nm/673 nm). Once extended, the DNA molecule passed through a focused laser spot, and the emission wavelengths are read out in real time to visualize the barcode. This unique sequence-specific marks along the DNA are shown in Figure 4.14.

The base line shows the DNA molecule, and the intensity increase at specific locations along the signal evidences the presence of other fluorophores at those sites. This detected increase in the signal is in agreement with the expected locations.

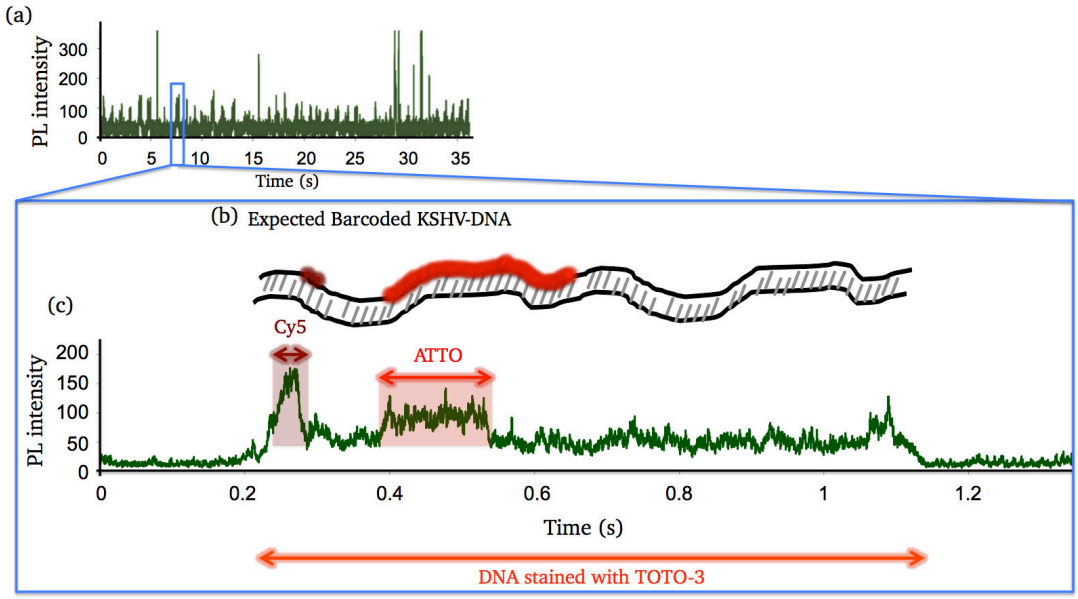

Figure 4.14. Real time optical mapping of barcoded KSHV-DNA molecule. Individual fluorescently tagged DNA containing a barcode is electrophoretically driven into the nanochannel and stretched by physical confinement. The fluorescent tags and the backbone dyes of the DNA molecule is excited by a focused laser spot. (a) The photoluminescence signal is recorded as it passed through under the point light source in real time. (b) schematic of the expected barcode of the DNA molecule. (c) the smooth PL recorded signal along time. The presence of the molecule is confirmed by an increase and then drop in intensity profile signal along time. The distance between the sequence-specific markers is comparable with expected schematic in (b).

Usually, thermal (Brownian) fluctuations of the molecule that induce distortions of the barcode. However, since we measure the molecules in real time at high sensitivity, small features are not blurred out due to thermal fluctuation and diffusion. All the measurements have been performed at room temperature. Any knowledge concerning the exact location of a large scale mutation is still unknown when using this technique.

Using this technique, the detection of changes along the DNA molecules takes place only in the time frame of seconds to minutes instead of day(s) to weeks as in the conventional

sequencing techniques. This technique can reveal the preliminary results in a quick manner and facilitates in decision making for further analysis using more sophisticated, time consuming, and expensive techniques.

4.4.2 Barcoded λ- bacteriophage DNA

The first technique can only be implemented on a specific DNA type, as the probes are designed to contain the complementary sequences of the repeat units of the DNA molecules. The second technique is however independent of the DNA type and can be implemented on any type of the DNA molecules. However, in the first technique, knowing the sequence of repeat units is only required to design their complementary probes. Although in the second technique, knowing the sequence of the whole DNA molecule is required. In the second technique the aim is rather to rapidly discriminate the different types of the DNA molecules by a comparison of the measured signal with the expected single using the available sequences from the library.

The aim of second method of optical mapping is to rapidly identify the DNA molecules by comparing the experimental barcodes to a database of the theoretical profile (reference). This technique is not limited to a specific type of the DNA molecule, but knowing the exact sequence of the molecule is required. A theoretical profile is created based on the sequence of understudied DNA, which allows identifying the molecule experimentally.

This technique is a complementary approach for labeling the DNA, based on competitive binding. In this technique we use a non-fluorescent molecule (netropsin) that binds specifically to the AT-rich regions of the DNA molecule. Creating a barcode in a competitive binding technique is based on a competition between the non-fluorescent molecule of netropsin and an intercalating dye. Netropsin binds to AT sites, blocking these bases from the intercalating dyes, creating an emission profile along the DNA, where the AT-rich regions are dark (low emission intensity), and GC-rich regions bright (high emission intensity). This leads to an inhomogeneous distribution of the intercalating dyes (TOTO-3) along the DNA molecule due to the counterstaining. The obtained intensity profile serves as a “barcode” for the type of the DNA molecule, based on the underlying sequence. Using this technique, the separation of different DNA molecules based on their sequence is feasible.

Barcoding protocol

Netropsin is a non-fluorescent molecule which binds to the AT-rich regions of the DNA molecule, limiting the binding of the fluorescent dyes at this position. When simultaneously adding the netropsin and TOTO-3, the molecules will compete for the binding sites on the λ-DNA. This competition generates a sequence specific pattern along the DNA molecule, resulting in an overall lower emission from AT-rich regions than from GC-rich regions along the extended DNA molecule.

For 100 µL of stained DNA, counterstained with netropsin, 1 µg of λ-DNA is mixed with netropsin and TOTO-3. The ratio of TOTO-3 molecules to DNA base pairs is 1:10, and the ratio of netropsin molecules (Sigma-Aldrich) to TOTO-3 molecules is 4000:1. The suspension is incubated for 2 hours at 50°C and, stored at -20C until use. Before each experiment, 0.2 μL Triton is added to the freshly degassed TBE buffer, and loaded on the one reservoir. The best results are obtained if experiments are performed shortly after staining of the DNA. Here, netropsin blocks the AT-sites, preventing TOTO-3 to bind, rendering an emission intensity profile along the DNA, where AT-rich regions appear dark, and GC-rich regions are bright.

Detection of photoluminescence signal of barcoded DNA

The generated barcode along the λ-DNA is served as a fingerprint of the underlying sequence. In order to reveal the sequence specific pattern, the electrophoretically driven DNA molecule is linearized by confinement. The intensity transverse to the nanochannel axis is plotted along the nanochannel in real time, as illustrated in Figure 4.15. Interpretation of the site-specific fluorescent tagging was achieved by comparing the single molecule fluorescence intensity profiles to a database of theoretically predicted templates (reference). The theory barcodes were generated based on a binary version of the genetic code, where ATs are converted into either ones or zeros, for netropsin. For the convolution, a Gaussian profile having a standard deviation of 200 nm is used to simulate broadening due to resolution limit of optical setup.

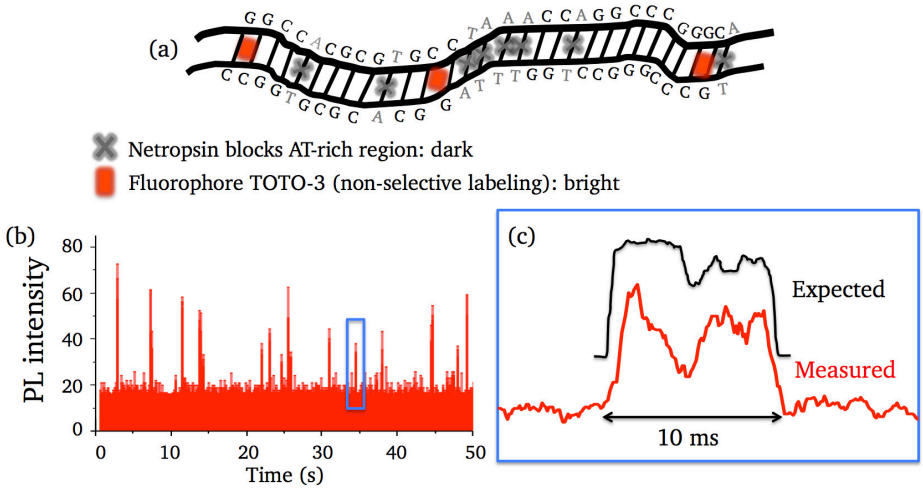

Figure 4.15. Real time optical mapping of the λ-DNA with competitive binding between netropsin and TOTO-3. (a) schematic representation of the sequence specific barcoding of the DNA molecules. Netropsin binds to the AT-rich regions of the DNA, lowering the binding of the TOTO-3 at those regions. The binding sites of netropsin are shown as gray cross, while TOTO-3 intercalates the DNA molecule base pairs at red lines. (b) emission intensity profile of the DNA molecules flowing in the nanochannel. (c) Comparison of the experimental consensus barcode of the DNA with the corresponding expected barcode. The smooth experimental data shows a clear correspondence to the smooth expected signals and the level of AT/CG content.

The smooth experimental data shows a clear correspondence to the expected signal, and the level of AT/GC content in the molecule.

The comparison of expected and experimental spectra demonstrates a proof of concept that direct barcoding using counterstaining against TOTO-3 with AT selective ligands can facilitate the fast identification of specific DNA samples. Competitive binding with netropsin is specifically beneficial to the molecules which have large GC concentration. In this case, netropsin molecules leave the GC sites mostly free, and the fluorophores will bind to the residual regions of the high AT concentration.

Chapter 5:

Summary and Outlook

5.1 Summary

This thesis describes the fabrication process of an integrated micro- and nanofluidic device for detection and optical mapping of the single molecules. The simple and robust nanofluidic platforms are capable of effectively detecting and identifying dyes binding sites along the stretched single DNA molecules. The optical maps of kaposi's sarcoma-associated herpesvirus and λ-DNA molecules are obtained in real time with single-molecule precision.

The robust fabrication of these lab-on-a-chip devices is based on the combination of the versatile, high resolution patterning capabilities of focused ion beam milling and electron beam lithography with the high throughput ultraviolet nanoimprint lithography. Complete fluidic circuits are sculptured first in a silicon stamp. These contain the microchannels, the nanochannels with different depths and layouts, together with the transient inlets to facilitate and smoothen the flow. Then, a negative polymeric replica is replicated from the silicon stamp, made by nanoimprint lithography. This negative stamp is further used to imprint the complete fluidic sample in a two-minute nanoimprint step. This approach greatly simplifies the fabrication of micro- and nanofluidic devices with well-controlled dimensions and layouts. The final disposable polymeric biochips are fabricated using a simple imprint-and-bond scheme in a parallel replication method, which is highly suitable for mass-production of high quality devices. Using disposable devices avoids the cross contamination, as a new chip can be used for each new experimental run.

The microfluidic part, fabricated by conventional photolithography, has 20 μm wide and 1 μm deep microchannels. The microchannels are served to transfer the molecules of interest from the reservoir inputs towards the nanofluidics. The nanofluidic part, fabricated with focused ion beam or electron beam lithography, contains nanochannels in the range of 50 nm – 400 nm wide, and 80 nm – 100 nm deep. Short or long nanochannels in the linear or meander shape configurations contain transient inlets at their both ends. The effect of different transient inlet configurations for DNA pre-stretching, before confinement in the nanochannel is also studied. We conclude that nanofunnel 3D inlets, in any shape of trapezoidal/triangular/rectangular, ensure a smooth transition of the DNA molecules from micro- to nanochannels. The best results of pre-stretching are achieved by longer 3D inlets with gradually increasing the width and depth. Those inlets decelerate the DNA molecules flow for a better control on the molecules while characterizing. The abrupt transitions from the microchannel to the nanochannels should be avoided, due to the low throughput and the clogging issues.

The molecules are examined while physically confined or elongated (in case of DNA molecules) in the nanochannels. The imprinted structures have a high pattern replication fidelity and no signs of stamp degradation have been observed after several tens of imprints. The fidelity of the imprinted polymer devices is evaluated by the flow measurements of

rhodamine B diluted in isopropanol, which proves the continuity of the nanochannels, and also by using the point-microspectroscopy which confirms the liquid confinement and discards the leaks. Physical confinement of the suspended QDs in toluene allows approaching the individual QDs inside the nanochannels, and also studying their blinking behavior.

The main application of such lab-on-chip micro- and nanofluidic devices is the rapid ultrasensitive screening of the DNA molecules, or counting of different DNA fragments. We demonstrated an effective elongation of the DNA molecules in the short/long linear or meander nanochannels. High sensitive real time observation of the fluorescently labeled DNA molecules is determined by differentiating the λ-DNA and kaposi's sarcoma-associated herpesvirus molecules based on their lengths along time.

The goal of this thesis is on-chip read out of the genetic maps (single optical DNA mapping) for rapidly identification of mutations. The real time recorded photoluminescence time traces visualize the sequence specific barcodes along the DNA molecules as they transit through a focused laser spot at the nanochannel. Two different techniques for barcoding the DNA molecules are used. Kaposi's sarcoma-associated herpesvirus DNA molecules are tagged with organic fluorophores (ATTO and Cy5) at sequence-specific sites (terminal repeat units). Furthermore, λ-DNA molecules were counterstained with netropsin molecule, which binds specifically to AT-rich regions of the DNA. A competitive binding between the netropsin and the intercalating dye (TOTO-3) leads to an inhomogeneous distribution of the dye, creating a barcode. The intensity profiles of the experimentally obtained genetic barcodes of both methods are compared to the expected signals. The developed techniques are based on the direct measurement of the recorded fluorescent signals, free from biases introduced by cloning, cleaving, amplification, reassembling or hybridization. Optical mapping provides a long range content of the molecule which can be a complement to sequencing for reassembling short reads obtained from DNA sequencing.

We conclude that we have developed a platform that is versatile and can be used for a simple and quick analysis of long barcoded DNA single-molecules. Our method has a variety of potential benefits relative to traditional techniques, such as screening and manipulating longer DNA fragments at high-speed and high-throughput, with greater reliability. The disposable, affordable and portable fabricated devices together with the proposed characterization techniques in this thesis showed a great potential as a first step of single DNA molecule characterization in personalized medicine, in point of care, and also early disease diagnostics.

5.2 Outlook

In this section, we will share our opinions on the future development, innovation, and optimization of the lab-on-a-chip techniques for single molecule studies.

A fundamental question related to DNA analysis is the sensitivity and the detection resolution. As an example, the ability to resolve two nearby barcodes on the DNA backbone in the optical mapping allows for the ultrasensitive analysis of mutation locations. The sensitivity is mostly referred to the strength of the light-matter interaction. The limit in detection depends on the resolution of the optical read out system and the experimental noise. We showed, an improvement in the resolution of detected signal using real time measurements by a photon counting system. However, the optical microscopes are inherently limited to the diffraction limit of light, and the best resolution for optical mapping of the DNA molecules is 1 kbp.[43] The sensitivity of the lab-on-a-chip devices can be further enhanced by integration of biosensors in the vicinity of nanochannels. Plasmonic nanoantenna pair creates a localized hot spot with enhanced local electromagnetic field intensity by confinement of the incident light energy at the nanoscale gaps.[101] If the molecule of interest is delivered to the hotspot, a higher sensitivity of the emission photoluminescence signal is obtained. In addition, plasmonic confinement of the light enables resolution of a higher tag density on the DNA molecules. As mentioned in the Chapter 3, we fabricated a silicon stamp with 50 nm wide nanochannels and the bowties adjacent to the nanochannel walls. The bowties were filled with gold to perform as a plasmonic nanoantenna. If resonated under the right conditions, the DNA molecules experience a very intense optical field and the resolution is enhanced. Since the signal enhancement is in direct relation with the bowties tip-to-tip gap, considering a gap of 55 nm as fabricated during this thesis, a resolution of about 150 base pair is achievable. This allows for resolving two nearby barcodes with the distance of 150 base pair, instead of 1 kbp resolution at the best condition with optical microscopes. Having double pairs of bowtie nanoantenna, the length of an extended DNA molecule can be measured precisely from the translocation time.

Another potential application in the sensitive optoelectronic devices is the label-free detection of the minimum amounts of substances. In the real life application, the optofluidics devices should be capable of detecting concentrations which are normally found in human fluids at the start of a disease (such as in cancer) or in contaminated water or food. The lower the limit of detection, the earlier the disease or the pollutant could be detected. In addition, label free measurements allow for the analysis of the intact molecules, and so, the expensive fluorophores are not required.

Our rapid single-molecule real time measurement system can be also automatized for even higher throughput. Automation allows for an enhanced functionality by integration of complex electrical control, mechanical properties, in situ sensing, and flow control.

6 Appendix

6.1 List of the chemicals

Chemicals	Symbol	Hazard statement	Precautionary statement
Acetone	GHS02 GHS07	H225 H319 H336	P210 P261 P303+P361+P353 P305+P351+P338 P405 P501
Poly(methyl methacrylate) 950	GHS02 GHS08 GHS09 GHS07	H226 H302+H332 H315 H319 H335 H372 H411	P210 P260 P280 P233 P273 P301+P312 P403+P235 P501
2-Propanol	GHS02 GHS07	H225 H319 H336	P210 P233 P305 + P351 + P338
Toluene	GHS02 GHS07 GHS08	H225 H304 H315 H336 H361d H373	P210 P261 P281 P301 + P310 P331
Netropsin	GHS06	H301	P301 310
Microposit S1813	GHS02	Not applicable	Not applicable
Anisole	GHS02 GHS07	H226 H303 H315 H319 H401 H332 H335	P305 P351 P338
Microposit MF-319 developer	GHS08 GHS07	Not applicable	Not applicable

Adhesion promotor AR 300-80	GHS02	H226	P210 P261 P303+P361+P353 P403+P235
Developer AR 600-56	GHS02 GHS07	H225 H319 H332 H335 H336	P210 P261 P280 P304+P340 P305+P351+P338 P312 P403+P233
1H,1H,2H,2H-Perfluorodecyltrichlorosilane	GHS05	H314	P260 P303+P361+P353 P305+P351+P338 P301+P330+P331 P405 P501

1. Metzker, M. L., Sequencing technologies - the next generation. *Nat Rev Genet* **2010,** *11* (1), 31-46.

2. Finishing the euchromatic sequence of the human genome. *Nature* **2004,** *431* (7011), 931-45.

3. Hert, D. G.; Fredlake, C. P.; Barron, A. E., Advantages and limitations of next-generation sequencing technologies: a comparison of electrophoresis and non-electrophoresis methods. *Electrophoresis* **2008,** *29* (23), 4618-26.

4. Alkan, C.; Sajjadian, S.; Eichler, E. E., Limitations of next-generation genome sequence assembly. *Nature methods* **2011,** *8* (1), 61-5.

5. Jokerst, J. V.; Jacobson, J. W.; Bhagwandin, B. D.; Floriano, P. N.; Christodoulides, N.; McDevitt, J. T., Programmable nano-bio-chip sensors: analytical meets clinical. *Analytical chemistry* **2010,** *82* (5), 1571-9.

6. Ligler, F. S., Perspective on Optical Biosensors and Integrated Sensor Systems. *Analytical chemistry* **2009,** *81* (2), 519-526.

7. Meng, X.; Benson, K.; Chada, K.; Huff, E. J.; Schwartz, D. C., Optical mapping of lambda bacteriophage clones using restriction endonucleases. *Nature Genetics* **1995,** *9*, 432.

8. Zhou, S.; Wei, F.; Nguyen, J.; Bechner, M.; Potamousis, K.; Goldstein, S.; Pape, L.; Mehan, M. R.; Churas, C.; Pasternak, S.; Forrest, D. K.; Wise, R.; Ware, D.; Wing, R. A.; Waterman, M. S.; Livny, M.; Schwartz, D. C., A single molecule scaffold for the maize genome. *PLoS genetics* **2009,** *5* (11), e1000711.

9. Levy-Sakin, M.; Ebenstein, Y., Beyond sequencing: optical mapping of DNA in the age of nanotechnology and nanoscopy. *Current opinion in biotechnology* **2013,** *24* (4), 690-8.

10. Levy-Sakin, M.; Grunwald, A.; Kim, S.; Gassman, N. R.; Gottfried, A.; Antelman, J.; Kim, Y.; Ho, S. O.; Samuel, R.; Michalet, X.; Lin, R. R.; Dertinger, T.; Kim, A. S.; Chung, S.; Colyer, R. A.; Weinhold, E.; Weiss, S.; Ebenstein, Y., Toward single-molecule optical mapping of the epigenome. *ACS nano* **2014,** *8* (1), 14-26.

11. Lam, E. T.; Hastie, A.; Lin, C.; Ehrlich, D.; Das, S. K.; Austin, M. D.; Deshpande, P.; Cao, H.; Nagarajan, N.; Xiao, M.; Kwok, P. Y., Genome mapping on nanochannel arrays for structural variation analysis and sequence assembly. *Nature biotechnology* **2012,** *30* (8), 771-6.

12. Inman, R. B., A denaturation map of the lambda phage DNA molecule determined by electron microscopy. *Journal of molecular biology* **1966,** *18* (3), 464-76.

13. Craighead, H., Future lab-on-a-chip technologies for interrogating individual molecules. *Nature* **2006,** *442* (7101), 387-93.

14. Kubitscheck, U., *Kubitscheck, U. 2013.* Principles of Light Microscopy, In "Fluorescence Microscopy: From Principles to Biological Applications*", edited by Ulrich Kubitscheck. Wiley-VCH, Weinheim, 1st edition, 527 pages*. 2013.

15. Rotman, B., Measurement of activity of single molecules of beta-D-galactosidase. *Proc. Natl. Acad. Sci. U. S. A.* **1961,** *47*, 1981-91.

16. Moerner, W. E.; Kador, L., Optical detection and spectroscopy of single molecules in a solid. *Physical review letters* **1989,** *62* (21), 2535-2538.

17. Rahman, M. A.; Zafar, G.; Shera, A. S., Changes in glycosylated proteins in long-term complications of diabetes mellitus. *Biomedicine & pharmacotherapy = Biomedecine & pharmacotherapie* **1990,** *44* (4), 229-34.

18. Sonnleitner, A.; Schutz, G. J.; Schmidt, T., Free Brownian motion of individual lipid molecules in biomembranes. *Biophysical journal* **1999,** *77* (5), 2638-42.

19. Bustamante, C.; Bryant, Z.; Smith, S. B., Ten years of tension: single-molecule DNA mechanics. *Nature* **2003,** *421* (6921), 423-7.

20. Altissimo, M., E-beam lithography for micro-nanofabrication. *Biomicrofluidics* **2010,** *4* (2).

21. Saifullah, M. S. M.; Ondarçuhu, T.; Koltsov, D. K.; Joachim, C.; Welland, M. E., A reliable scheme for fabricating sub-5 nm co-planar junctions for single-molecule electronics. *Nanotechnology* **2002,** *13* (5), 659.

22. Gierak, J.; Jede, R.; Hawkes, P., Nanofabrication with Focused Ion Beams. In *Nanofabrication Handbook*, 2012; pp 41-84.

23. Raffa, V.; Castrataro, P.; Menciassi, A.; Dario, P., Focused Ion Beam as a Scanning Probe: Methods and Applications. In *Applied Scanning Probe Methods II: Scanning Probe Microscopy Techniques*, Bhushan, B.; Fuchs, H., Eds. Springer Berlin Heidelberg: Berlin, Heidelberg, 2006; pp 361-412.

24. Lindquist, N. C.; Nagpal, P.; McPeak, K. M.; Norris, D. J.; Oh, S. H., Engineering metallic nanostructures for plasmonics and nanophotonics. *Reports on progress in physics. Physical Society (Great Britain)* **2012,** *75* (3), 036501.

25. Turner, S. W.; Cabodi, M.; Craighead, H. G., Confinement-induced entropic recoil of single DNA molecules in a nanofluidic structure. *Physical review letters* **2002,** *88* (12), 128103.

26. Bonthuis, D. J.; Meyer, C.; Stein, D.; Dekker, C., Conformation and dynamics of DNA confined in slitlike nanofluidic channels. *Physical review letters* **2008,** *101* (10), 108303.

27. Stein, D.; van der Heyden, F. H.; Koopmans, W. J.; Dekker, C., Pressure-driven transport of confined DNA polymers in fluidic channels. *Proc. Natl. Acad. Sci. U. S. A.* **2006,** *103* (43), 15853-8.

28. Shelton, E.; Jiang, Z.; Wang, S.; Stein, D., Controlling the conformations and transport of DNA by free energy landscaping. **2011,** *99* (26), 263112.

29. Zhou, W.; Huang, y.-s.; Menard, E.; R. Aluru, N.; Rogers, J. A.; Alleyne, A. G., *Mechanism for stamp collapse in soft lithography*. 2005; Vol. 87, p 251925-251925.

30. Goswami, A.; Umashankar, R.; Gupta, A. K.; Aravindan, S.; Rao, P. V., Development of a microstructured surface using the FIB. *Journal of Micromanufacturing* **2018,** *1* (1), 53-61.

31. Gierak, J., *Focused Ion Beam nano-patterning from traditional applications to single ion implantation perspectives*. 2014; Vol. 1.

32. Han, J.; Turner, S. W.; Craighead, H. G., Entropic Trapping and Escape of Long DNA Molecules at Submicron Size Constriction. *Physical review letters* **1999,** *83* (8), 1688-1691.

33. Forbest, R. G., Understanding how the liquid-metal ion source works. *Vacuum* **1997,** *48* (1), 85-97.

34. Schift, H.; Kristensen, A., Nanoimprint Lithography – Patterning of Resists Using Molding. 2009; pp 271-312.

35. Duan, C.; Wang, W.; Xie, Q., Review article: Fabrication of nanofluidic devices. *Biomicrofluidics* **2013,** *7* (2), 26501.

36. Xia, D.; Yan, J.; Hou, S., Fabrication of nanofluidic biochips with nanochannels for applications in DNA analysis. *Small (Weinheim an der Bergstrasse, Germany)* **2012,** *8* (18), 2787-801.

37. Tegenfeldt, J. O.; Prinz, C.; Cao, H.; Chou, S.; Reisner, W. W.; Riehn, R.; Wang, Y. M.; Cox, E. C.; Sturm, J. C.; Silberzan, P.; Austin, R. H., From the Cover: The dynamics of genomic-length DNA molecules in 100-nm channels. *Proc. Natl. Acad. Sci. U. S. A.* **2004,** *101* (30), 10979-83.

38. Pu, Q.; Yun, J.; Temkin, H.; Liu, S., Ion-Enrichment and Ion-Depletion Effect of Nanochannel Structures. *Nano Letters* **2004,** *4* (6), 1099-1103.

39. Stamatoyannopoulos, J. A.; Adzhubei, I.; Thurman, R. E.; Kryukov, G. V.; Mirkin, S. M.; Sunyaev, S. R., Human mutation rate associated with DNA replication timing. *Nature Genetics* **2009,** *41*, 393.

40. Chaffey, N., Alberts, B., Johnson, A., Lewis, J., Raff, M., Roberts, K. and Walter, P. Molecular biology of the cell. 4th edn. *Annals of Botany* **2003,** *91* (3), 401-401.

41. Watson, J. D.; Crick, F. H., The structure of DNA. *Cold Spring Harbor symposia on quantitative biology* **1953,** *18*, 123-31.

42. Levy, S. L.; Craighead, H. G., DNA manipulation, sorting, and mapping in nanofluidic systems. *Chemical Society reviews* **2010,** *39* (3), 1133-52.

43. Wang, Y.; Reinhart, W. F.; Tree, D. R.; Dorfman, K. D., Resolution limit for DNA barcodes in the Odijk regime. *Biomicrofluidics* **2012,** *6* (1), 14101-141019.

44. Houseal, T. W.; Bustamante, C.; Stump, R. F.; Maestre, M. F., Real-time imaging of single DNA molecules with fluorescence microscopy. *Biophysical journal* **1989,** *56* (3), 507-516.

45. Das, S. K.; Austin, M. D.; Akana, M. C.; Deshpande, P.; Cao, H.; Xiao, M., Single molecule linear analysis of DNA in nano-channel labeled with sequence specific fluorescent probes. *Nucleic acids research* **2010,** *38* (18), e177-e177.

46. Lam, E. T.; Hastie, A.; Lin, C.; Ehrlich, D.; Das, S. K.; Austin, M. D.; Deshpande, P.; Cao, H.; Nagarajan, N.; Xiao, M.; Kwok, P.-Y., Genome mapping on nanochannel arrays for structural variation analysis and sequence assembly. *Nature biotechnology* **2012,** *30* (8), 771-776.

47. Reisner, W.; Larsen, N. B.; Silahtaroglu, A.; Kristensen, A.; Tommerup, N.; Tegenfeldt, J. O.; Flyvbjerg, H., Single-molecule denaturation mapping of DNA in nanofluidic channels. *Proc. Natl. Acad. Sci. U. S. A.* **2010,** *107* (30), 13294-13299.

48. Welch, R. L.; Sladek, R.; Dewar, K.; Reisner, W. W., Denaturation mapping of Saccharomyces cerevisiae. *Lab on a Chip* **2012,** *12* (18), 3314-3321.

49. Baumann, C. G.; Smith, S. B.; Bloomfield, V. A.; Bustamante, C., Ionic effects on the elasticity of single DNA molecules. *Proc. Natl. Acad. Sci. U. S. A.* **1997,** *94* (12), 6185-90.

50. Thamdrup, L. H.; Klukowska, A.; Kristensen, A., Stretching DNA in polymer nanochannels fabricated by thermal imprint in PMMA. *Nanotechnology* **2008,** *19* (12), 125301.

51. Bouchiat, C.; Wang, M. D.; Allemand, J.; Strick, T.; Block, S. M.; Croquette, V., Estimating the persistence length of a worm-like chain molecule from force-extension measurements. *Biophysical journal* **1999,** *76* (1 Pt 1), 409-13.

52. Dai, L.; Renner, C. B.; Doyle, P. S., The polymer physics of single DNA confined in nanochannels. *Advances in colloid and interface science* **2016,** *232*, 80-100.

53. Becker, H.; Locascio, L. E., Polymer microfluidic devices. *Talanta* **2002,** *56* (2), 267-87.

54. Manneschi, C.; Fanzio, P.; Ala-Nissila, T.; Angeli, E.; Repetto, L.; Firpo, G.; Valbusa, U., Stretching of DNA confined in nanochannels with charged walls. *Biomicrofluidics* **2014,** *8* (6), 064121.

55. Ladoux, B.; P Quivy, J.; Doyle, P.; Almouzni, G.; L Viovy, J., *Direct imaging of single molecules: from dynamics of a single DNA chain to the study of complex DNA-protein interactions*. 2001; Vol. 84, p 267-90.

56. Reisner, W.; Beech, J. P.; Larsen, N. B.; Flyvbjerg, H.; Kristensen, A.; Tegenfeldt, J. O., Nanoconfinement-enhanced conformational response of single DNA molecules to changes in ionic environment. *Physical review letters* **2007,** *99* (5), 058302.

57. Jo, K.; Dhingra, D. M.; Odijk, T.; de Pablo, J. J.; Graham, M. D.; Runnheim, R.; Forrest, D.; Schwartz, D. C., A single-molecule barcoding system using nanoslits for DNA analysis. *Proc. Natl. Acad. Sci. U. S. A.* **2007,** *104* (8), 2673-8.

58. Riehn, R.; Austin, R. H.; Sturm, J. C., A nanofluidic railroad switch for DNA. *Nano Lett* **2006,** *6* (9), 1973-6.

59. Reisner, W.; Larsen, N. B.; Silahtaroglu, A.; Kristensen, A.; Tommerup, N.; Tegenfeldt, J. O.; Flyvbjerg, H., Single-molecule denaturation mapping of DNA in nanofluidic channels. *Proc. Natl. Acad. Sci. U. S. A.* **2010,** *107* (30), 13294-9.

60. Kim, Y.; Kim, K. S.; Kounovsky, K. L.; Chang, R.; Jung, G. Y.; dePablo, J. J.; Jo, K.; Schwartz, D. C., Nanochannel confinement: DNA stretch approaching full contour length. *Lab Chip* **2011,** *11* (10), 1721-9.

61. Odijk, T., The statistics and dynamics of confined or entangled stiff polymers. *Macromolecules* **1983,** *16* (8), 1340-1344.

62. Persson, F.; Utko, P.; Reisner, W.; Larsen, N. B.; Kristensen, A., Confinement spectroscopy: probing single DNA molecules with tapered nanochannels. *Nano Lett* **2009,** *9* (4), 1382-5.

63. Reisner, W.; Morton, K. J.; Riehn, R.; Wang, Y. M.; Yu, Z.; Rosen, M.; Sturm, J. C.; Chou, S. Y.; Frey, E.; Austin, R. H., Statics and dynamics of single DNA molecules confined in nanochannels. *Physical review letters* **2005,** *94* (19), 196101.

64. Reha, D.; Kabelac, M.; Ryjacek, F.; Sponer, J.; Sponer, J. E.; Elstner, M.; Suhai, S.; Hobza, P., Intercalators. 1. Nature of stacking interactions between intercalators (ethidium, daunomycin, ellipticine, and 4',6-diaminide-2-phenylindole) and DNA base pairs. Ab initio quantum chemical, density functional theory, and empirical potential study. *Journal of the American Chemical Society* **2002,** *124* (13), 3366-76.

65. Krishnamoorthy, G.; Duportail, G.; Mely, Y., Structure and dynamics of condensed DNA probed by 1,1'-(4,4,8,8-tetramethyl-4,8-diazaundecamethylene)bis[4-[[3- methylbenz-1,3-oxazol-2-yl]methylidine]-1,4-dihydroquinolinium] tetraiodide fluorescence. *Biochemistry* **2002,** *41* (51), 15277-87.

66. Reddy, B. S.; Sharma, S. K.; Lown, J. W., Recent developments in sequence selective minor groove DNA effectors. *Current medicinal chemistry* **2001,** *8* (5), 475-508.

67. Niidome, T.; Ohmori, N.; Ichinose, A.; Wada, A.; Mihara, H.; Hirayama, T.; Aoyagi, H., Binding of cationic alpha-helical peptides to plasmid DNA and their gene transfer abilities into cells. *The Journal of biological chemistry* **1997,** *272* (24), 15307-12.

68. Eckel, R.; Ros, R.; Ros, A.; Wilking, S. D.; Sewald, N.; Anselmetti, D., Identification of binding mechanisms in single molecule-DNA complexes. *Biophysical journal* **2003,** *85* (3), 1968-73.

69. Gunther, K.; Mertig, M.; Seidel, R., Mechanical and structural properties of YOYO-1 complexed DNA. *Nucleic Acids Res* **2010,** *38* (19), 6526-32.

70. Armitage, B. A., Cyanine Dye–DNA Interactions: Intercalation, Groove Binding, and Aggregation. In *DNA Binders and Related Subjects*, Waring, M. J.; Chaires, J. B., Eds. Springer Berlin Heidelberg: Berlin, Heidelberg, 2005; pp 55-76.

71. Reuter, M.; Dryden, D. T., The kinetics of YOYO-1 intercalation into single molecules of double-stranded DNA. *Biochemical and biophysical research communications* **2010,** *403* (2), 225-9.

72. Mannion, J. T.; Reccius, C. H.; Cross, J. D.; Craighead, H. G., Conformational analysis of single DNA molecules undergoing entropically induced motion in nanochannels. *Biophysical journal* **2006,** *90* (12), 4538-45.

73. Jameson, D., Introduction to Fluorescence. 2014.

74. Nie, S.; Zare, R. N., Optical detection of single molecules. *Annual review of biophysics and biomolecular structure* **1997,** *26*, 567-96.

75. James, D. I., Microscopy techniques for materials science*: A.R. Clarke and C.N. Eberhardt. Woodhead Publishing Ltd., Abington, Cambridge, CB1 6AH. 2002; 448pp; £145, $225, €225; ISBN 1 85573 587 3; Hardback*. 2003; Vol. 22, p 721.

76. Schwartz, D. C.; Li, X.; Hernandez, L. I.; Ramnarain, S. P.; Huff, E. J.; Wang, Y. K., Ordered restriction maps of Saccharomyces cerevisiae chromosomes constructed by optical mapping. *Science* **1993,** *262* (5130), 110-4.

77. Neely, R. K.; Deen, J.; Hofkens, J., Optical mapping of DNA: single-molecule-based methods for mapping genomes. *Biopolymers* **2011,** *95* (5), 298-311.

78. Bensimon, A.; Simon, A.; Chiffaudel, A.; Croquette, V.; Heslot, F.; Bensimon, D., Alignment and sensitive detection of DNA by a moving interface. *Science* **1994,** *265* (5181), 2096-8.

79. Michalet, X.; Ekong, R.; Fougerousse, F.; Rousseaux, S.; Schurra, C.; Hornigold, N.; van Slegtenhorst, M.; Wolfe, J.; Povey, S.; Beckmann, J. S.; Bensimon, A., Dynamic molecular combing: stretching the whole human genome for high-resolution studies. *Science* **1997,** *277* (5331), 1518-23.

80. Chou, S. Y.; Krauss, P. R.; Renstrom, P. J., Imprint Lithography with 25-Nanometer Resolution. *Science* **1996,** *272* (5258), 85.

81. Chou, S.; R. Krauss, P.; Zhang, W.; Guo, L.; Zhuang, L., Sub-10 nm Imprint Lithography and Applications. 1997; Vol. 15, p 2897-2904.

82. Schift, H., Nanoimprint lithography: An old story in modern times? A review. 2008; Vol. 26.

83. Salieb-Beugelaar, G. B.; Teapal, J.; Nieuwkasteele, J.; Wijnperle, D.; Tegenfeldt, J. O.; Lisdat, F.; van den Berg, A.; Eijkel, J. C., Field-dependent DNA mobility in 20 nm high nanoslits. *Nano Lett* **2008,** *8* (7), 1785-90.

84. Duffy, D. C.; McDonald, J. C.; Schueller, O. J.; Whitesides, G. M., Rapid Prototyping of Microfluidic Systems in Poly(dimethylsiloxane). *Analytical chemistry* **1998,** *70* (23), 4974-84.

85. Li, Y. J.; Xie, H. M.; Guo, B. Q.; Luo, Q.; Gu, C. Z.; Xu, M. Q., Fabrication of high-frequency moiré gratings for microscopic deformation measurement using focused ion beam milling. *Journal of Micromechanics and Microengineering* **2010,** *20* (5), 055037.

86. Cao, H.; Tegenfeldt, J. O.; Austin, R. H.; Chou, S. Y., Gradient nanostructures for interfacing microfluidics and nanofluidics. **2002,** *81* (16), 3058-3060.

87. Arne, S.; Helmut, S., Fabrication of 3D nanoimprint stamps with continuous reliefs using dose-modulated electron beam lithography and thermal reflow. *Journal of Micromechanics and Microengineering* **2010,** *20* (9), 095002.

88. Schleunitz, A.; Guzenko, V. A.; Messerschmidt, M.; Atasoy, H.; Kirchner, R.; Schift, H., Novel 3D micro- and nanofabrication method using thermally activated selective topography equilibration (TASTE) of polymers. *Nano convergence* **2014,** *1* (1), 7.

89. Kirchner, R.; Guzenko, V.; Rohn, M.; Sonntag, E.; Mühlberger, M.; Bergmair, I.; Schift, H., Bio-inspired 3D funnel structures made by grayscale electron-beam patterning and selective topography equilibration. 2015; Vol. 141, p 107-111.

90. Schuck, P. J.; Fromm, D. P.; Sundaramurthy, A.; Kino, G. S.; Moerner, W. E., Improving the mismatch between light and nanoscale objects with gold bowtie nanoantennas. *Physical review letters* **2005,** *94* (1), 017402.

91. Reisner, W.; Pedersen, J. N.; Austin, R. H., DNA confinement in nanochannels: physics and biological applications. *Reports on progress in physics. Physical Society (Great Britain)* **2012,** *75* (10), 106601.

92. Persson, F.; Tegenfeldt, J. O., DNA in nanochannels—directly visualizing genomic information. *Chemical Society reviews* **2010,** *39* (3), 985-999.

93. Stellwagen, N. C., Electrophoresis of DNA in agarose gels, polyacrylamide gels and in free solution. *Electrophoresis* **2009,** *30 Suppl 1*, S188-95.

94. Muller, V.; Westerlund, F., Optical DNA mapping in nanofluidic devices: principles and applications. *Lab Chip* **2017,** *17* (4), 579-590.

95. Menard, L.; Ramsey, J. M., Nanofluidic device architectures for the controlled transport and high throughput analysis of single dna molecules in nanochannels. 2013; Vol. 1, p 2-4.

96. Zhou, J.; Wang, Y.; Menard, L. D.; Panyukov, S.; Rubinstein, M.; Ramsey, J. M., Enhanced nanochannel translocation and localization of genomic DNA molecules using three-dimensional nanofunnels. *Nature communications* **2017,** *8* (1), 807.

97. Freitag, C.; Noble, C.; Fritzsche, J.; Persson, F.; Reiter-Schad, M.; Nilsson, A. N.; Graneli, A.; Ambjornsson, T.; Mir, K. U.; Tegenfeldt, J. O., Visualizing the entire DNA from a chromosome in a single frame. *Biomicrofluidics* **2015,** *9* (4), 044114.

98. Reccius, C. H.; Stavis, S. M.; Mannion, J. T.; Walker, L. P.; Craighead, H. G., Conformation, length, and speed measurements of electrodynamically stretched DNA in nanochannels. *Biophysical journal* **2008,** *95* (1), 273-86.

99. Levene, M. J.; Korlach, J.; Turner, S. W.; Foquet, M.; Craighead, H. G.; Webb, W. W., Zero-mode waveguides for single-molecule analysis at high concentrations. *Science* **2003,** *299* (5607), 682-6.

100. Kress, W. J.; Erickson, D. L., DNA barcodes: methods and protocols. *Methods in molecular biology (Clifton, N.J.)* **2012,** *858*, 3-8.

101. Dostalek, J.; Knoll, W., Biosensors based on surface plasmon-enhanced fluorescence spectroscopy (Review). 2008; Vol. 3, p FD12-22.

102. Bayat, P.; Esmek, F.; Perez-Willard, F.; Volkenandt, T.; Blick, R. H.; Fernandez-Cuesta, I.; Sculpturing Wafer-scale Nanofluidic Devices for Single Molecule Analysis, Submitted to Nanoscale **2018**.

103. https://bionanogenomics.com

104. http://www.opgen.com

105. https://nanoporetech.com

106. https://www.pacb.com

107. https://www.pacb.com/products-and-services/sequel-system/

I would like to sincerely thank the following people for their direct or indirect support.

I offer my deep and sincere gratitude to my supervisor, Prof. Robert H. Blick, who has supported and guided me throughout this project with his patience, encouragement and commitment. It was a great joy working together over the last 3.5 years with his positive energy, passion for science and strong leadership.

My sincerest gratitude goes to my family for their continuous and unparalleled love, help and support; especially my lifelong hero, my dad, whom I wish I could have had forever. He gave me the greatest gift anyone could give another person; he believed in me and taught me to be strong.

The PIER Helmholtz Graduate School (PHGS) and the super-friendly coordinators, Ms. Stefanie Tepass, Mr. Mirko Siemssen, and Ms. Gabriele Keidel are gratefully acknowledged for their appreciable financial and organizational supports during my doctoral project. This doctoral thesis was funded with a prestige scholarship for 3.5 years from University of Hamburg in cooperation with Deutsches Elektronen-Synchrotron (DESY). PHGS also supported my attendance in international conferences over the last 3.5 years, which resulted in three best poster awards and an invited speech from a prestige conference in Canada.

I would also like to thank Prof. Gabriel Bester for his encouragement and insightful comments in our annual meetings, Prof. Frank Lehner and also Prof. Franz X. Kärtner as my mentors at DESY. Many thanks are addressed to Prof. Wolfgang Parak for accepting to be the second evaluator of my dissertation, despite his busy schedule.

I would offer my special thanks to our collaborators, Prof. Adam Grundhoff and Dr. Thomas Günther at the Heinrich Pette Institute, Leibniz Institute for Experimental Virology, University Medical Center Hamburg-Eppendorf for providing us the knowledge and expertise of DNA barcoding, as well as Dr. Fabian Perez-Willard, and Tobias Volkenandt from Carl Zeiss Microscopy for their help and support in electron and ion beam microscopy techniques.

Special appreciation goes to my colleagues at my work group, Dr. Lars Tiemann, Paul Gwozdz, Stefanie Haugg, and also Jonas Sichau, Dr. Robert Zierold for proof reading of my thesis. I was very lucky to have many volunteers for proof reading and commenting on my thesis. I would also like to thank my Bachelor and Master students, Franziska Esmek, Manuel Mueller, Thomas Klings, Filippo Ciabattini, and Jon Polensky for their helps during the project. I would like to thank Dr. Irene Fernandez-Cuesta for our scientific discussions and for teaching me the secrets in the lab, and also the Rhodamine and QD spectroscopy measurements.

I thank all members of the Center for Hybrid Nanostructures for their technical and organizational supports, Mr. Thomas Finger and Mr. Matthias Hein for their support in the

clean room, especially after the relocation of our building and the whole labs. I also thank our secretory, Ms. Katja Finger, for her kind administrational helps, Cornelius Fendler and Jann Harberts for all the fun we had over the lunch time and group activities.

My special thanks goes to my fiancé, Dr. Wolfgang Hollik for his patience and having my back all the time, and also for proof reading of my dissertation. This means a lot to me.

Declaration

I hereby declare on oath, that I have written the present dissertation by my own and have not used other than the acknowledged resources and aids. The submitted written version corresponds to the version on the electronic storage medium. I hereby declare that I have not previously applied or pursued for a doctorate (Ph.D. studies).

Parisa Bayat.

Hamburg 2018

Date: Signature: